Chapter 3

RESULTS

The results in this investigation were divided into 6 sections as followed :

3.1 Syntheses of ligands

3.2 Characterization of ligands

3.3 Synthesis and characterization of *cis*-$Ru(bpy)_2Cl_2$

3.4 Synthesis and characterization of $[Ru(bpy)_3](BF_4)_2$

3.5 Syntheses of $[Ru(bpy)_2L](BF_4)_2$

3.6 Characterization of $[Ru(bpy)_2L](BF_4)_2$

3.1 Syntheses of ligands

There are five ligands which were synthesized in this work as followed:

- 2-(phenylazo)pyridine (azpy)
- 2-(4′-*N,N*-dimethylaminophenylazo)pyridine (dmazpy)
- 2-(4′-*N,N*-diethylaminophenylazo)pyridine (deazpy)
- 2-(phenylazo)pyrimidine (azpym)
- 2-(4′-*N,N*-diethylaminophenylazo)pyrimidine (deazpym)

Azpy, dmazpy and deazpy ligands were synthesized by coupling of 2-aminopyri dine with nitrosobenzene, *N,N*-dimethyl-4-nitrosoaniline and *N,N*-diethyl-4-nitroso aniline, respectively. For azpym and deazpym ligands were synthesized by coupling of 2-aminopyrimidine with nitrosobenzene and *N,N*-diethyl-4-nitrosoaniline, respectively. Purification was done by column chromatography which described previously. The reactions are shown in equation (1)-(5).

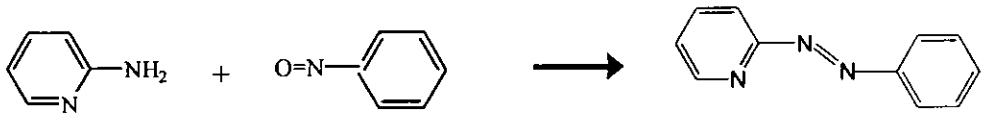

(1)

2-aminopyridine nitrosobenzene azpy

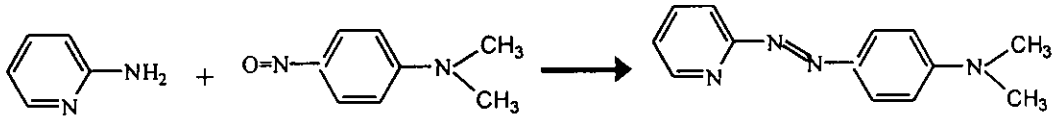

(2)

2-aminopyridine *N,N*-dimethyl-4-nitrosoaniline dmazpy

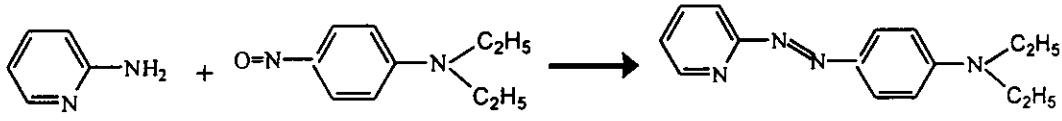

(3)

2-aminopyridine *N,N*-diethyl-4-nitrosoaniline deazpy

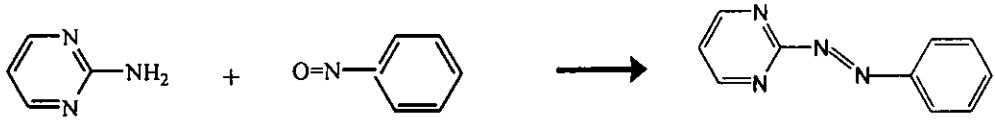

(4)

2-aminopyrimidine nitrosobenzene azpym

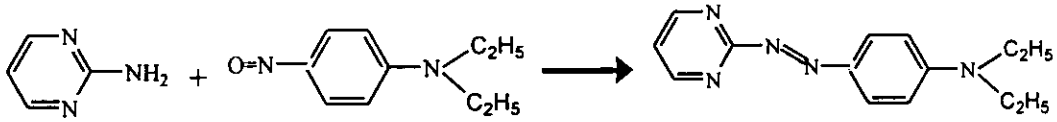

(5)

2-aminopyrimidine *N,N*-diethyl-4-nitrosoaniline deazpym

Ligands were obtained in small yield because of many side reactions. The yield of azpy, dmazpy, deazpy, azpym and deazpym ligands were 35%, 28%, 13%, 27% and 5%, respectively. The physical properties of those ligands are summarized in Table 1.

Table 1 The physical properties of ligands

Ligand	Physical properties		
	Appearance	Color	Melting point (^{o}C)
azpy	Liquid	Orange	32-34[a]
dmazpy	Monoclinic	Red	104-105
deazpy	Orthorhombic	Red	109-110
azpym	Liquid	Orange	Liquid at room temperature
deazpym	Orthorhombic	Red	96-97

[a]Results from Krause and Krause (1980)

Those ligands were well dissolved in almost solvents. The solubility was tested by using 0.0012 g of each ligand in 10 mL of selected solvent (water, methanol, acetronitrile, acetone, ethanol, ethyl acetate, dichloromethane and hexane). However, the deep pink color solution was obtained when dissolve in water.

3.2 Characterization of ligands

The structures of azpy, dmazpy, deazpy, azpym and deazpym were determined by using these techniques

- Electrospray mass spectrometry (ES-MS)
- Proton Nuclear Magnetic resonance spectroscopy (^{1}H NMR)
- Infrared spectroscopy (IR)
- UV-Visible absorption spectroscopy (UV-Visible)
- Cyclic Voltammetry (CV)

3.2.1 Electrospray mass spectrometric results of ligands

Electrospray mass spectroscopic is one important technique to study molecular weight of ligands. The electrospray mass spectra of dmazpy, deazpy, azpym and deazpym ligands are shown in Figure 2-5, respectively. The electrospray mass spectroscopic data of these ligands, which co response to the relative abundance are shown in Table 2.

The parent peak, which gave 100% relative abundance, corresponded to calculated molecular weight of each ligand, one protonation at m/z 227.1, 255.3, 184.9 and 256.2 for dmazpy, deazpy, azpym and deazpym, respectively.

Table 2 The electrospray mass spectrometric data of ligands

Compound	Expected molecular weight	m/z	Assignment	Rel. Abund. (%)
Dmazpy	226.2	227.1	$[M + H]^+$	100
Deazpy	254.3	255.3	$[M + H]^+$	100
Azpym	184.2	184.9	$[M + H]^+$	100
Deazpym	255.3	256.2	$[M + H]^+$	100

M = formula of a ligand

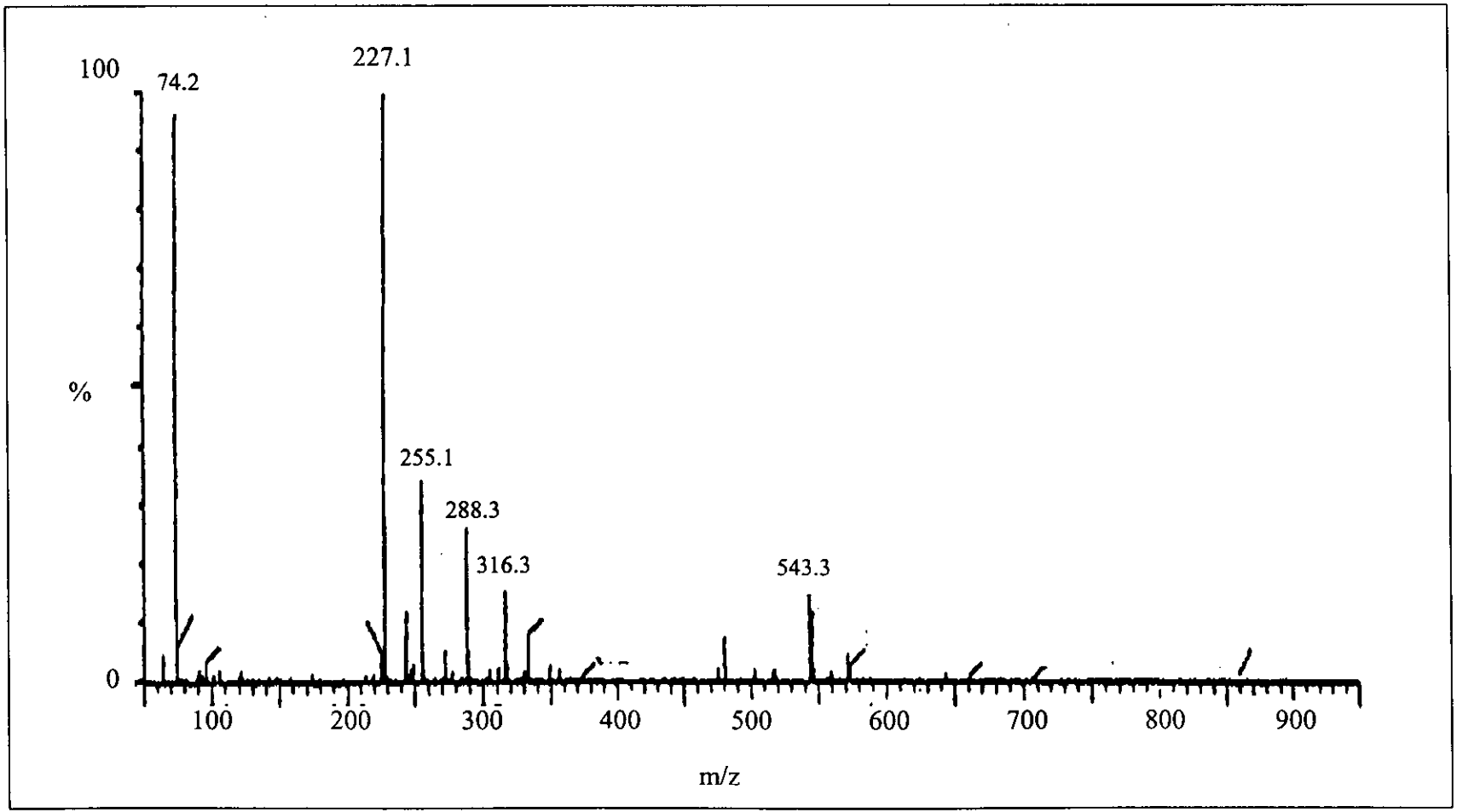

Figure 2 Electrospray mass spectrum of dmazpy

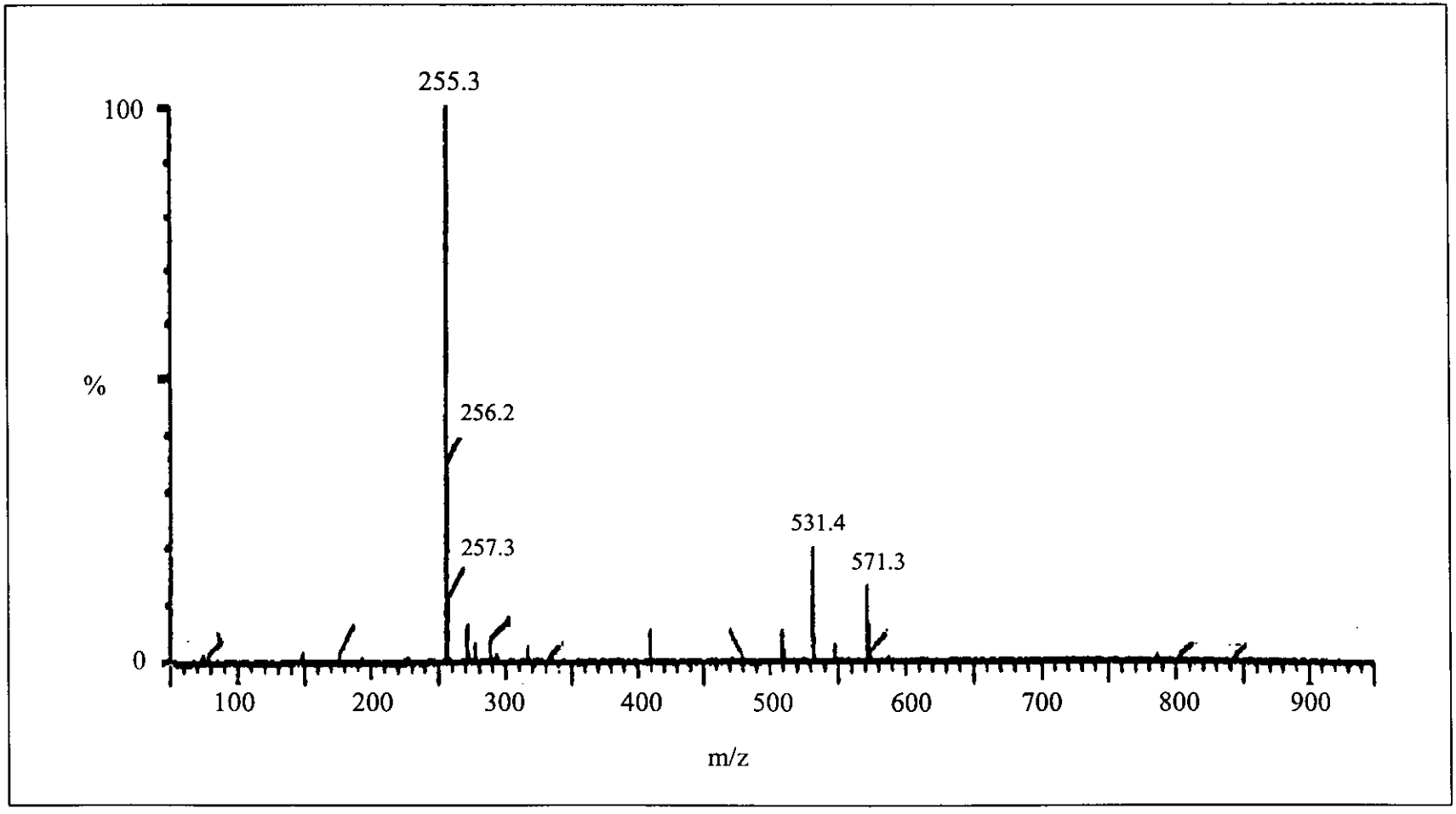

Figure 3 Electrospray mass spectrum of deazpy

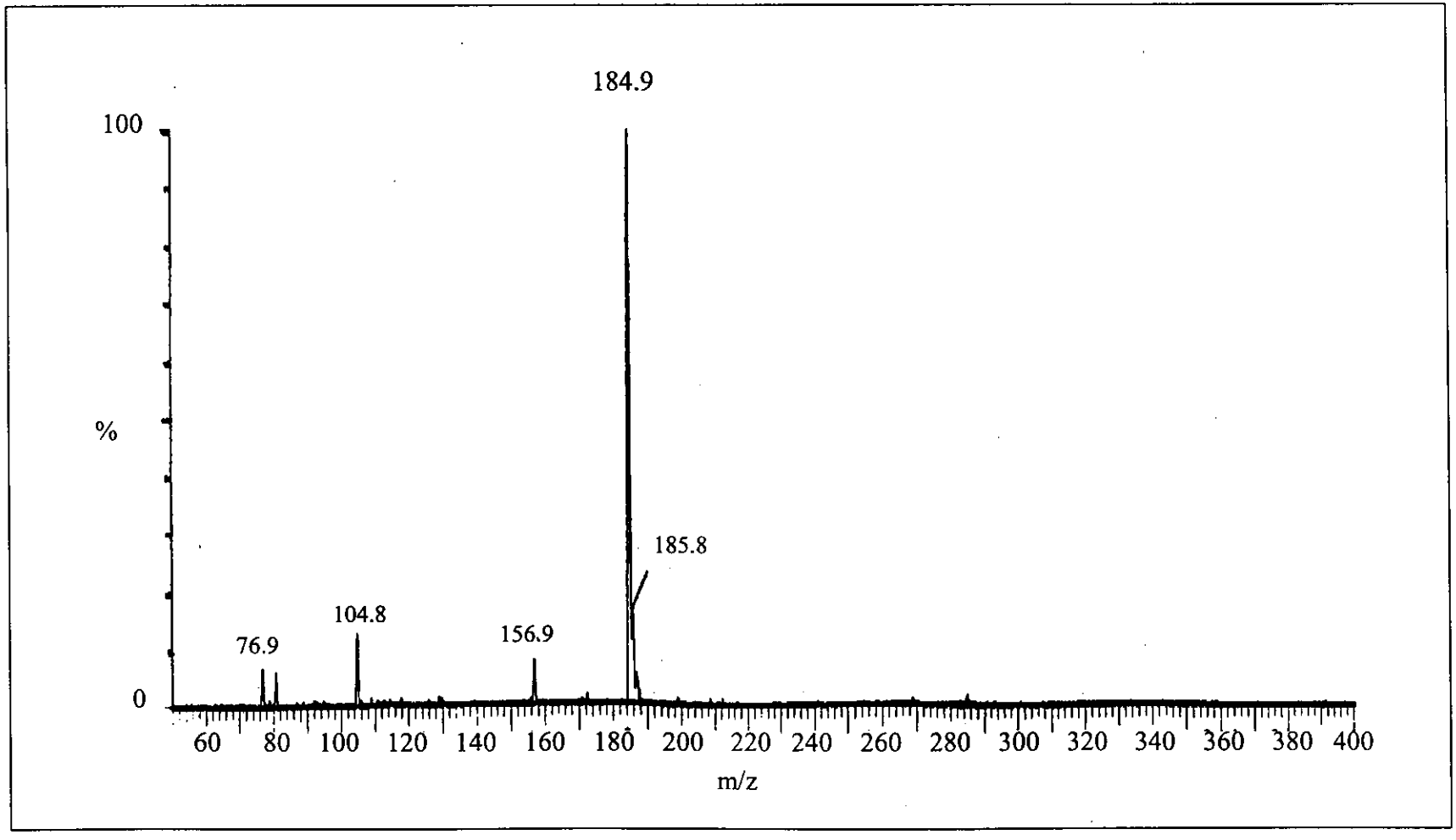

Figure 4 Electrospray mass spectrum of azpym

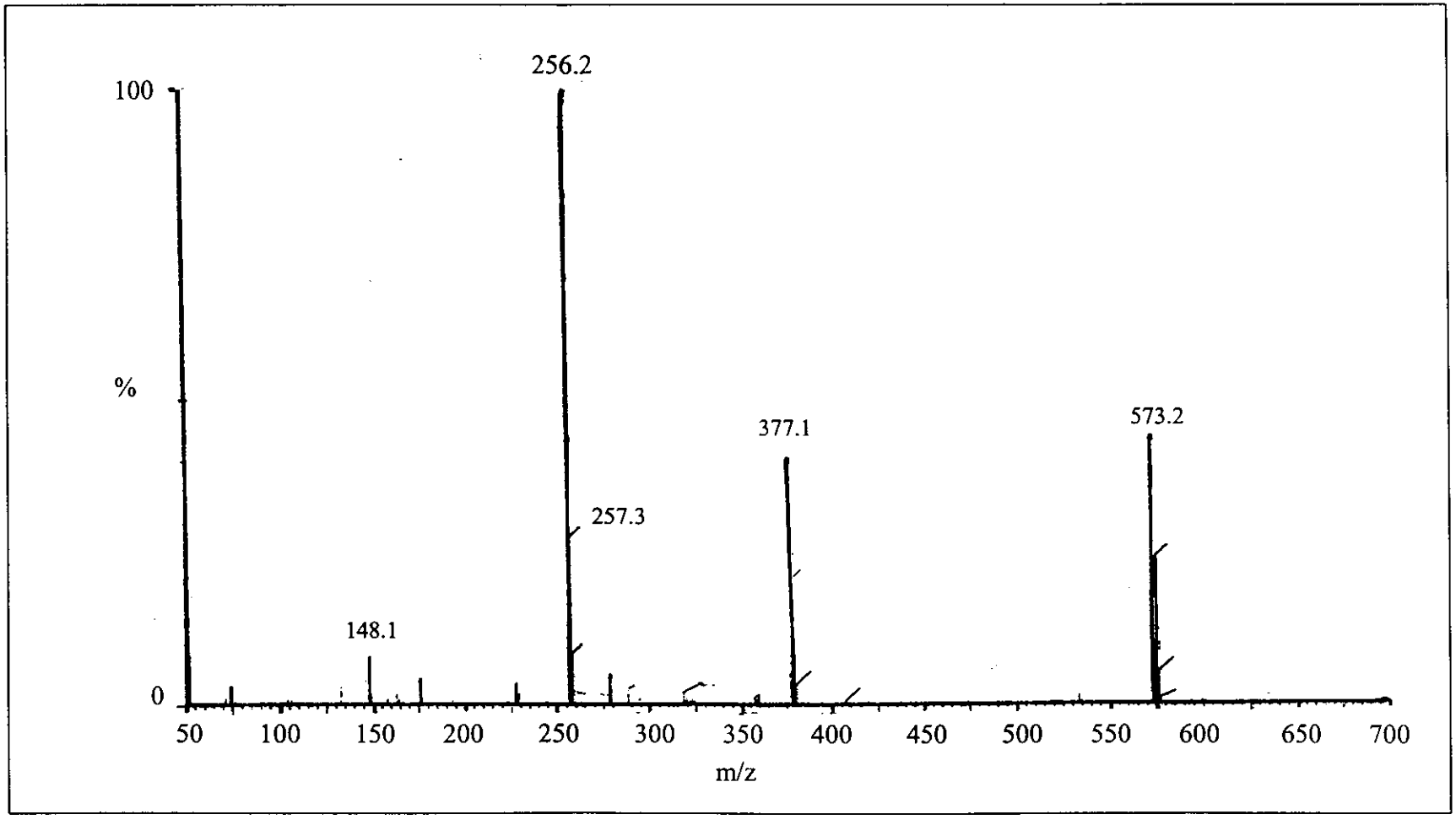

Figure 5 Electrospray mass spectrum of deazpym

3.2.2 ^{1}H NMR spectroscopic results of ligands

^{1}H NMR spectroscopy is an important technique to determine molecular structures of compounds because different protons in a molecular structure will show different chemical shifts. The chemical shifts (δ, ppm) and J-coupling (Hz) of free ligands are reported in part per million (ppm) downfield from tetramethylsilane (TMS, $(CH_3)_4Si$) which used as an internal standard. The ^{1}H NMR spectroscopic data of azpy, dmazpy and deazpy ligands are given in Table 3 and Table 4 for azpym and deazpym ligands. The ^{1}H NMR spectra and structures with proton numbering systems of azpy, dmazpy, deazpy, azpym and deazpym ligands in acetone-d_6 are shown in Figure 8-12, respectively.

Table 3 ^{1}H NMR spectroscopic data of azpy, dmazpy and deazpy

Position	δ(ppm)			J (Hz)	Amount of H
	Azpy	Dmazpy	Deazpy		
H6	8.75 (ddd)	8.66 (ddd)	8.65 (ddd)	5.0, 2.0, 1.0	1
H4	8.04 (ddd)	7.94 (ddd)	7.93 (ddd)	7.0, 8.0, 2.0	1
H7	8.02 (dd)	7.93 (d)	7.92 (d)	2.0, 8.5 and 9.0	2
H3	7.77 (ddd)	7.70 (ddd)	7.70 (ddd)	8.0, 1.0, 1.0	1
H5	7.55 (ddd)	7.41 (ddd)	7.40 (ddd)	7.0, 1.0, 5.0	1
H8	7.64 (m)	6.89 (d)	6.88 (d)	9.0	2
H9		3.15 (s)	3.55 (q)	7.0	1, 6 and 4
H10	-	-	1.25 (t)	7.0	6

s = singlet, d = doublet, dd = doublet of doublet, ddd = doublet of doublet of doublet, t = triplet, q = quartet, m = multiplet

Protons in azpy and dmazpy ligands are divided into 7 groups but 8 groups for deazpy which are shown in Figure 6.

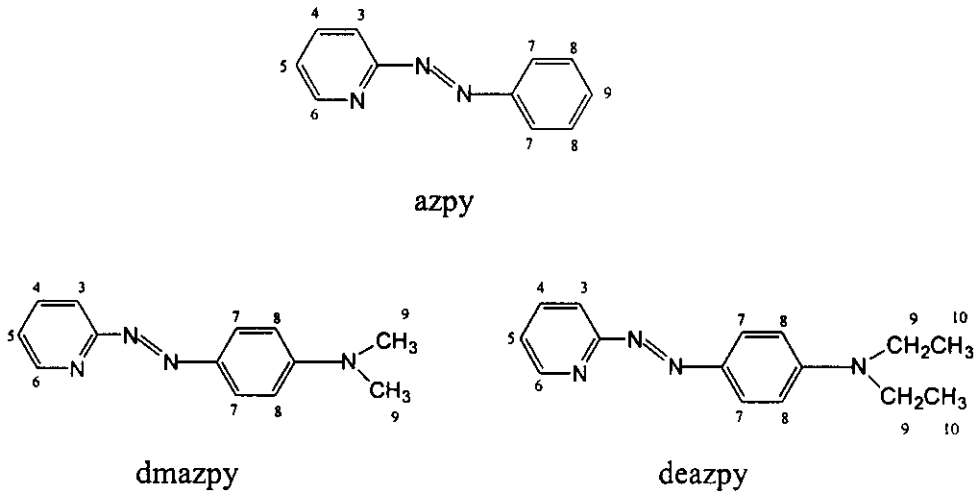

Figure 6 The structures of azpy, dmazpy and deazpy with proton numbering systems

The ^{1}H NMR results were used to support the structures of all ligands. The results of ^{1}H NMR of dmazpy and deazpy were very similar to each other. The chemical shift of corresponding protons in both ligands resonate at slightly different values. The details of each signal of azpy, dmazpy and deazpy (Table 3) are described below.

The H3 located next to the H4 and it was effected from nitrogen of azo function. The signal of H3 proton might be located at downfield more than H5 and upfield than that in H6, H4 and H7. This signal showed doublet of doublet of doublet peak which was splitted by the H4 (J = 8.0 Hz) and H5 (J = 1.0 Hz) and the H6 (J = 1.0 Hz).

The H4 was opposite to pyridine nitrogen. The proton was less effected from nitrogen atom than that of the H6, thus the chemical shift value was less than that

of H6. The signal of this proton was also doublet of doublet of doublet peak. It was splitted by the H5 (J = 7.0 Hz), H3 (J = 8.0 Hz) and the H6 (J = 2.0 Hz).

The signal of H5 proton, next to H6, was doublet of doublet of doublet peak. The splitting of doublet peak (J = 7.0 Hz) was observed for coupling with H4. Then each of doublet peak was splitted to doublet peaks (J = 1.0 Hz) from long range coupling with H3 and then each of doublet peak was splitted to doublet peaks by H_1 (J = 5.0 Hz). This H5 signal of azpy ligand occurred at downfield more than dmazpy and deazpy ligands.

The H6 was located on pyridine next to pyridine nitrogen atom which gave signal at the most downfield. The proton signal was splitted by the H_2 (J = 5.0 Hz). Then each of doublet peak was splitted to doublet peaks from long range coupling with H4 (J = 2.0 Hz) and H3 (J = 1.0 Hz). Therefore, the signal was doublet of doublet of doublet peak.

The H7 had two equivalent protons on phenyl ring located closed to azo nitrogen. This signal showed at downfield than H3. The H7 of azpy ligand interacted with H9 (J = 2.0 Hz) gave the doublet peak and then each of doublet peak was splitted to doublet peaks by H8 (J = 8.5 Hz). For the H7 of dmazpy and deazpy ligands interacted with H8 gave the doublet peak with J-coupling 9.0 Hz. This H7 signal of azpy ligand occurred at downfield more than dmazpy and deazpy ligands.

The H8 had two equivalent protons located next to the H7. The signal showed doublet peak which was splitted by the H7 (J = 9.0 Hz for dmazpy and deazpy). The signal of H8 proton for azpy ligand showed multiplet peaks which resonated at the same position of H9.

The H9 were the -H, $-CH_3$ and $-CH_2-$ protons of azpy, dmazpy and deazpy ligands, respectively. This signal of azpy ligand was multiplet peak. The splitting of multiplet peak was observed for coupling with H7 and H8 which resonated

at the same position of H8. In case of dmazpy, the H9 signal was singlet peak of 6 protons whereas, deazpy showed quartet peak of 4 proton. The signal in deazpy was due to the methyl ($-CH_3$) protons.

The H10 were methyl ($-CH_3$) proton of deazpy ligand. The signal of this proton was triplet peak from the interaction with methylene ($-CH_2-$) protons.

Table 4 ^{1}H NMR spectroscopic data of azpym and deazpym

Position	δ(ppm)		J (Hz)	Amount of H
	Azpym	Deazpym		
H4, H6	9.01 (d)	8.92 (d)	5.0	2
H7	8.05 (dd)	7.96 (d)	2.5, 8.0 and 9.0	2
H5	7.61 (t)	7.46 (t)	5.0	1
H8	7.66 (m)	6.89 (d)	9.0	2
H9		3.57 (q)	7.0	1 and 4
H10	-	1.25 (t)	7.0	6

d = doublet, dd = doublet of doublet, t = triplet, q = quartet, m = multiplet

Protons in azpym ligand are divided into 6 groups but 7 groups for deazpym are shown in Figure 7.

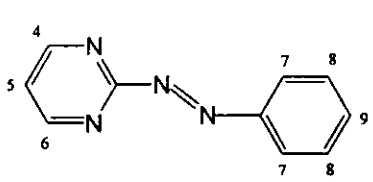

azpym

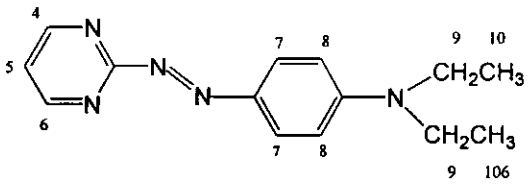

deazpym

Figure 7 The structures of azpym and deazpym with proton numbering systems

For the details of each signal of azpym, and deazpym (Table 4) could be described below.

The H4 and H6 are equivalent protons on pyrimidine ring. These protons were located next to pyrimidine nitrogen atoms which gave signal at the most downfield. The proton signal was splitted by the H5 (J = 5.0 Hz). Therefore, the signal was doublet peak.

The signal of H5 proton located next to H4 and H6 of both ligands were triplet peaks. The splitting of triplet peak was observed from coupling with H4 and H6 (J = 5.0 Hz). The chemical shift of H5 occurred with less values than that of H4, H6 and H7.

The H7 had two equivalent protons on phenyl ring. These protons interacted with H8 and gave the doublet peak with J-coupling 9.0 Hz for deazpym ligand. The signal of H7 for azpym ligand was doublet of doublet peak. The splitting of doublet peak (J = 2.5 Hz) was observed from long range coupling with H9. Then signal of doublet peak was splitted into doublet of doublet peak (J = 8.0 Hz) from coupling with H8. These signals of both azpym and deazpym ligands occurred at downfield more than H5 but upfield than that in H4 and H6.

The H8 had two equivalent protons located next to the H7. The signal was multiplet for azpym ligand which overlap with the signal of H9. For the H8 signal

of deazpym ligand showed doublet peak which affected from the H7 (δ = 6.89 ppm, J=9.0 Hz). It occurred at upfield than that of H5 (δ = 7.46 ppm).

The H9 signals were the -H and -CH_2- protons of azpym and deazpym ligands, respectively. This signal of azpym ligand was multiplet. The multiplet peaks were due to the overlap of H9 and H8 signals. In case of deazpym ligand, the methylene (-CH_2-) protons showed quartet peaks of 4 protons from the interaction with methyl protons (J = 7.0 Hz).

The H10 signals were the methyl (-CH_3) protons of deazpym ligand. The signal of this proton was triplet peak of 6 protons from the interaction with methylene protons (J = 7.0 Hz).

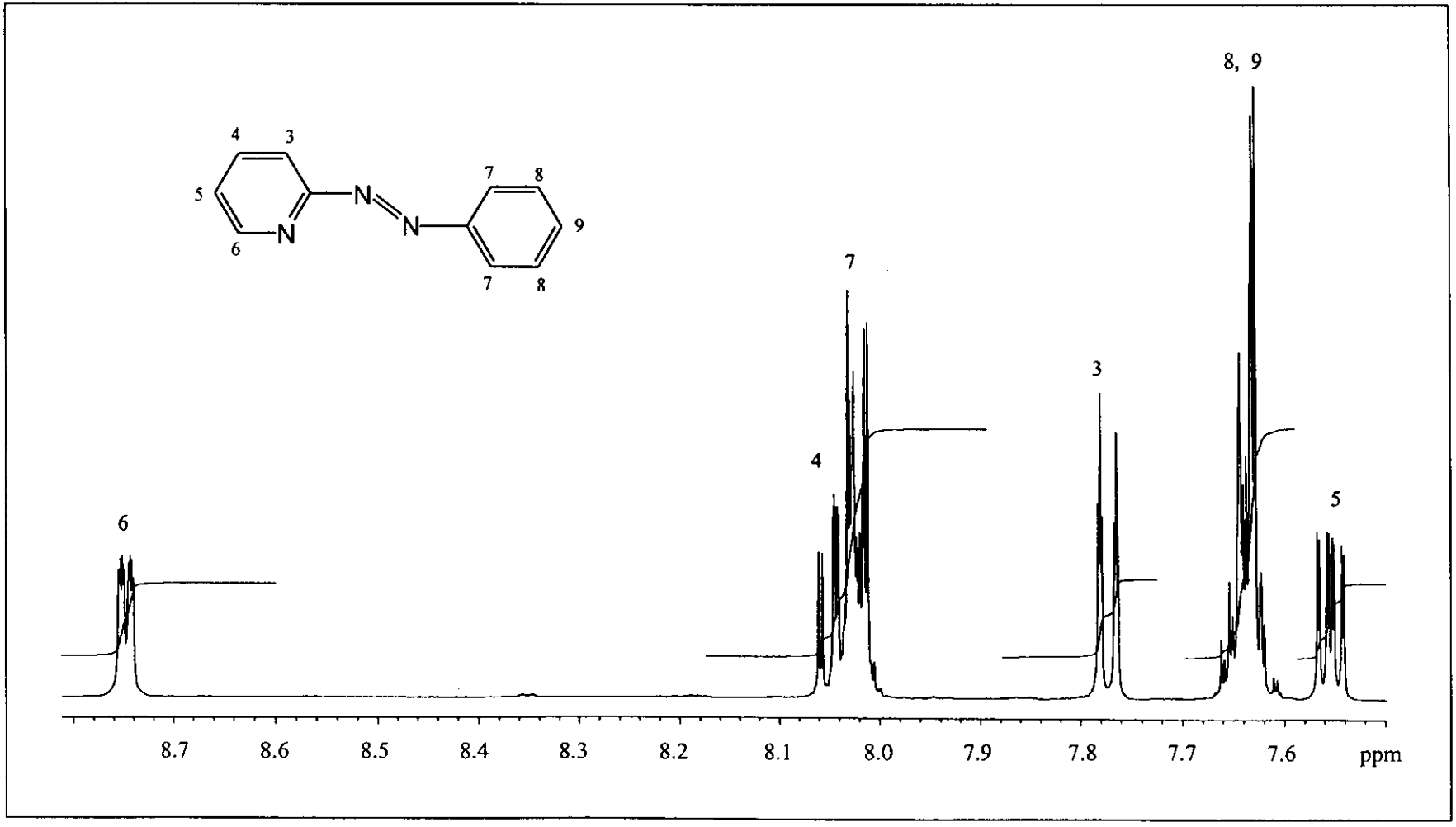

Figure 8 ^{1}H NMR spectrum of azpy in acetone-d_6 solution

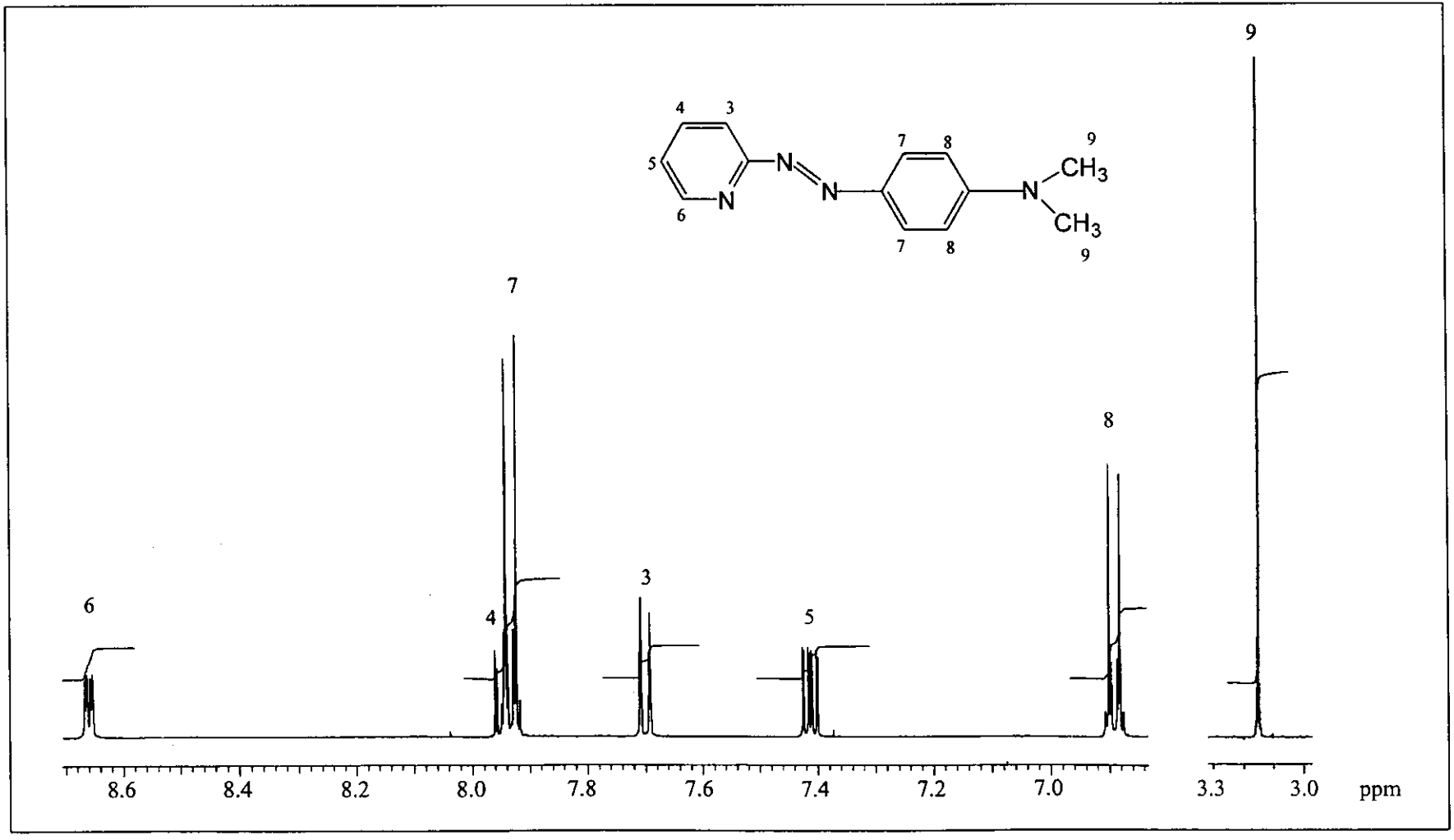

Figure 9 ^{1}H NMR spectrum of dmazpy in acetone-d_6 solution

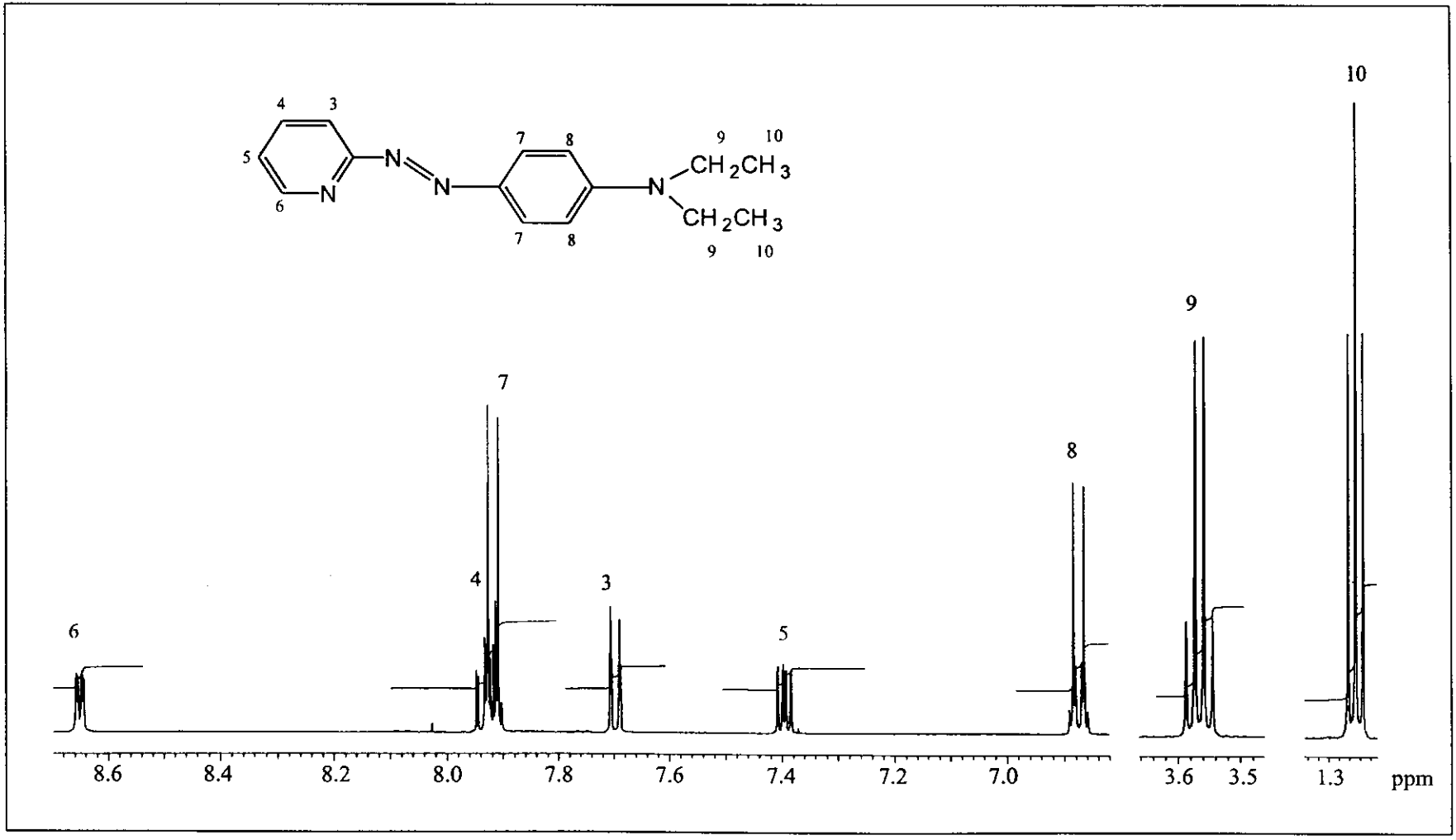

Figure 10 ^{1}H NMR spectrum of deazpy in acetone-d_6 solution

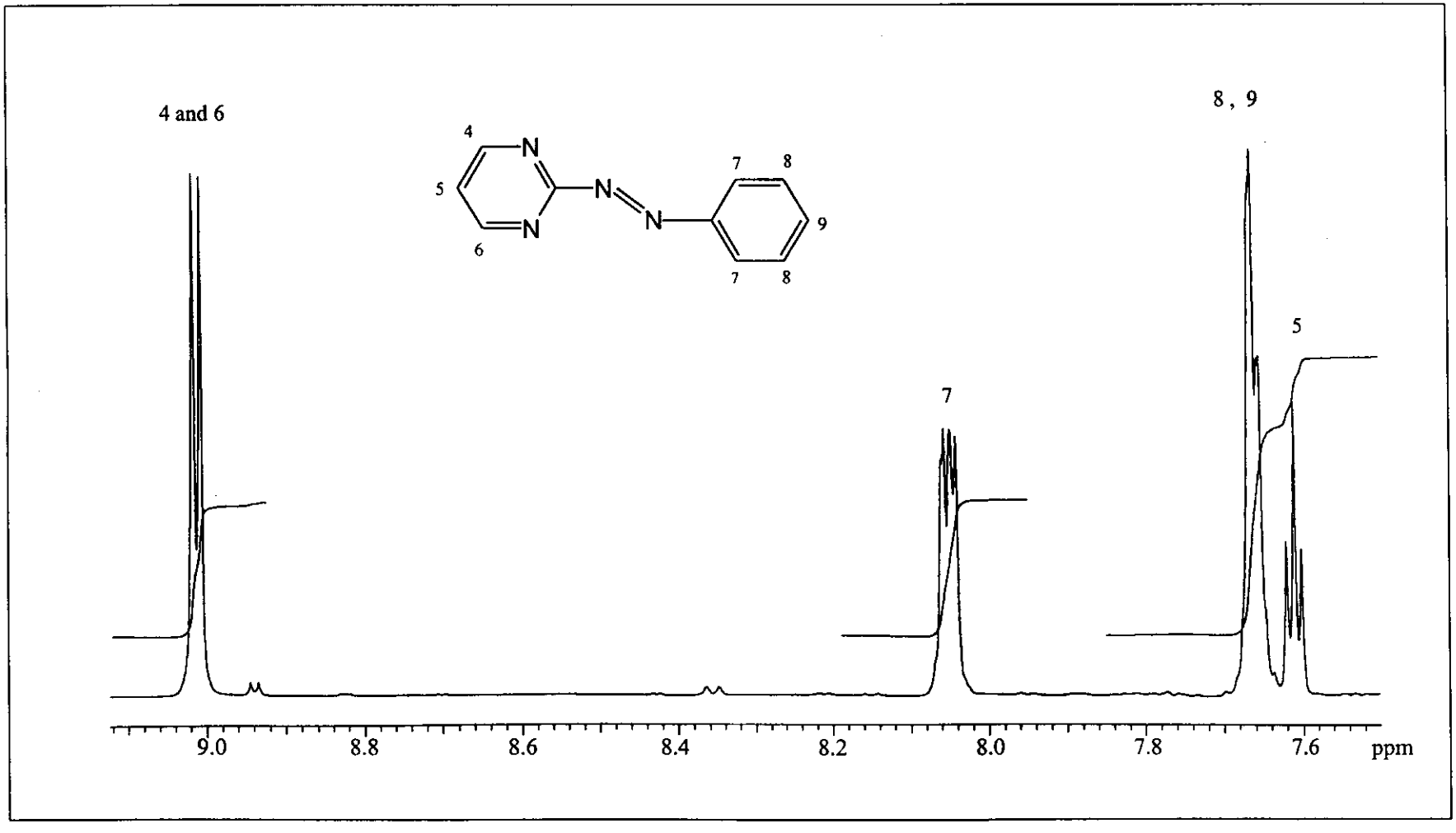

Figure 11 ^{1}H NMR spectrum of azpym in acetone-d_6 solution

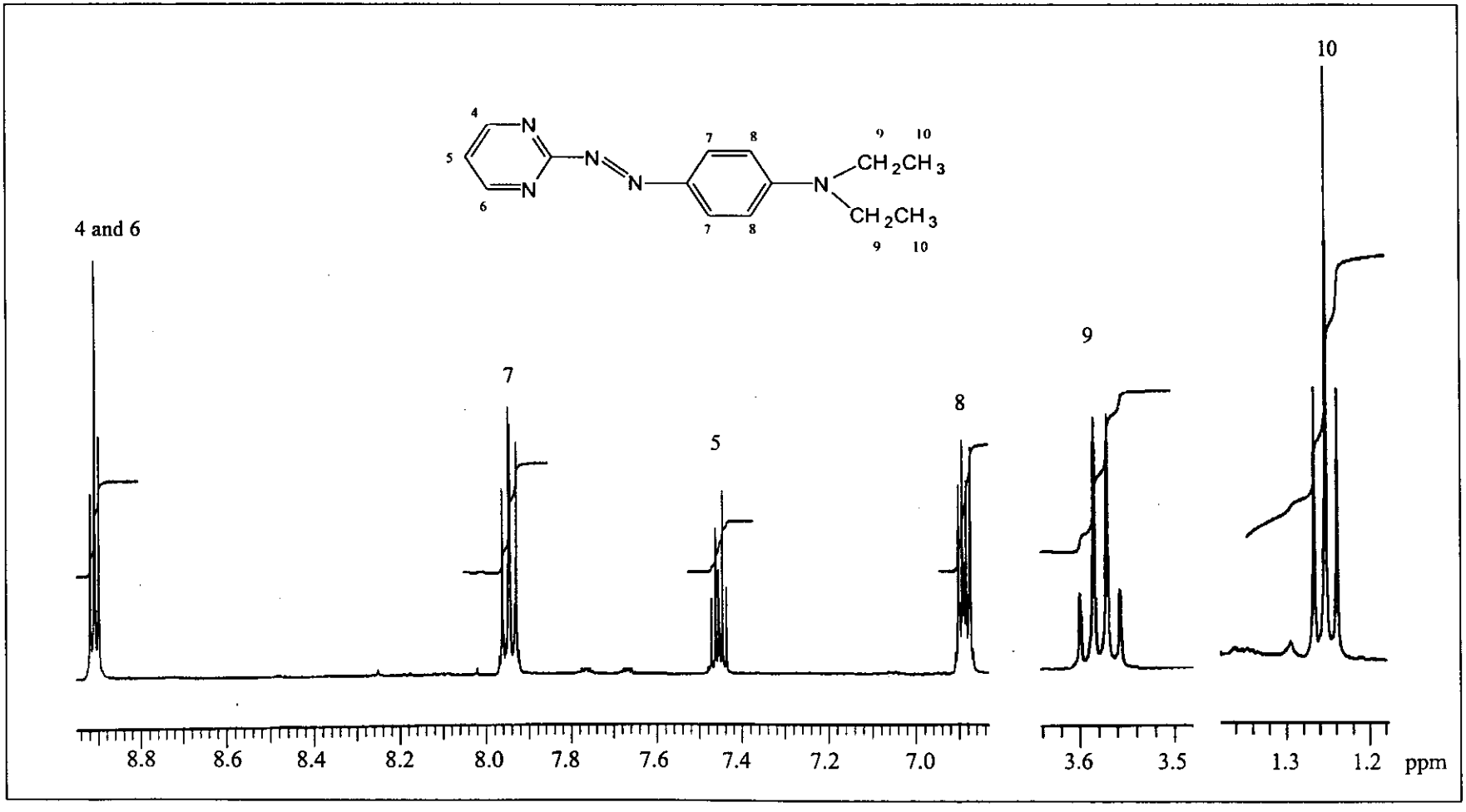

Figure 12 ^{1}H NMR spectrum of deazpym in acetone-d_6 solution

3.2.3 Infrared spectroscopic results of ligands

Infrared spectra of free ligands in the KBr pellet were recorded in the range 4000-400 cm^{-1} which were helpful in the characterization of the ligands. The infrared spectra in the range 1800-400 cm^{-1} of azpy, dmazpy, deazpy, azpym and deazpym are shown in Figure 13-17, respectively. All of the ligands exhibited several characteristic strong bands near 1600 to 500 cm^{-1}. Some characteristic frequencies are summarized in Table 5.

The ring modes for 2-substituted pyridine and monosubstituted benzene appeared in the 1600-1400 cm^{-1} region. They were the C=C and C=N stretching of pyridine and benzene ring modes. These modes in the case of dmazpy, deazpy, azpym and deazpym ligands showed strong to medium absorption at the frequencies similar to azpy results. The C=C and C=N stretching of azpy appeared at 1584, 1578, 1498 and 1495 cm^{-1} (Krause and Krause, 1980).

Objective of the studying, the IR spectra were to locate the N=N stretching mode which used for considering the acid property in azo complexes. From the data in Table 5 it could be seen that the N=N stretching vibration for azpy find a strong absorption at 1421 cm^{-1} which corresponded to the previous work (Krause and Krause, 1980). This band shifted to lower energy for dmazpy, deazpy, azpym and deazpym ligands which occurred at 1400, 1397, 1392 and 1379 cm^{-1}, respectively. This result indicates that the N=N bond of the free azpy ligand was stronger than those of free dmazpy, deazpy, azpym and deazpym ligands. The decrease of N=N bond order in dmazpy, deazpy and deazpym could be due to the substituents ($-NR_2$) which were electron donating groups and will be discussed in details later.

Table 5 Infrared data of ligands in the KBr pellet

Vibrational modes	Wavenumber (cm^{-1})				
	Azpy	Dmazpy	Deazpy	Azpym	Deazpym
sp^2 C-H stretching	3056(w)	3055(w)	3067(m)	3060(w)	3033(w)
N=N (azo) stretching	1421(s)	1400(s)	1397(s)	1392(s)	1379(s)
C=N stretching	1581(s)	1604(s)	1602(s)	1563(s)	1600(s)
C=C stretching	1581(s) 1493(m) 1464(m) 1448(m)	1604(s) 1524(s) 1450(m)	1602(s) 1516(s) 1467(m)	1563(s) 1497(m) 1452(m)	1600(s) 1562(s) 1516(s)
C-H bending of para disubstituted benzene	-	819(s)	826(s)	-	838(s)
C-H out of plane	791(s) 738(s) 687(s)	800(m) 744(m)	792(s) 746(m)	815(s) 765(s) 690(s)	811(m) 794(m)

s = strong, m = medium, w = weak

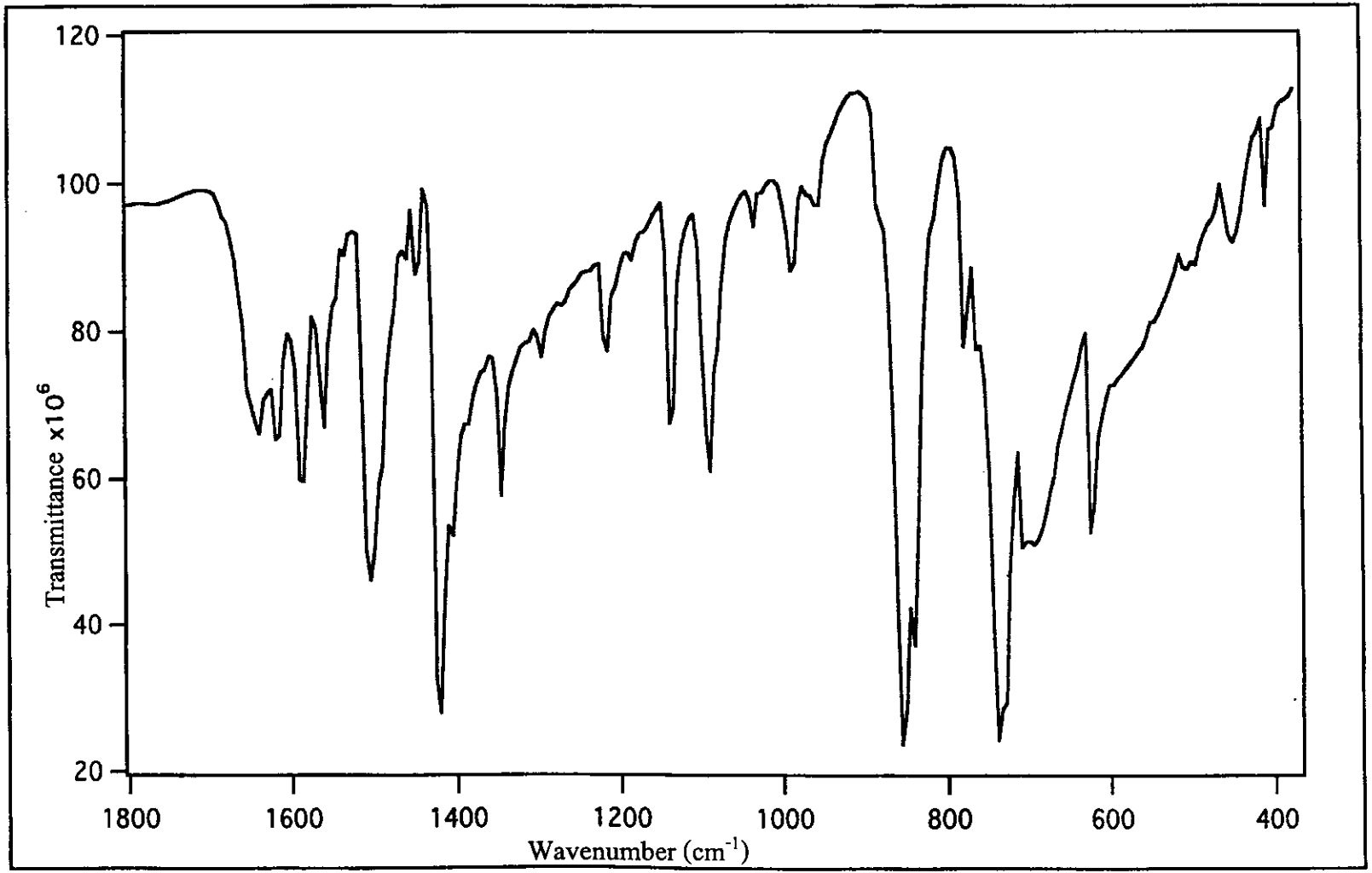

Figure 13 Infrared spectrum of azpy in the KBr pellet

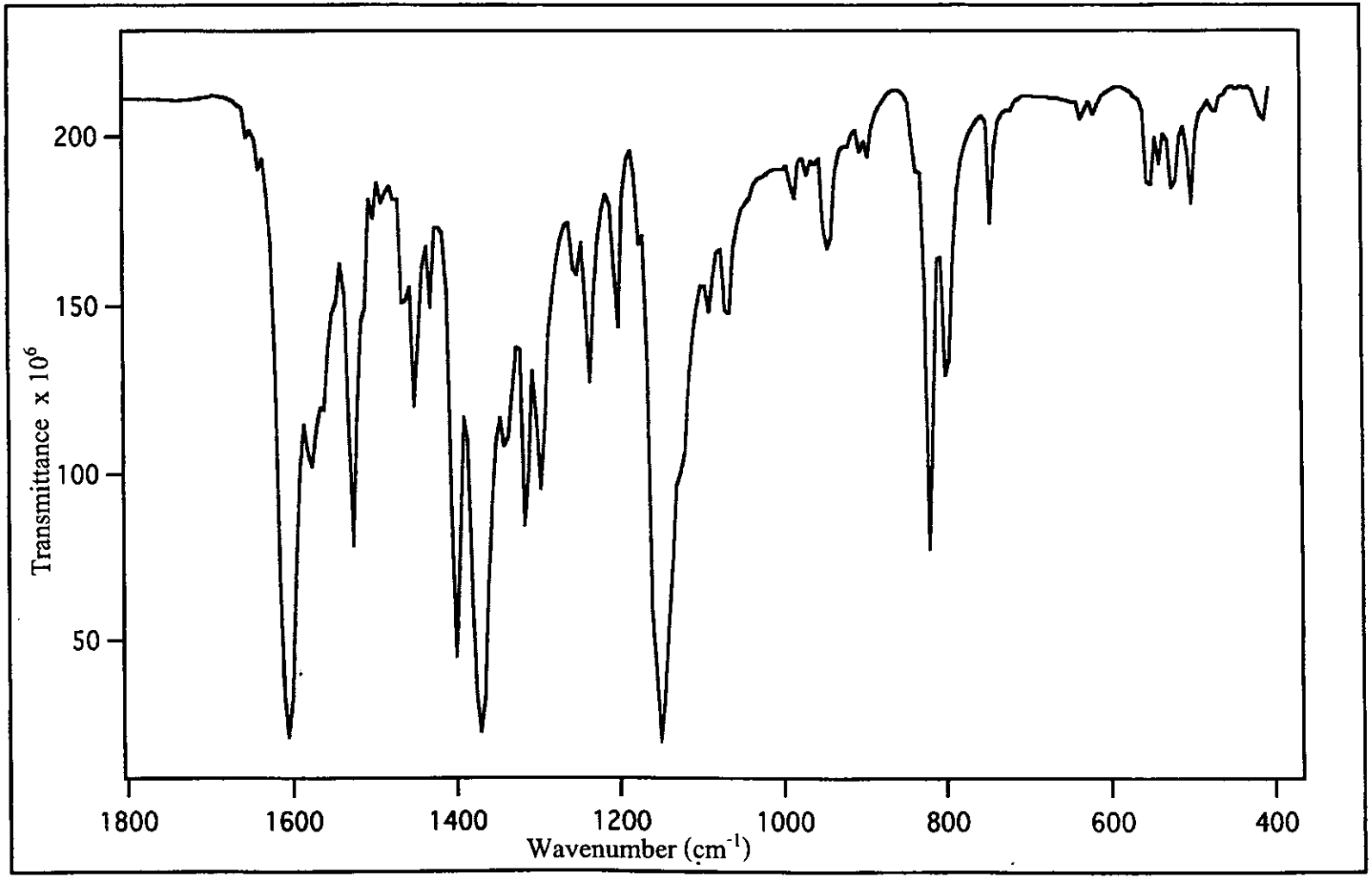

Figure 14 Infrared spectrum of dmazpy in the KBr pellet

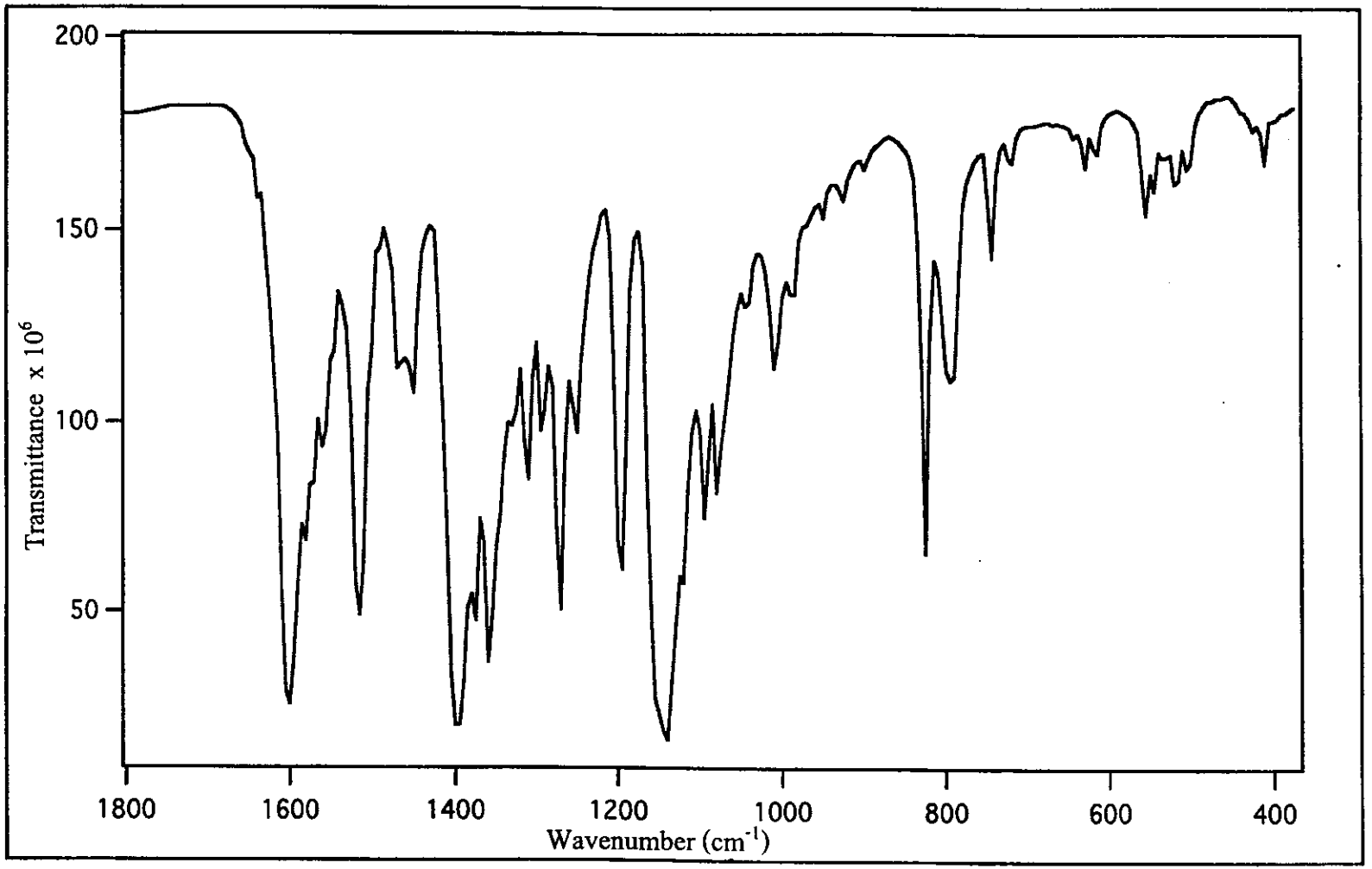

Figure 15 Infrared spectrum of deazpy in the KBr pellet

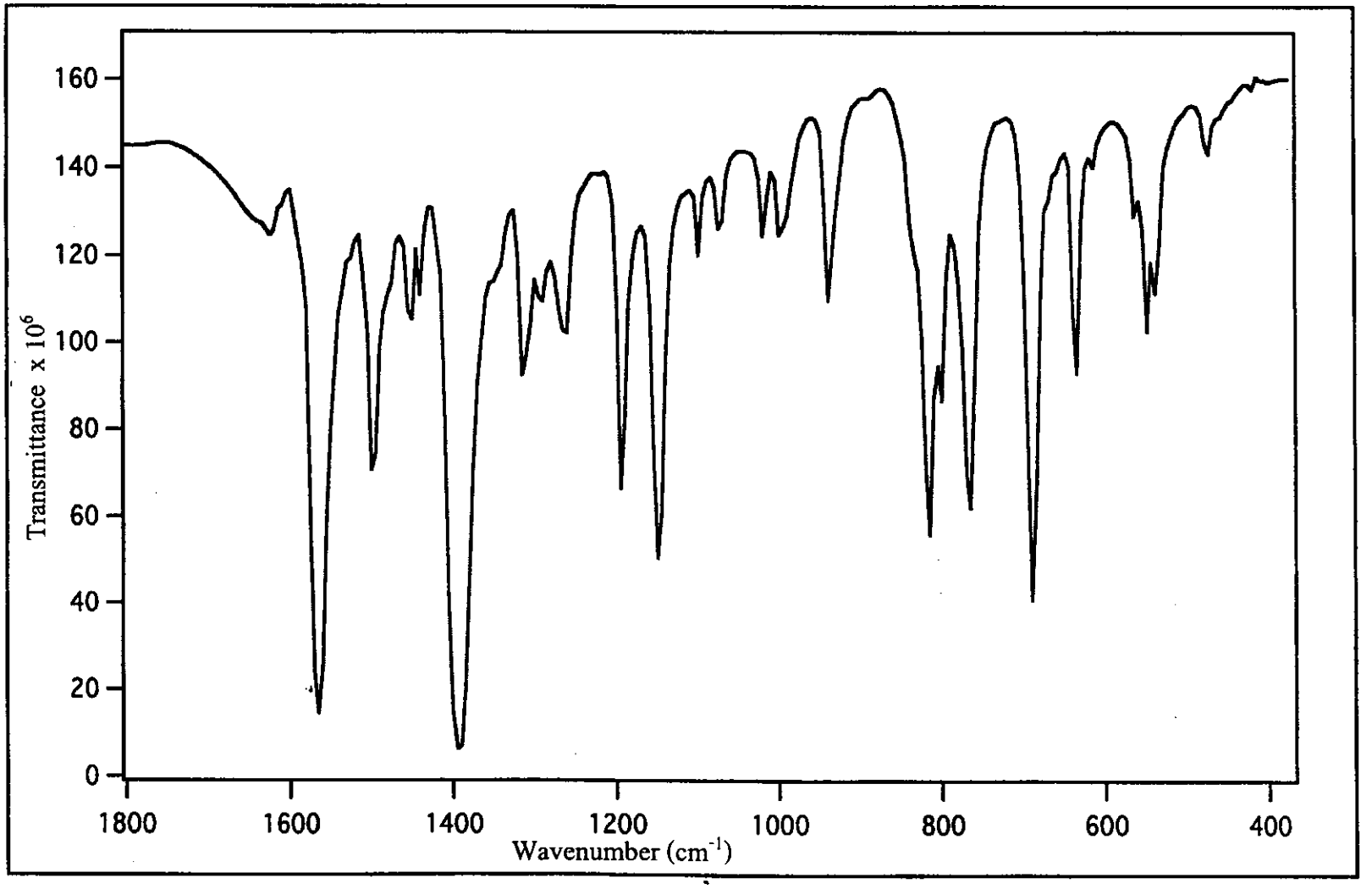

Figure 16 Infrared spectrum of azpym in the KBr pellet

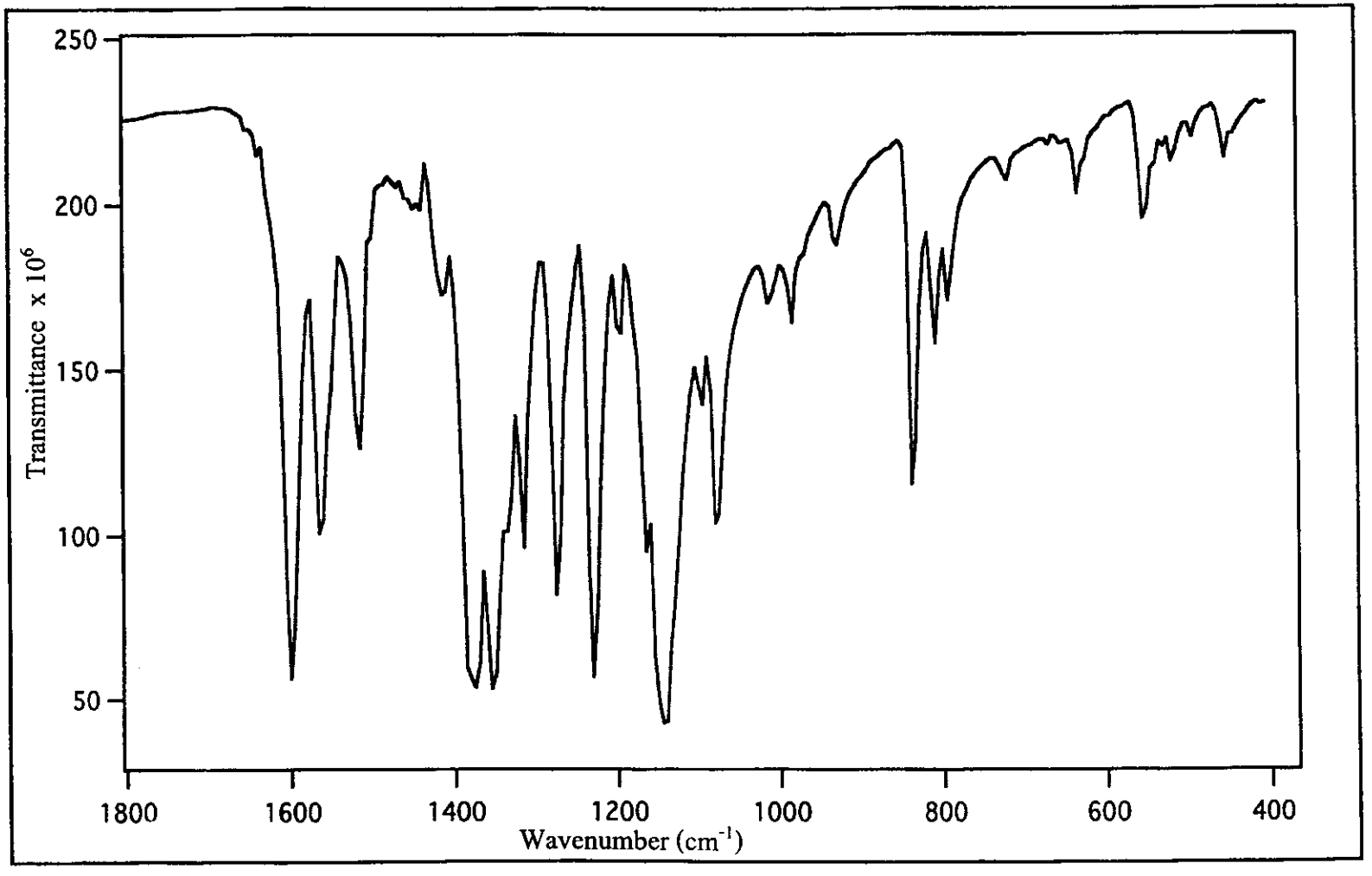

Figure 17 Infrared spectrum of deazpym in the KBr pellet

3.2.4 UV-Visible absorption spectroscopic results of ligands

The UV-Visible spectra of free ligands in various solvents were measured in the range 200-800 nm. The electronic absorption spectra of azpy, dmazpy, deazpy, azpym and deazpym solution in acetonitrile are shown in Figure 18-22, respectively.

Table 6 UV-Visible data of ligands in various solvents

Compound	λ_{max}, nm (ε^a x 10^{-4}, $M^{-1}cm^{-1}$)			
	$\pi \rightarrow \pi^*$			
	CH_2Cl_2	$CHCl_3$	DMSO	CH_3CN
Azpy	318 (1.8)	319 (1.8)	319 (1.8)	314 (1. 8)
	[b]448 (0.05)	[b]449 (0.05)	[b]450 (0.05)	[b]448 (0.05)
Dmazpy	426 (3.4)	428 (3.4)	437 (2.5)	423 (3.7)
	270 (1.1)	270 (1.2)	269 (1.0)	267 (1.2)
Deazpy	437 (3.5)	438 (3.5)	444 (2.5)	431 (3.4)
	273 (1.0)	273 (1.1)	271 (0.9)	271 (0.9)
Azpym	304 (1.7)	311 (1.6)	303 (1.3)	298 (1.5)
	[b]447 (0.04)	[b]448 (0.04)	[b]438 (0.05)	[b]439 (0.04)
Deazpym	444 (3.0)	451 (3.4)	442(3.0)	431 (2.9)
	274 (1.2)	276 (1.2)	273 (1.2)	267 (1.1)

[a] Molar extinction coefficient

[b] $n \rightarrow \pi^*$ transition

The azoimine ligand groups always show two absorption bands which assigned to $n \rightarrow \pi^*$ and $\pi \rightarrow \pi^*$ transitions as observed in 200-500 nm. The absorption spectra of all ligands were prepared in acetonitrile. The absorption spectrum of free azpy ligand displayed absorption bands at 448 nm ($\varepsilon \approx 500\ M^{-1}cm^{-1}$) and at ~ 314 nm ($\varepsilon \approx 18000\ M^{-1}cm^{-1}$). These could be respectively assigned to $n \rightarrow \pi^*$ and $\pi \rightarrow \pi^*$ transitions.

The absorption spectra of dmazpy and deazpy ligands showed two absorption bands at 260-270 nm ($\varepsilon \approx 10000\ M^{-1}cm^{-1}$) in UV region which referred to $\pi \rightarrow \pi^*$ (1) transition, and bands at 420-430 nm ($\varepsilon \approx 35000\ M^{-1}cm^{-1}$) in visible region which belonged to $\pi \rightarrow \pi^*$ (2) transition. These derivatives of azpy ligand had $\pi \rightarrow \pi^*$ transition at the lowest energy, whereas that in azpy was $n \rightarrow \pi^*$ transition.

The spectrum of azpym ligand displayed absorption bands of $\pi \rightarrow \pi^*$ transition at 298 nm ($\varepsilon \approx 15{,}000\ M^{-1}cm^{-1}$) in UV region and the broad band of $n \rightarrow \pi^*$ transition at ~440 nm ($\varepsilon \approx 400\ M^{-1}cm^{-1}$) in visible region. For deazpym ligand showed two absorption bands which were assigned as $\pi \rightarrow \pi^*$ transition in UV at ~270 ($\varepsilon \approx 10000\ M^{-1}cm^{-1}$) and visible region at ~430 nm ($\varepsilon \approx 30000\ M^{-1}cm^{-1}$). In addition, their absorption spectra were also studies in CH_2Cl_2, $CHCl_3$ and DMSO solution. All the ligands showed slightly solvent effect. The polar solvents lead to bathochromic shift (red shift) of $\pi \rightarrow \pi^*$ transition.

The data in Table 6 showed that the absorption intense band of $\pi \rightarrow \pi^*$ transition shifted to lower energies for dmazpy, deazpy and deazpym ligands. Whereas, the azpym ligand shifted to higher energy when compared to azpy ligand. The energy of $\pi \rightarrow \pi^*$ transition increased in the order deazpym $\approx$ deazpy < dmazpy < azpy < azpym.

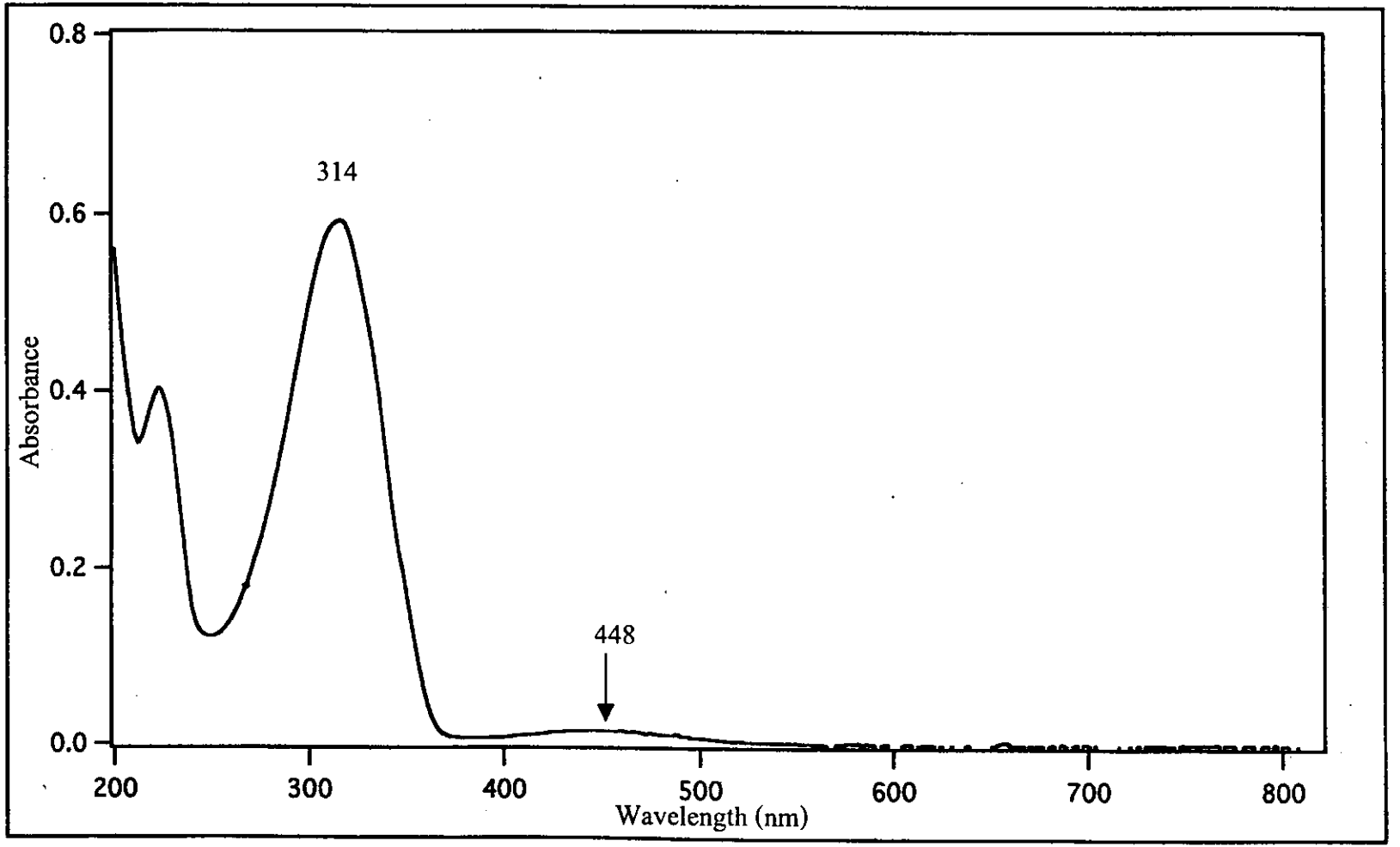

Figure 18 Absorption spectrum of azpy in CH_3CN solution

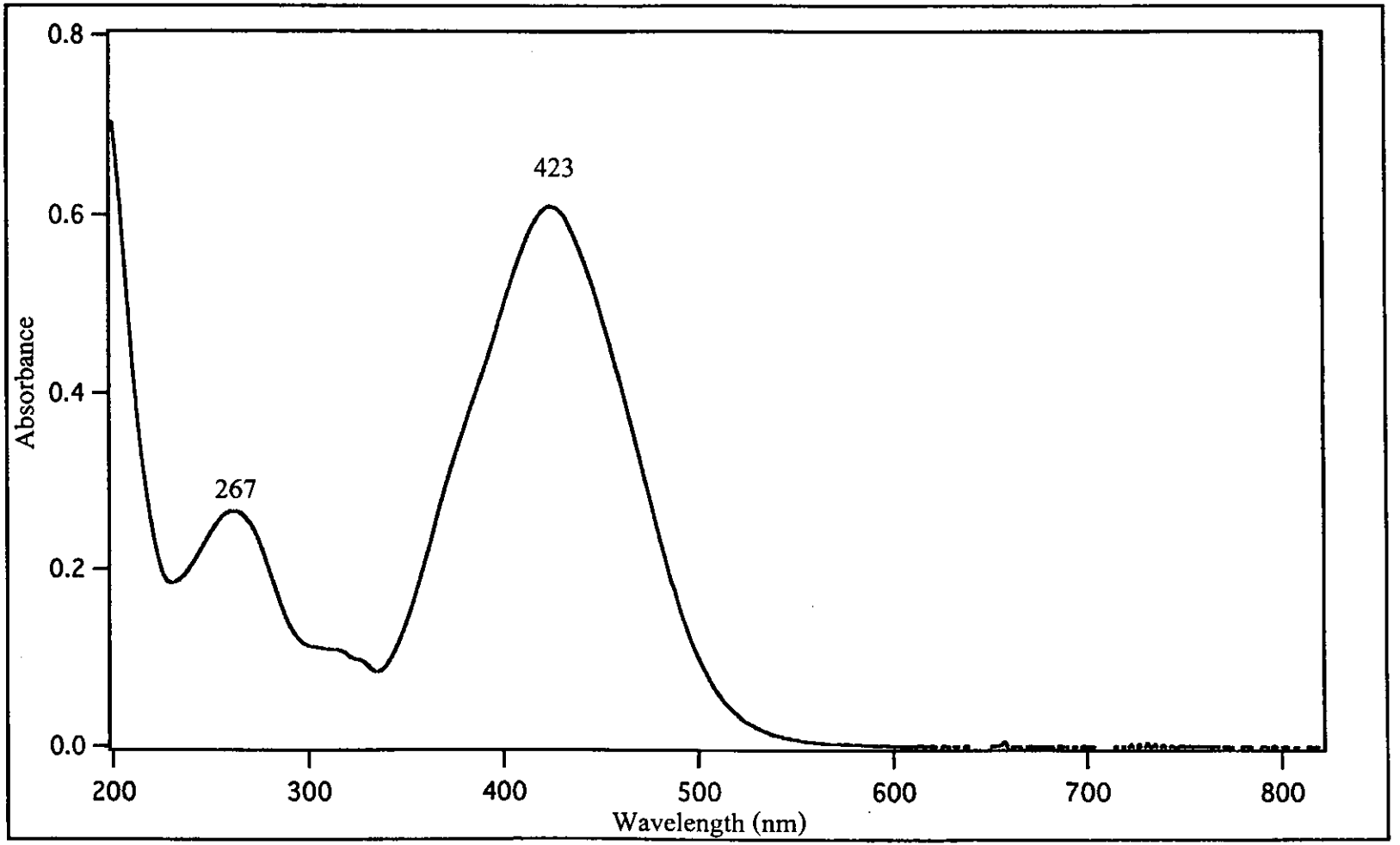

Figure 19 Absorption spectrum of dmazpy in CH_3CN solution

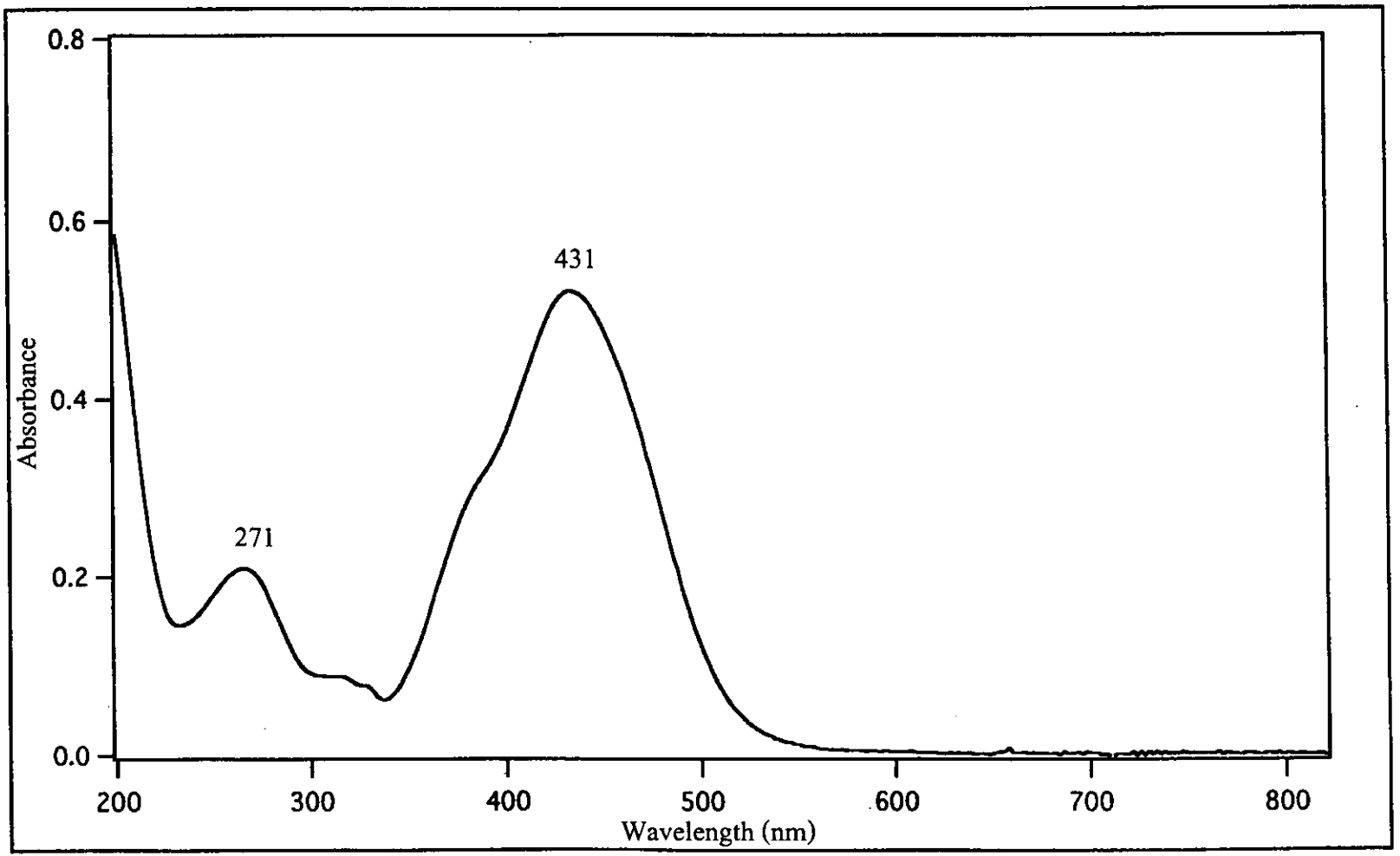

Figure 20 Absorption spectrum of deazpy in CH_3CN solution

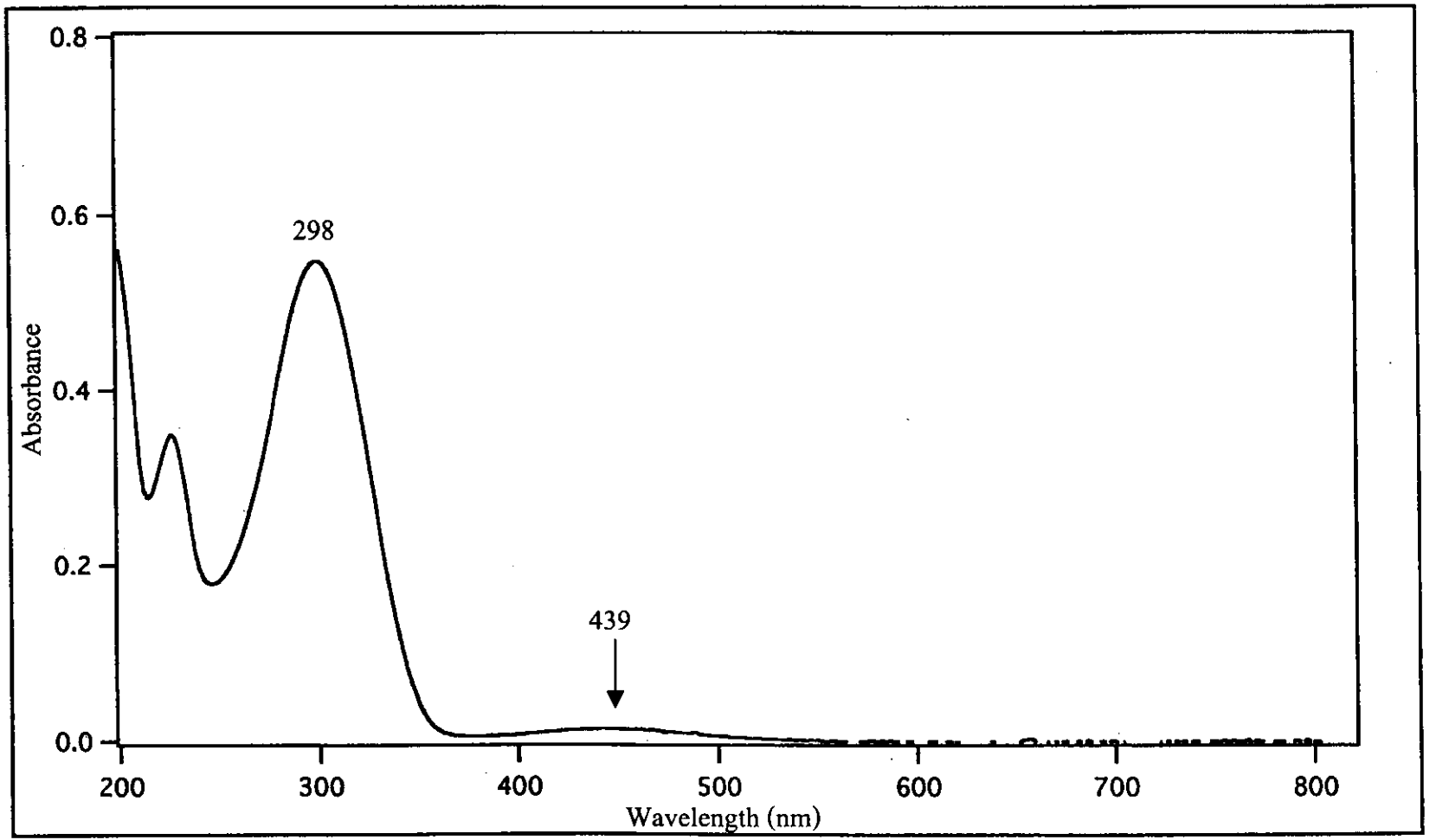

Figure 21 Absorption spectrum of azpym in CH_3CN solution

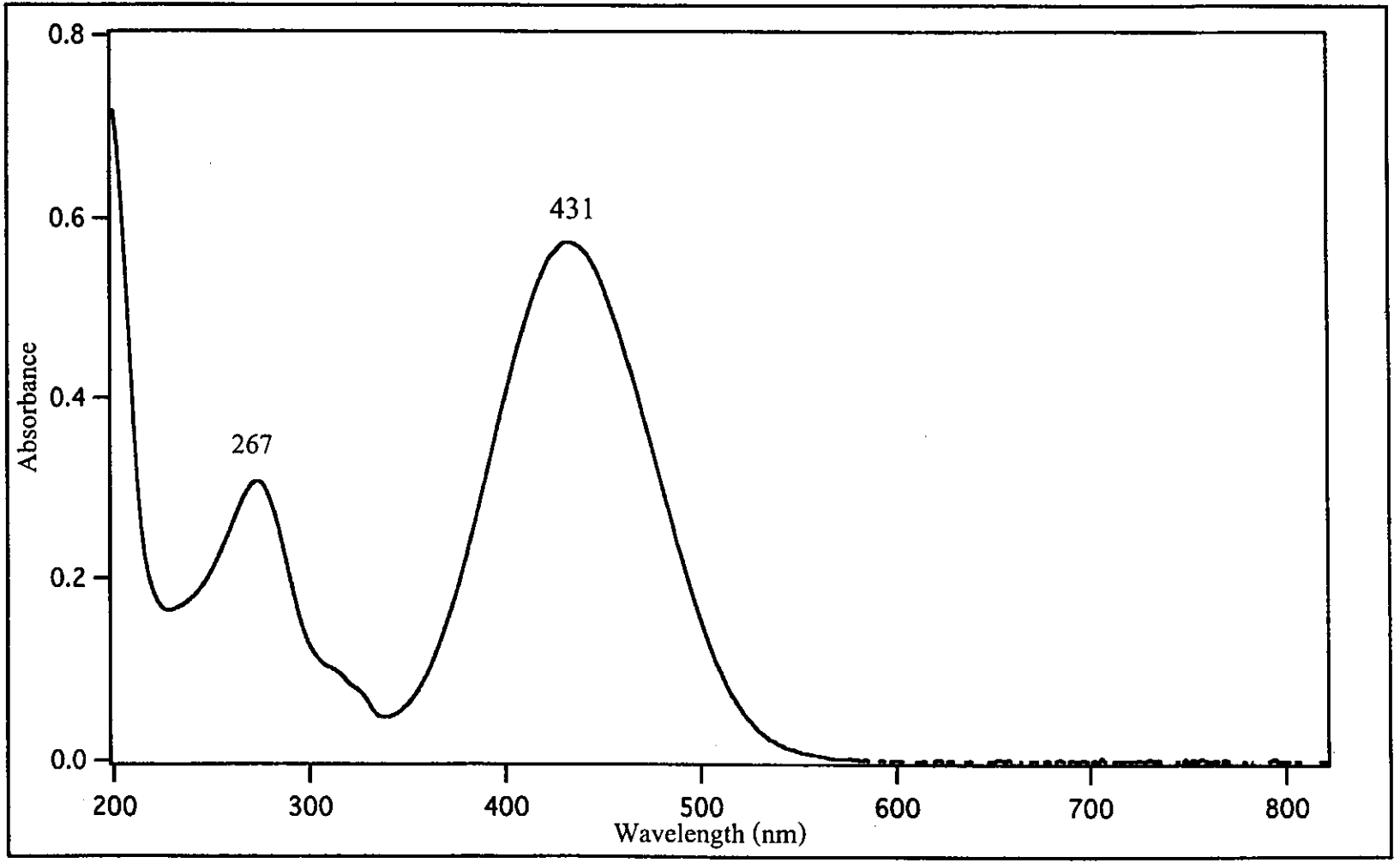

Figure 22 Absorption spectrum of deazpym in CH_3CN solution

3.2.5 Cyclic voltammetric results of ligands

The oxidation-reduction processes of those ligands were investigated by cyclic voltammetric technique. The cyclic voltammograms of azpy, dmazpy, deazpy, azpym and deazpym ligands solution in acetonitrile are shown in Figure 23-27, respectively. Ferrocene was used as an internal standard (ΔE_p = 70 mV). $E_{1/2}$ values are calculated from the average of anodic and cathodic peak potentials ($E_{1/2} = (E_{pa} + E_{pc})/2$) at scan rate of 100 mV/s and ΔE_p value was calculated from the difference of the both peaks ($\Delta E_p = E_{pa} - E_{pc}$). The cyclic voltammograms displayed ligand reduction at the negative potential. However, the positive potential may be the couple of ligands substituted. The cyclic voltammograms of dmazpy, deazpy and deazpym ligands exhibited positive and negative potential, whereas, azpy and azpym ligands displayed no peaks in positive potential. The cyclic voltammetric data of all ligands in acetonitrile solution are summarized in Table 7.

In this experiment, the different scan rates were used to check the couple or the redox reaction. The couple gave equal anodic and cathodic currents which refer to reversible couple. The unequal currents referred to the unequally transfer of the electron in the reduction and oxidation. This led to irreversible couple. When different scan rates were applied and these currents gave equal anodic and cathodic currents at higher scan rate, which led to quasi-reversible couple.

Table 7 Cyclic voltammetric data of free ligands in 0.1 M TBAH acetonitrile at scan rate 100 mV/s (ferrocene as an internal standard, $\Delta Ep = 70$ mV)

Ligand	$E_{1/2}$,V (ΔE_p, mV)			
	Oxidation Potential		Reduction Potential	
	E_{pa}	$E_{1/2}$	E_{pc}	E_{pa}
Azpy	-	-	-1.62	-1.34
Dmazpy	+0.60	+0.83 (94)	-1.79	-1.38
Deazpy	+0.59	+0.80 (96)	-1.82	-1.42
Azpym	-	-	-1.47	-1.14
Deazpym	+0.64	+0.89 (86)	-1.66	-1.28

E_{pc} = cathodic peak potential, E_{pa} = anodic peak potential

Reduction potential

Reduction potential of the ligands were studied in the range –2.0 to 0.0 V. The cyclic voltammogram of all ligands gave similar patterns but the peak potentials were shifted. The reduction potential of all ligands showed irreversible peaks (Figure 80 and 81, Appendix A). The cathodic peaks appeared at E_{pc} = -1.62, -1.79, -1.82, -1.47 and –1.66 V for azpy, dmazpy, deazpy, azpym and deazpym ligands, respectively.

Oxidation potential

The cyclic voltammogram of azpy and azpym ligands did not give any signals in the range 0.0 to 1.4 V. The dmazpy, deazpy and deazpym ligands showed one irreversible peak in the range 0.4-0.7 V and a quasi-reversible couple in the range 0.75-1.15 V. The cyclic voltammograms of substituted ligands showed the irreversible peaks at E_{pa} = +0.60 V (dmazpy), +0.59 V (deazpy) and +0.64 V (deazpym). These ligands displayed the irreversible peaks at low scan rate (50-100 mV/s) and higher scan rate (200-1000 mV/s) (Figure 82, Appendix A). For dmazpy ligand showed quasi-reversible couple at $E_{1/2}$ = +0.83 V (ΔE_p = 94 mV). The quasi-reversible couple of deazpy and dazpym ligands gave similar results to those in dmazpy at $E_{1/2}$ = +0.80 V (ΔE_p = 96 mV) for deazpy and $E_{1/2}$ = +0.89 V (ΔE_p = 86 mV) for deazpym ligand (Figure 83, Appendix A).

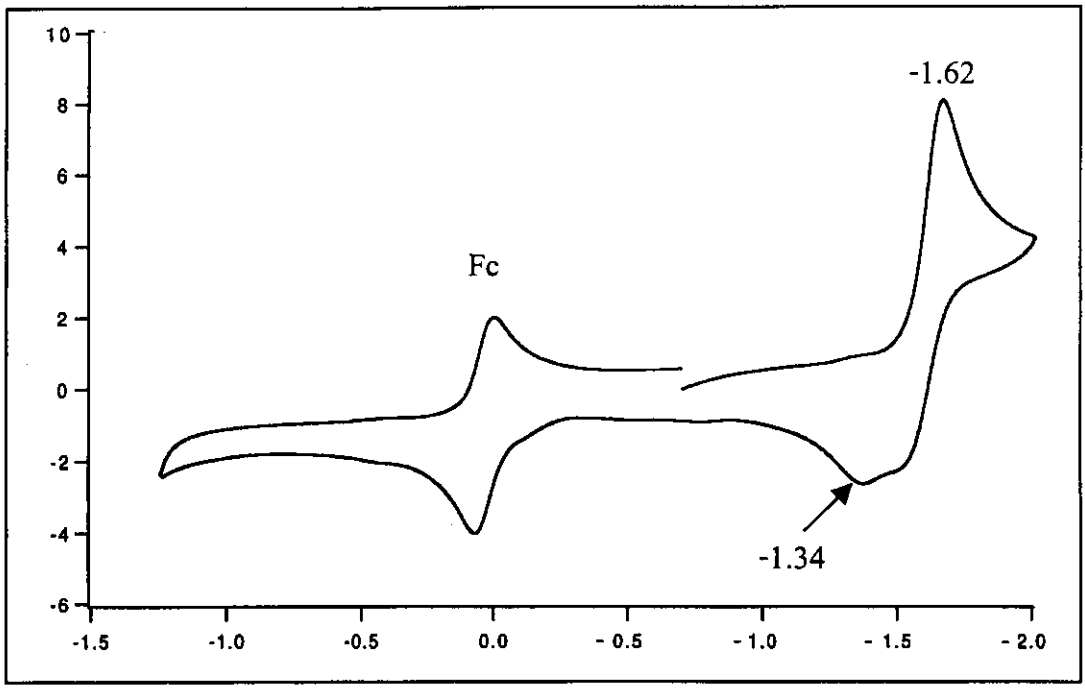

Figure 23 Cyclic voltammogram of azpy in CH_3CN at scan rate 100 mV/s

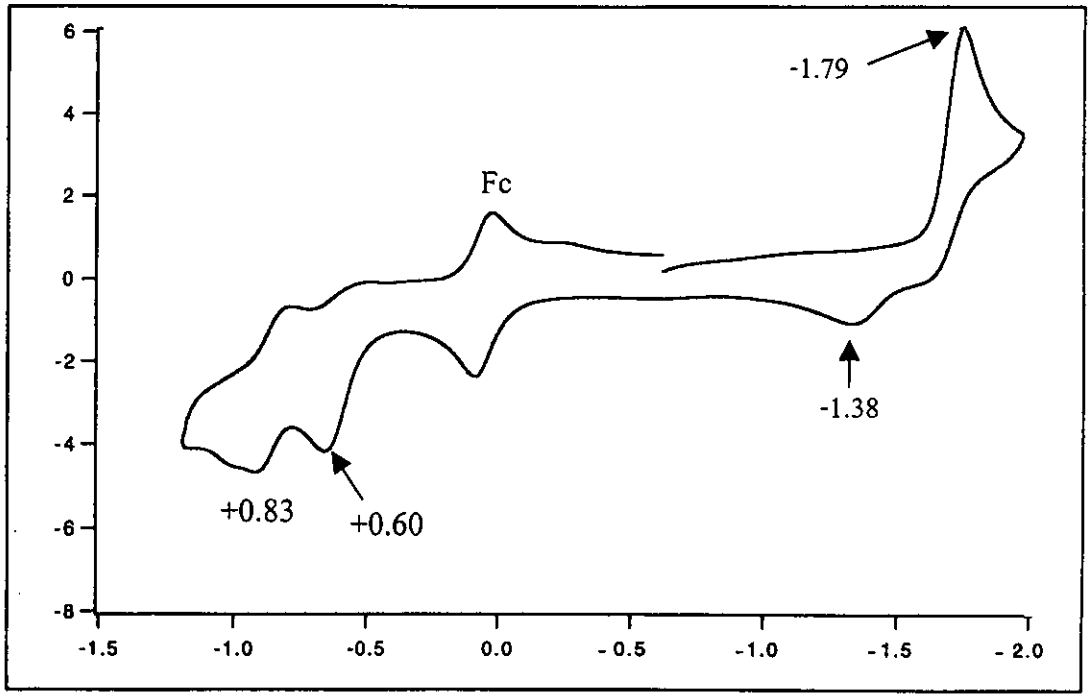

Figure 24 Cyclic voltammogram of dmazpy in CH_3CN at scan rate 100 mV/s

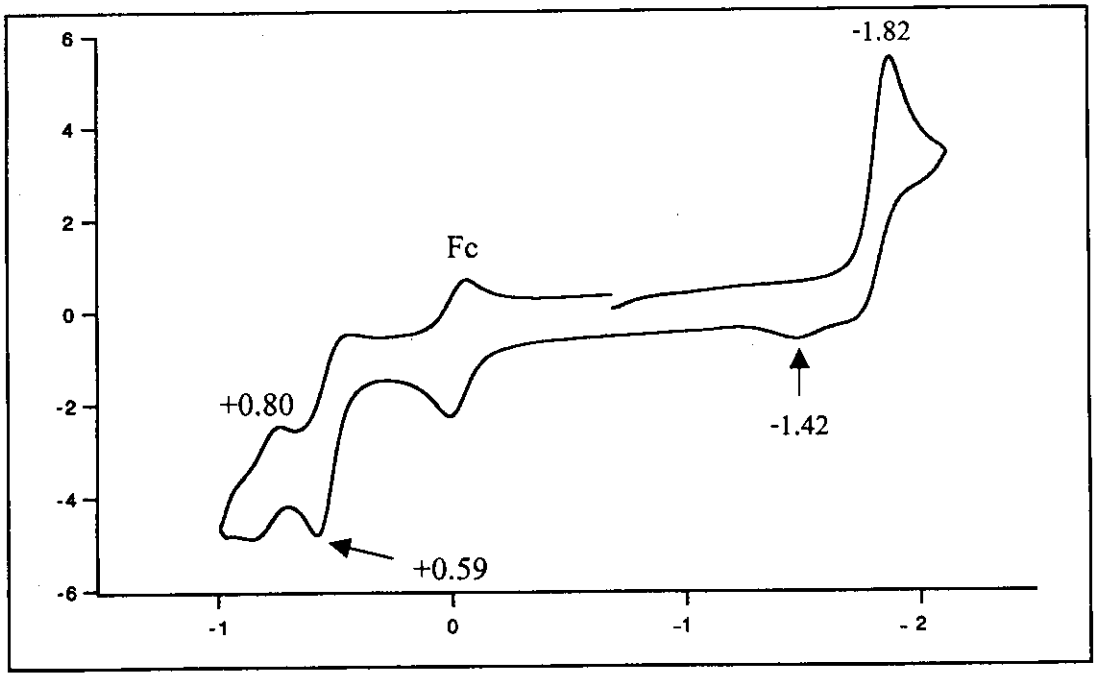

Figure 25 Cyclic voltammogram of deazpy in CH_3CN at scan rate 100 mV/s

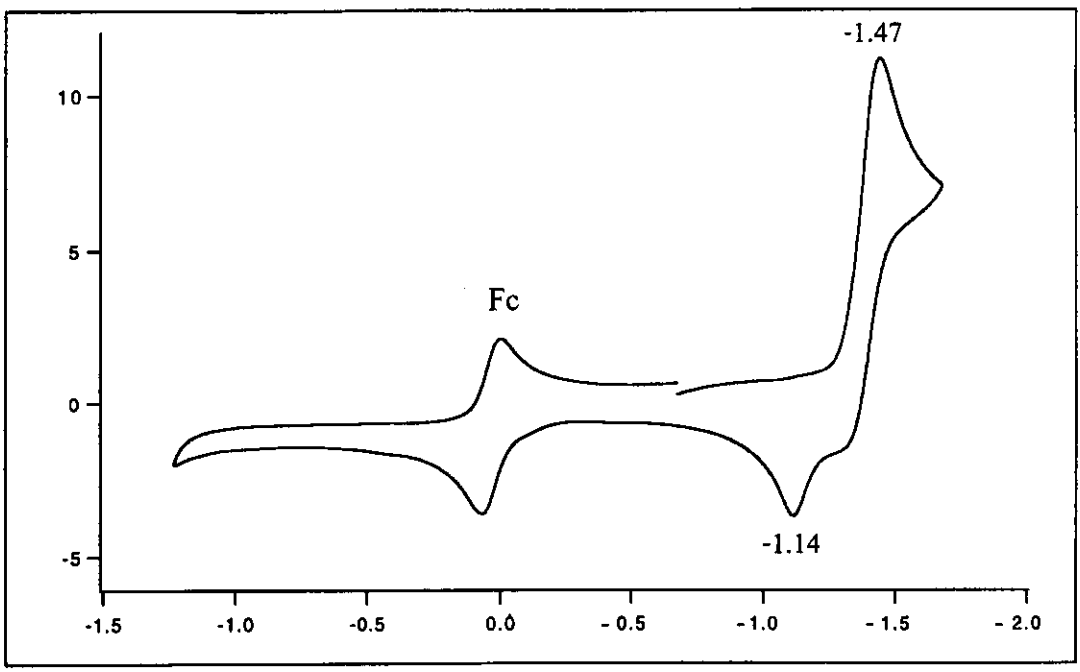

Figure 26 Cyclic voltammogram of azpym in CH_3CN at scan rate 100 mV/s

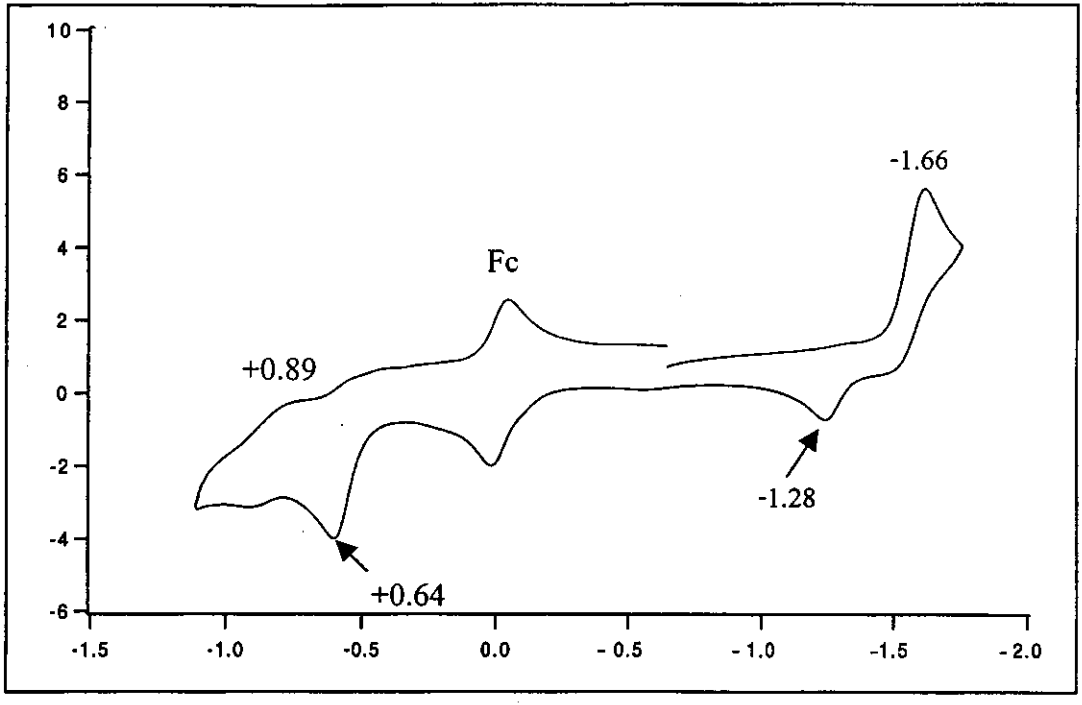

Figure 27 Cyclic voltammogram of deazpym in CH_3CN at scan rate 100 mV/s

3. 3 Synthesis and characterization of *cis*-$Ru(bpy)_2Cl_2$

The *cis*-$Ru(bpy)_2Cl_2$ complex was used as starting material for syntheses $[Ru(bpy)_2L](BF_4)_2$ (L = azpy, dmazpy, deazpy, azpym and deazpym) complexes and according to the literature procedure (Sullivan, *et al.*, 1978). The structure of *cis*-$Ru(bpy)_2Cl_2$ complex was studied by IR and ^1H NMR spectroscopic techniques. The infrared spectrum in the range 1800-370 cm^{-1} of this complex is shown in Figure 28. The results obtained on examining the infrared spectra are listed in Table 8.

Table 8 Infrared data of *cis*-$Ru(bpy)_2Cl_2$ in the KBr pellet

Vibrational modes	Frequencies (cm^{-1})
sp^2 C-H stretching	3066(w)
C=N and C=C stretching in aromatic compounds	1601(m), 1561(m) 1478(m), 1460(s) 1442(m), 1418(s)
C-H out of plane	800(w), 763(vs), 728(s)
Ru-Cl	325(m)
Ru-N	265(m), 245(m)

s = strong, m = medium, w = weak, vs = very strong

A complete assignment of all bands were in the range 4000-200 cm^{-1}. The infrared spectrum of this complex in the regions of 1600-1400 and 900-700 cm^{-1} showed bands typical for coordinated bipyridine (Lewis, *et al.*, 1967). There were some important bands to specify the isomer of this complex. Krause showed that the characteristic difference in the infrared spectra of *cis*-$Ru(bpy)_2Cl_2$ and *cis-trans* mixture exhibited at two regions, ~700-800 cm^{-1} and ~300-350 cm^{-1}. A few additional bands in the mixture attributed to the *trans*-isomer. Perhaps the most important differences were: a) splitting of the 760 cm^{-1} band, *trans* at 767 cm^{-1}, *cis* at 759 cm^{-1} with higher energy shoulders; b) splitting of the 800 cm^{-1} band, *trans* at 807 cm^{-1}, *cis* at 800 cm^{-1}; c) the *trans* appeared to have a peak at 342 cm^{-1}, while the *cis* had one at 322 cm^{-1} (Krause, 1978). In this work, the band at 325 cm^{-1} was assigned to Ru^{II}-Cl, corresponded to the value reported by Krause. The two bands near 265 and 245 cm^{-1} were assigned to Ru-N stretching modes. Thus, in this work was assumed that the synthesized $Ru(bpy)_2Cl_2$ complex produced mostly the *cis*-isomer.

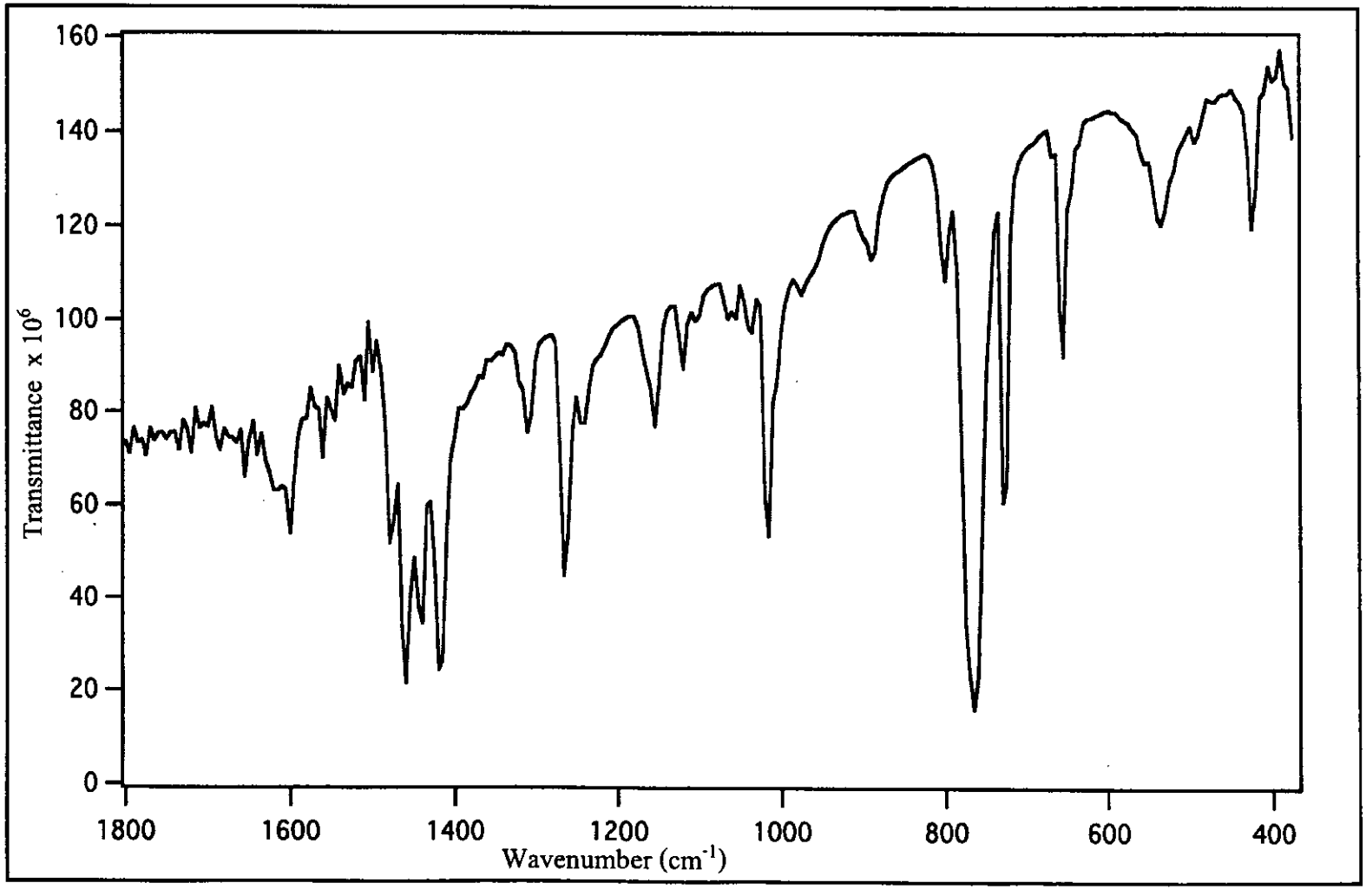

Figure 28 Infrared spectrum of *cis*-$Ru(bpy)_2Cl_2$ in the KBr pellet

The ^{1}H NMR spectrum of *cis*-$Ru(bpy)_2Cl_2$ complex indicated the binding mode and stereochemistry compared to the $[Ru(bpy)_2L](BF_4)_2$ complexes (L = azpy, dmazpy, deazpy, azpym and deazpym). The ^{1}H NMR spectrum and proton-numbering pattern of this complex in DMSO-d_6 was illustrated in Figure 29 and is clearly assigned in Table 9.

The eight signals identifiable with the bipyridine protons, one set of four (defined as H3′, H4′, H5′ and H6′) associated with the rings *trans* to another bipyridine ring, the other set of four (defined as H3, H4, H5 and H6) associated with the ring *trans* to chloride atom (see Figure 29, inset), by comparison with assignments previously reported for $[Ru(bpy)_2py_2]^{2+}$ (Hitchcock, *et al.*, 1988), The doublet peak of H6′ protons were expected to appear at lowest field.

Table 9 ^{1}H NMR data of *cis*-$Ru(bpy)_2Cl_2$ in DMSO-d_6 solution

Position	δ (ppm)	J (Hz)	Amounts of H
H6′	9.92 (d)	5.5	2
H3′	8.57 (d)	7.5	2
H3	8.42 (d)	7.5	2
H4′	8.09 (dd)	7.5, 7.5	2
H5′	7.76 (dd)	6.0, 6.0	2
H4	7.68 (dd)	7.5, 7.5	2
H6	7.51 (d)	4.5	2
H5	7.12 (dd)	6.0, 6.0	2

d = doublet dd = doublet of doublet

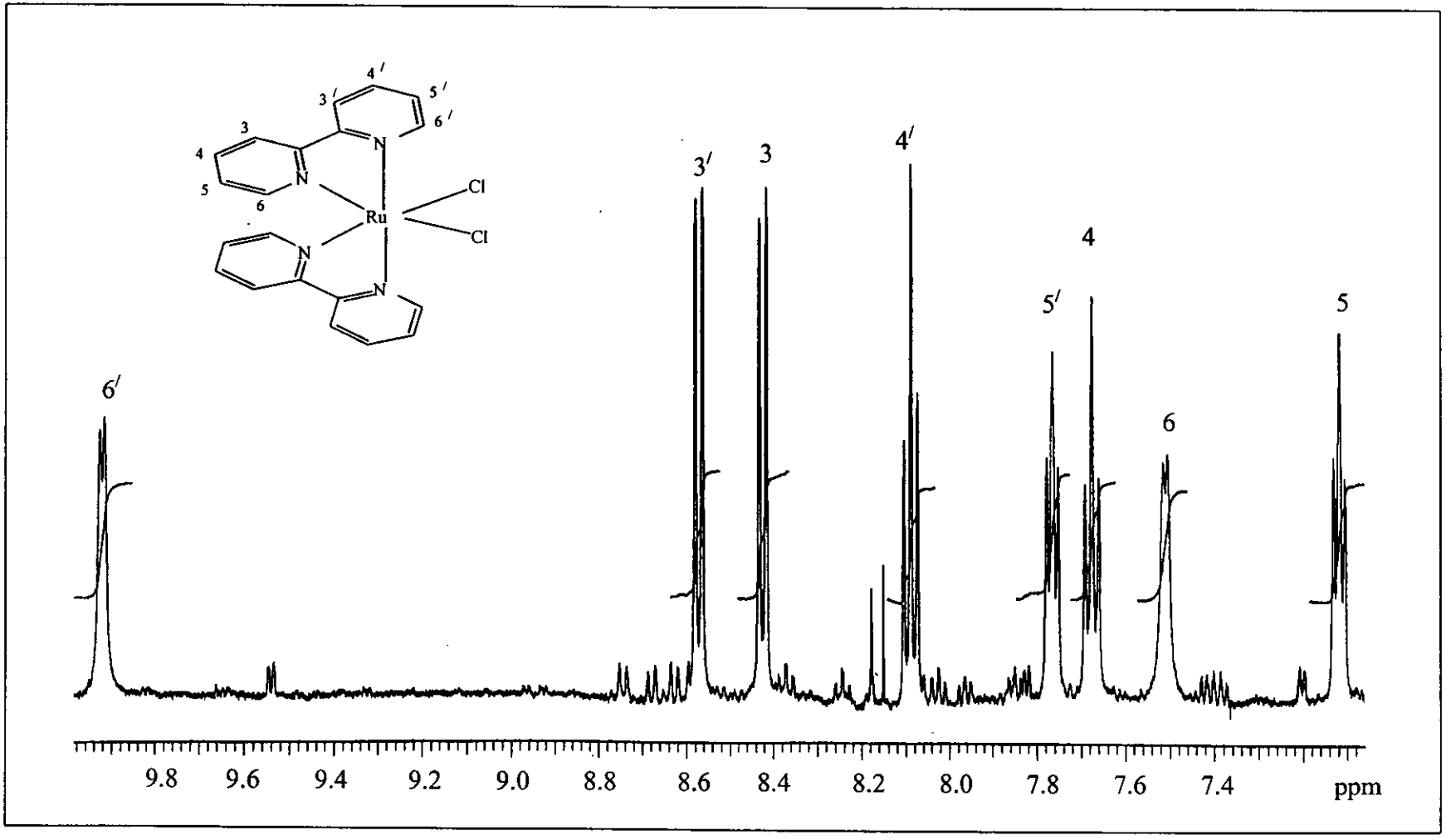

Figure 29 ^{1}H NMR spectrum of *cis*-Ru(bpy)$_2$Cl$_2$ in DMSO-d_6 solution

3.4 Synthesis and characterization of $[Ru(bpy)_3](BF_4)_2$

$[Ru(bpy)_3](BF_4)_2$ was prepared from $RuCl_3.xH_2O$ and 2,2′-bipyridine according to the literature procedure (Palmer and Piper, 1966). This complex was used for comparing the chemical properties with those $[Ru(bpy)_2L](BF_4)_2$ (L = azpy, dmazpy, deazpy, azpym and deazpym) complexes. The structure of this complex was characterized by IR, UV-Visible and Nuclear Magnetic Resonance spectroscopic techniques.

Infrared spectra were helpful in the characterization of the bipyridine complexes. The infrared spectrum of the complex $[Ru(bpy)_3](BF_4)_2$ in the region 2000-400 cm^{-1} is presented in Figure 30. The strong bands at 1600, 1460, 1420, 780 and 730 cm^{-1} were due to the C=C and C=N stretchings of the coordinated bpy molecules for $[Ru(bpy)_3]N_3Cl{\cdot}2H_2O$ (Wang, *et al.*, 2001) and $[Ru(bpy)_3]^{2+}[W_{10}O_{32}]^{4-}{\cdot}3DMSO$ (Han, *et al.*, 2001). For the infrared spectrum of $[Ru(bpy)_3](BF_4)_2$ in this work exhibited several characters strong bands at 1602, 1559, 1439, 1421, 777 and 732 (Table 10), corresponded to characteristic of bpy molecules

Table 10 Infrared data of $[Ru(bpy)_3](BF_4)_2$ in the KBr pellet

Vibrational modes	Frequencies (cm^{-1})
C=N and C=C stretching in aromatic compounds	1602(s), 1459(s) 1439(s), 1421(s)
C-H out of plane bending	777(vs) 732(s)

s = strong, vs = very strong

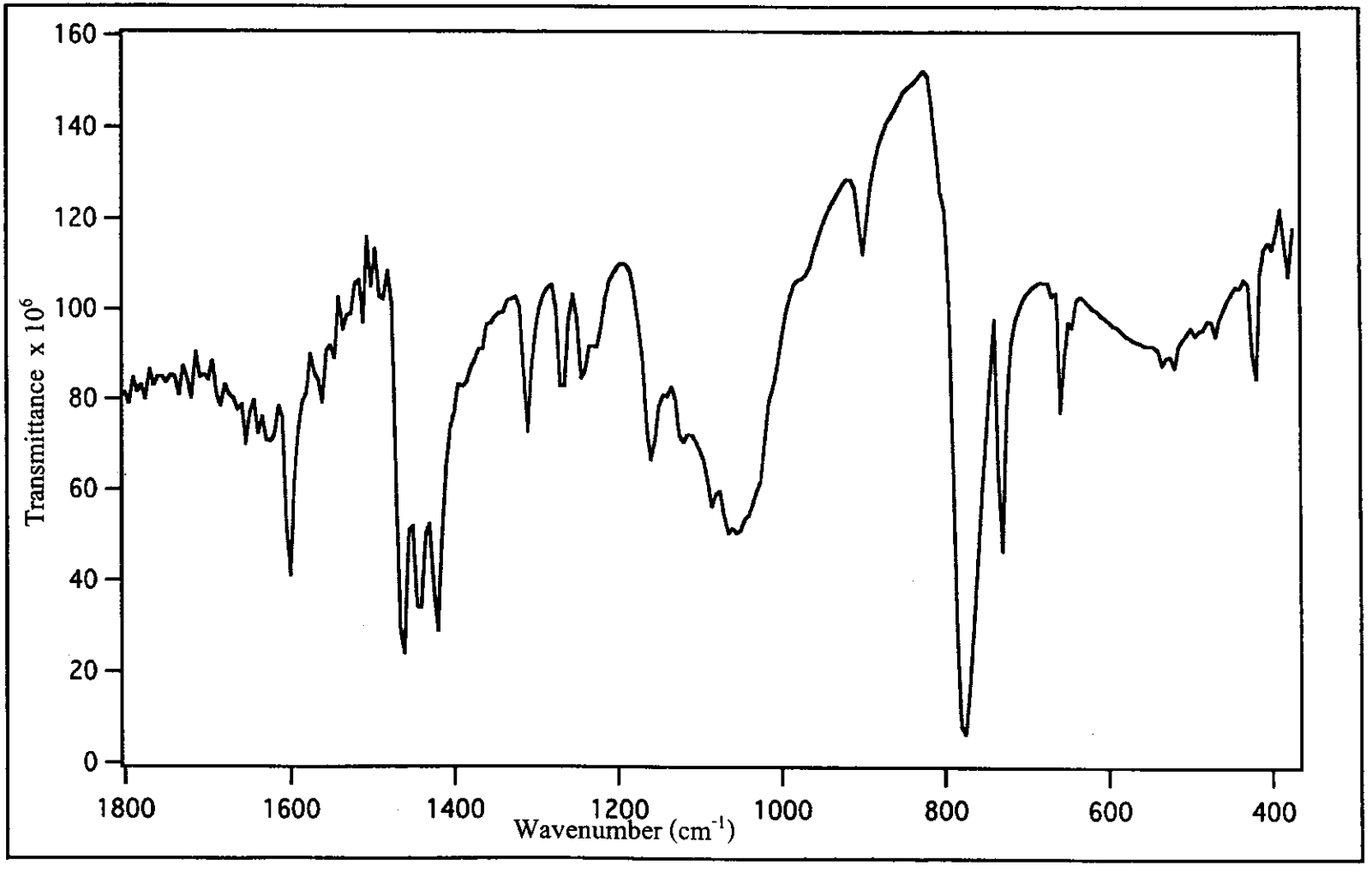

Figure 30 Infrared spectrum of $[Ru(bpy)_3](BF_4)_2$ in the KBr pellet

Fast atomic bombardment mass spectrometry (FAB-MS) is one important techniques to study molecular weight of $[Ru(bpy)_3](BF_4)_2$ complex. FAB-MS of the positive ion of this complex gave the abundant peaks which were listed in Table 11.

Table 11 FAB-mass spectrometric data of $[Ru(bpy)_3](BF_4)_2$

Compound	Expected molecular weight	m/z	Assignment	Rel. Abund. (%)
$[Ru(bpy)_3](BF_4)_2$	743.2	657 605	$[M-BF_4]^+$ $[M-BF_4$, − cyclobutadiene $]^+$	82 100

M = formula of a complex

The parent peak, which gave 100% relative abundance, was molecular weight of complex. This method could be used to confirm the molecular structure and molecular mass of these complexes as expected. The FAB mass spectra of $[Ru(bpy)_3](BF_4)_2$ complex is displayed in Figure 31.

The FAB mass spectrum of the $[Ru(bpy)_3](BF_4)_2$ complex showed only two peak at m/z = 657 and 605. The intense peak at m/z = 657 was assigned to $[Ru(bpy)_3](BF_4)^+$ ion. The parent peak at m/z = 605 was probably from the dissociation of $[Ru(bpy)_3](BF_4)^+$ to loss the cyclobutadiene molecule.

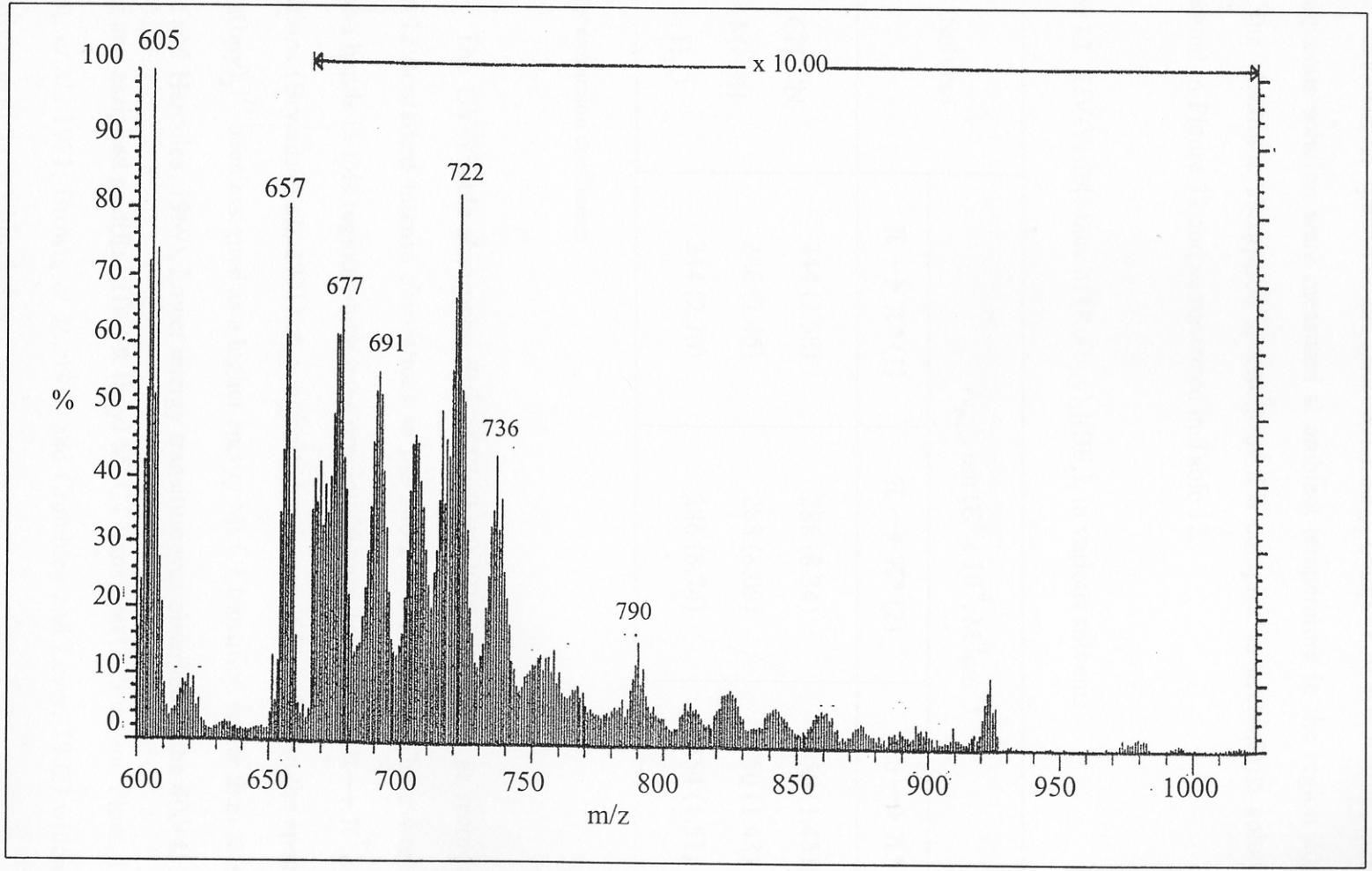

Figure 31 FAB mass spectrum of $[Ru(bpy)_3](BF_4)_2$

UV-Visible spectra of the $[Ru(bpy)_3](BF_4)_2$ complex in acetonitrile, methanol and aqueous solution were measured at ambient temperature in the region 200-800 nm. The electronic absorption spectrum of this complex in acetonitrile solution is illustrated in Figure 32 and summarized in Table 12.

Table 12 UV-Visible data of $[Ru(bpy)_3](BF_4)_2$ in various solvents

Solvent	λ_{max}, nm (ε^a x 10^{-4}, $M^{-1}cm^{-1}$)		
	$\pi \rightarrow \pi^*$ (1)	$\pi \rightarrow \pi^*$ (2)	Ru $\rightarrow \pi^*$
CH_3CN	244 (2.58)	288 (8.34)	450 (1.45)
MeOH	246 (2.45)	288 (8.09)	450 (1.43)
H_2O	244 (2.76)	286 (8.74)	454 (1.51)

[a] Molar extinction coefficient

The UV-Visible absorption data of $[Ru(bpy)_3](BF_4)_2$ complex as recorded in Table 12 contained intense absorptions in the 240-290 nm region. There were two maxima bands in this region which have previously been assigned to $\pi \rightarrow \pi^*$ ligand transitions (Bryant, *et al.*, 1971). A composite band near 250 nm had in the spectrum of $[Ru(bpy)_3]^{2+}$ been assigned as a higher energy MLCT transition rather than $\pi \rightarrow \pi^*$ (Lytle and Hercules, 1969). Lower energy transition was observed in the 400-450 nm region and assigned as d(Ru(II))$\rightarrow\pi^*$(bpy) MLCT transition (Palmer and Piper, 1966; Bryant, *et al.*, 1971; Brown, *et al.*, 1976 and Crutchley and Lever, 1982) which had typically one in the visible region.

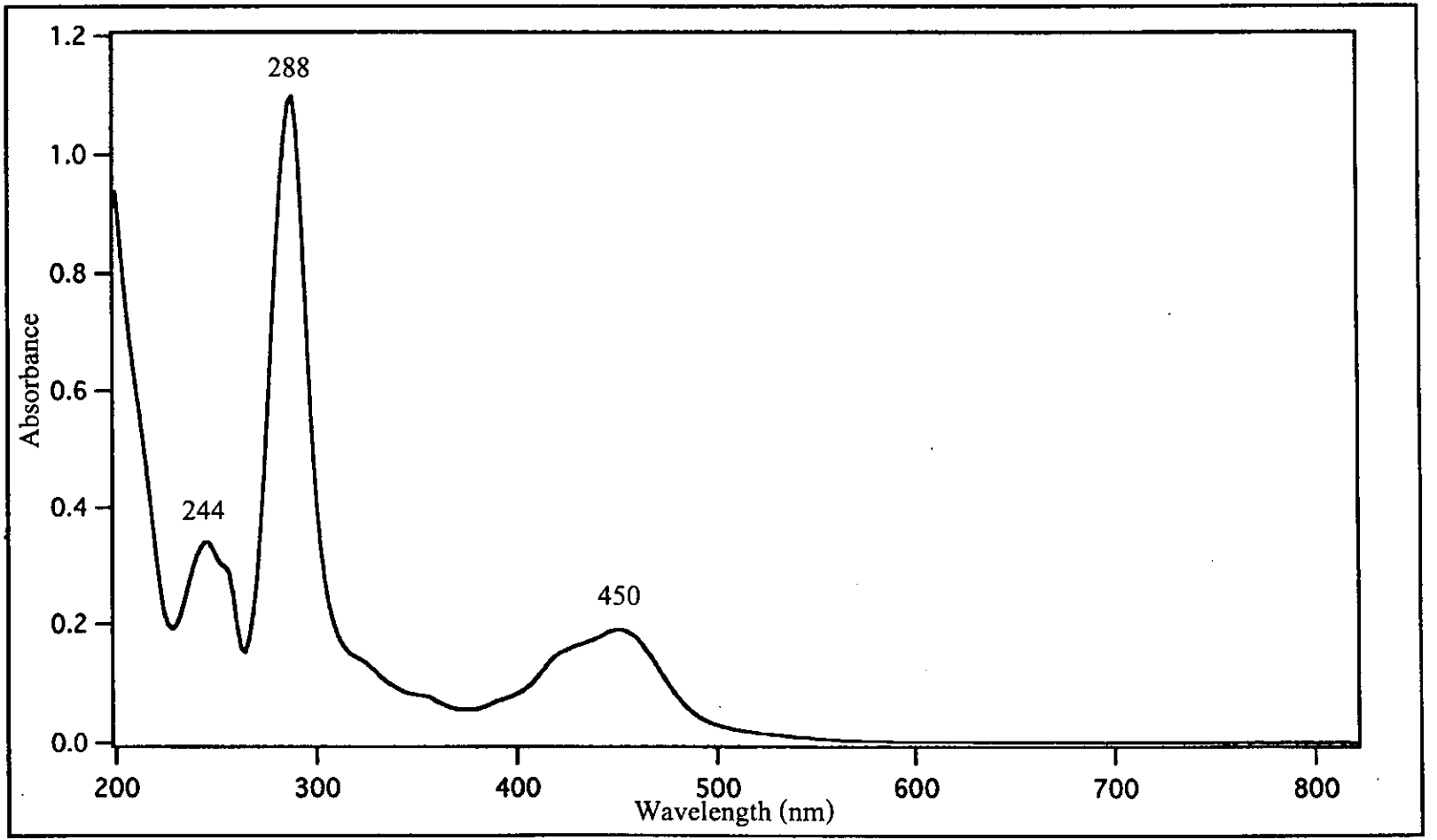

Figure 32 Aabsorption spectrum of $[Ru(bpy)_3](BF_4)_2$ in CH_3CN solution

The ^{1}H NMR spectrum (Figure 33) of $[Ru(bpy)_3](BF_4)_2$ in acetone-d_6 showed 4 signals for 24 protons. There were four signals due to the structure of this complex which was D_3 symmetry. This means the two pyridine rings in the bpy ligands were chemical and magnetically equivalent. The ^{1}H-^{1}H COSY spectra (Figure 34) of this complex revealed that the four signals 8.86 (ddd), 8.23 (ddd), 8.06 (ddd) and 7.60 (ddd) ppm could be assigned to H3, H4, H6 and H5, respectively, by comparison with those already reported (Constable and Seddon, 1982). The ^{1}H NMR data of this complex is detailed in Table 13.

Table 13 ^{1}H NMR data of $[Ru(bpy)_3](BF_4)_2$ in acetone-d_6 solution

Position	δ (ppm)	J (Hz)	Amount of H
H3	8.86 (ddd)	8.5, 1.0, 1.5	6
H4	8.23 (ddd)	8.5, 8.0,1.5	6
H6	8.06 (ddd)	5.5, 1.5, 1.0	6
H5	7.60 (ddd)	8.0, 1.5, 5.5	6

ddd = doublet of doublet of doublet

The ^{13}C NMR spectrum (Figure 35) and HMQC spectra (Figure 36) showed 5 signals for 30 carbon atoms : four methine carbons (δ 125.80, 139.47, 129.20 and 153.24 ppm) and a quaternary carbon (δ 158.74 ppm). The HMQC correlation data of $[Ru(bpy)_3](BF_4)_2$ in acetone-d_6 solution is shown in Table 14.

Table 14 HMQC correlation data for $[Ru(bpy)_3](BF_4)_2$ in acetone-d_6 solution

Position	δ (ppm)	
	^{1}H	^{13}C (C-Type)
H2	-	159.09 (C)
H3	8.86 ddd	126.16 (CH)
H4	8.23 ddd	139.83 (CH)
H5	7.60 ddd	129.56 (CH)
H6	8.06 ddd	153.60 (CH)

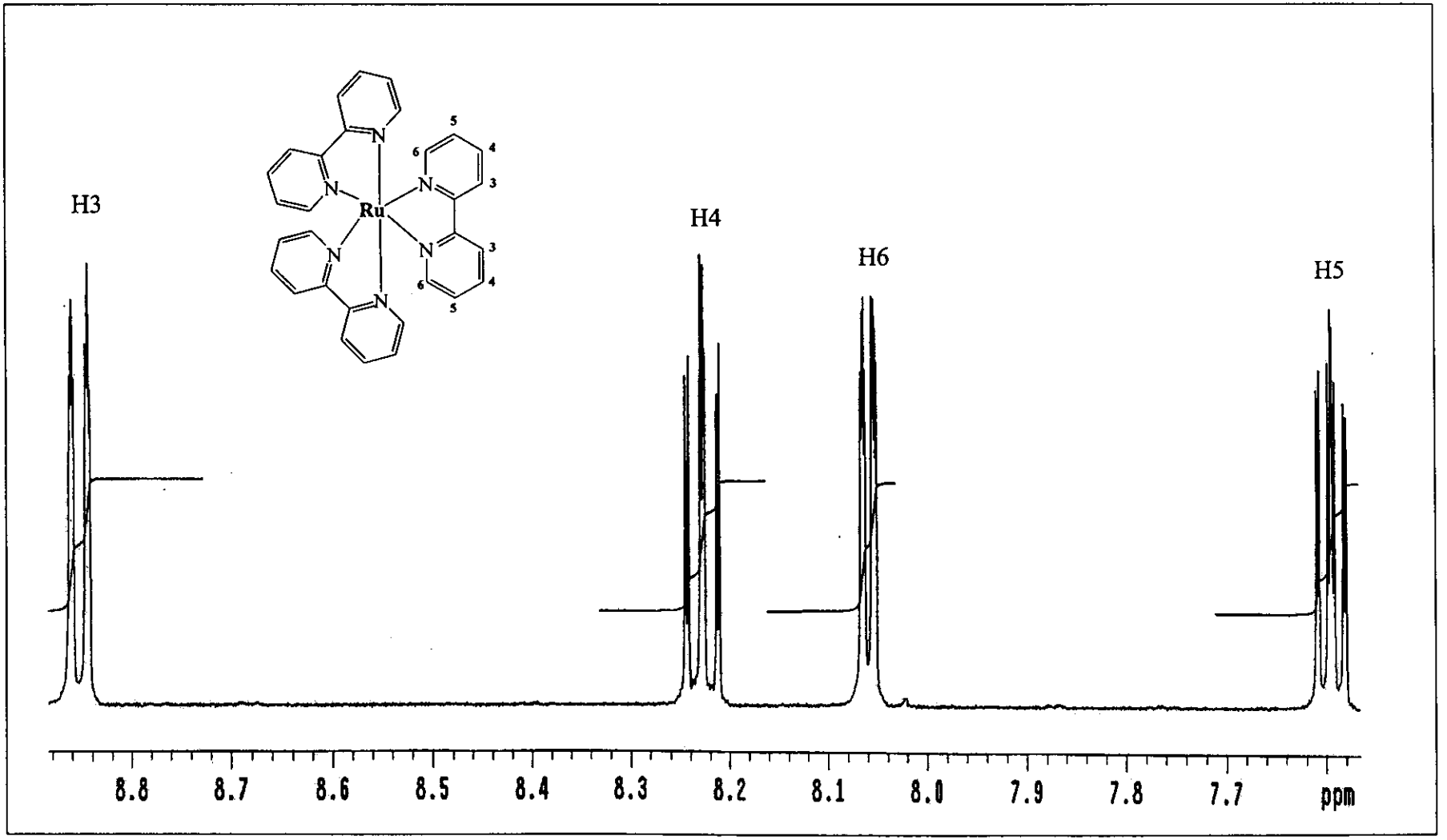

Figure 33 ^{1}H NMR spectrum of $[Ru(bpy)_3](BF_4)_2$ in acetone-d_6 solution

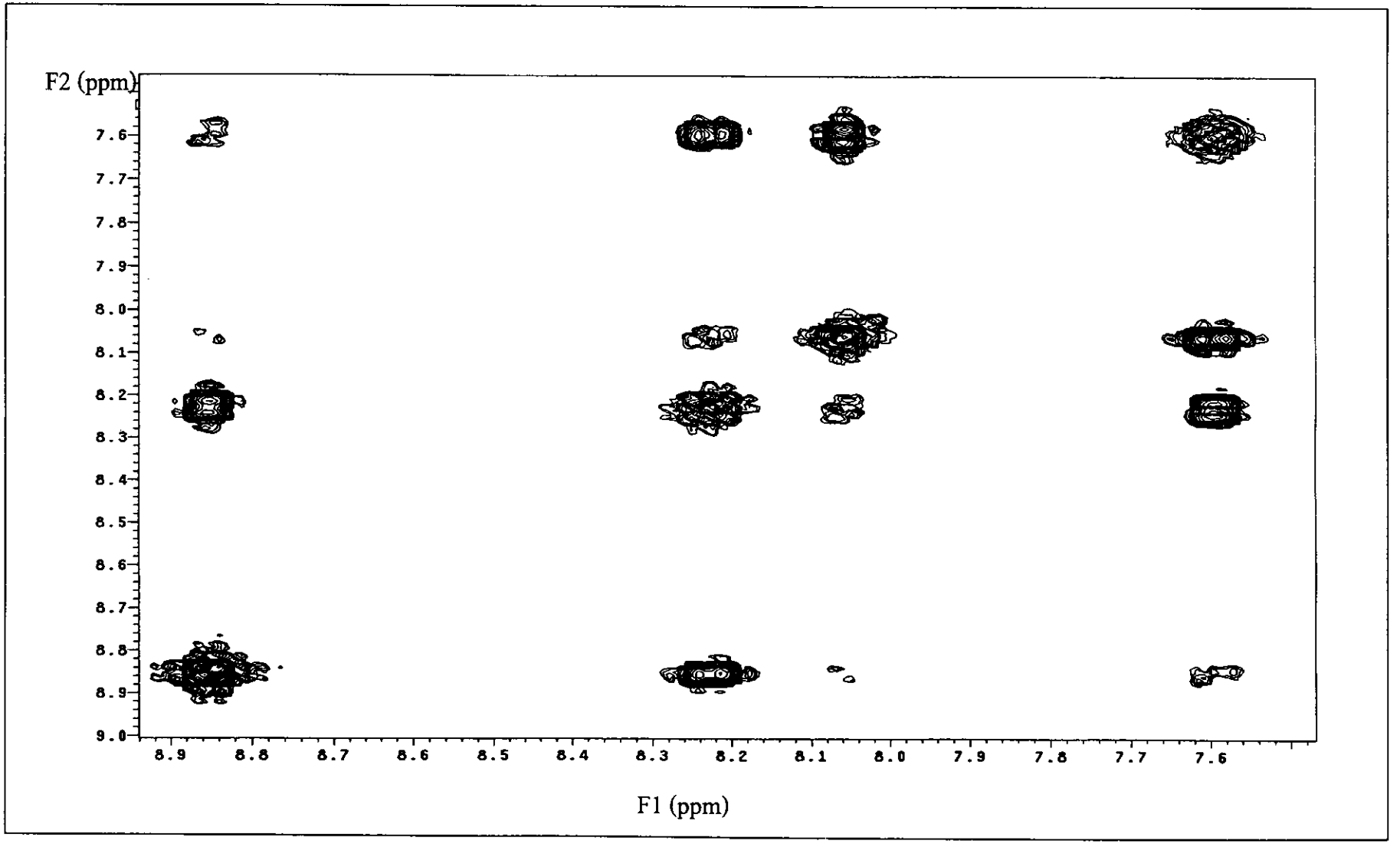

Figure 34 ^{1}H-^{1}H COSY spectrum of $[Ru(bpy)_3](BF_4)_2$ in acetone-d_6 solution

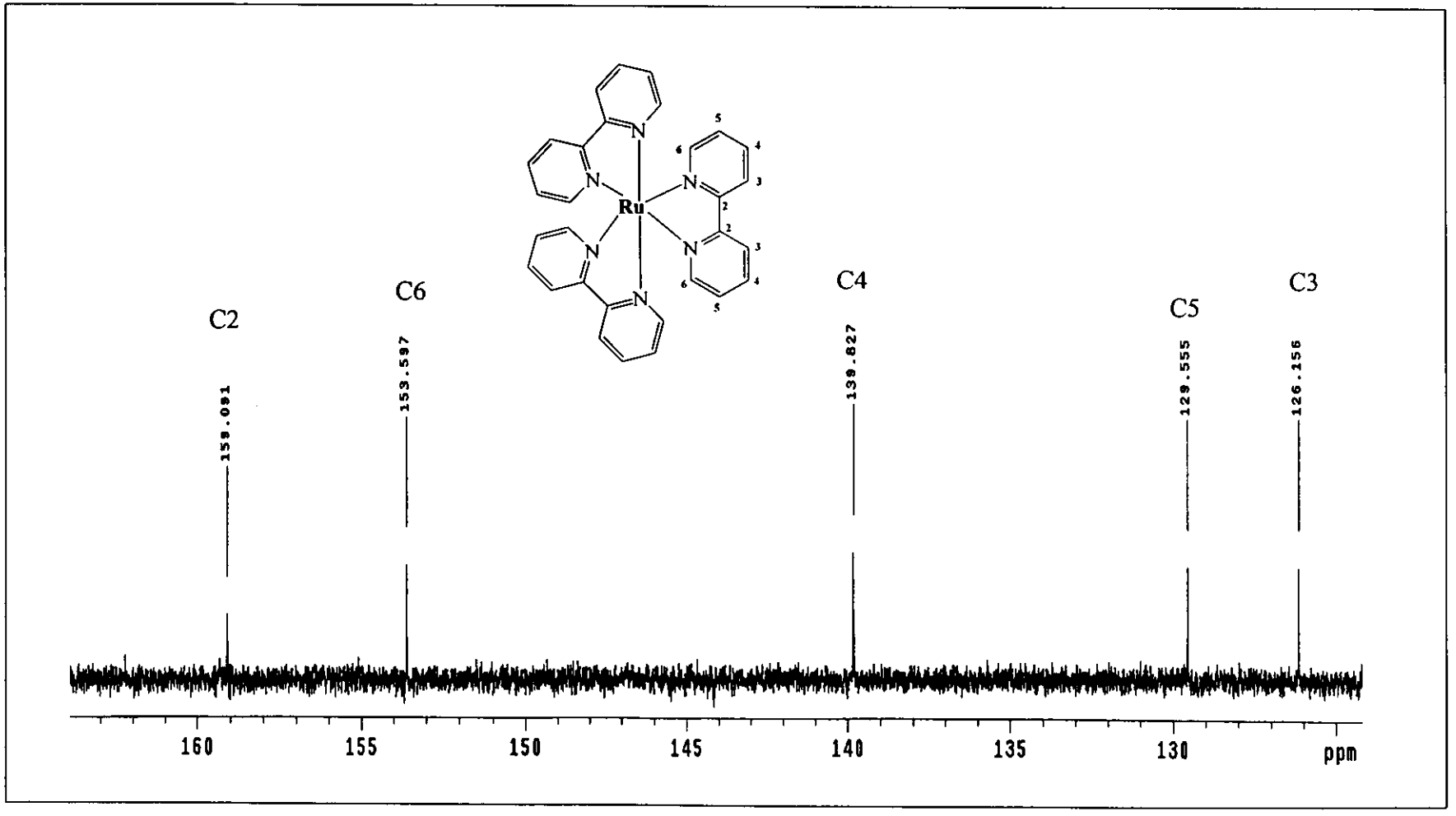

Figure 35 ^{13}C NMR spectrum of $[Ru(bpy)_3](BF_4)_2$ in acetone-d_6 solution

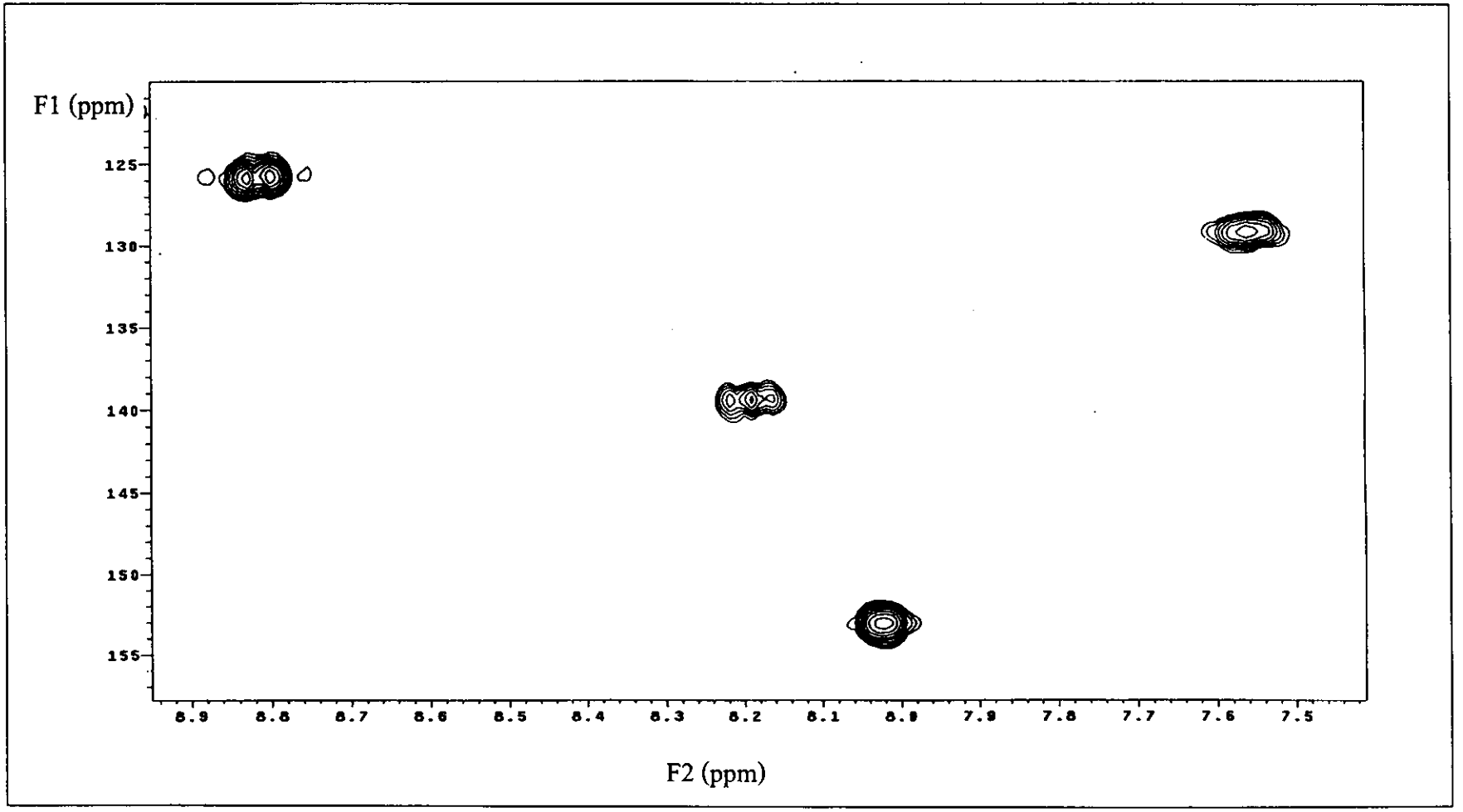

Figure 36 HMQC spectrum of $[Ru(bpy)_3](BF_4)_2$ in acetone-d_6 solution

3.5 Syntheses of $[Ru(bpy)_2L](BF_4)_2$

The $[Ru(bpy)_2L](BF_4)_2$ complexes (L = azpy, dmazpy, deazpy, azpym and deazpym) were synthesized from the reaction between *cis*-$Ru(bpy)_2Cl_2$ with L ligands in 1:1 (v/v) methanol/water, respectively. The red reaction mixture of $[Ru(bpy)_2azpy]^{2+}$ and $[Ru(bpy)_2azpym]^{2+}$ complexes were refluxed for 3 h. For the reaction mixture of $[Ru(bpy)_2L](BF_4)_2$ complexes where L were dmazpy (violet-blue solution), deazpy (blue solution) and deazpym (green-blue solution) ligands were refluxed for 6 h. All complexes were obtained in high yield (> 75%) and stable in air. Some of the physical properties of complexes are summarized in Table 15.

Table 15 The physical properties of $[Ru(bpy)_2L](BF_4)_2$ (L = azpy, dmazpy, deazpy, azpym and deazpym)

Complex	Physical properties			
	Appearance	Color		Melting point
		solid	solution	(°C)
$[Ru(bpy)_2azpy](BF_4)_2$	Needle like	red	red	> 300
$[Ru(bpy)_2dmazpy](BF_4)_2$	Needle like	black	violet-blue	> 300
$[Ru(bpy)_2deazpy](BF_4)_2$	Powder like	black	blue	> 300
$[Ru(bpy)_2azpym](BF_4)_2$	Needle like	red	red	> 300
$[Ru(bpy)_2deazpym](BF_4)_2$	Powder like	black	green- blue	> 300

The solubilities of all complexes are similar as summarized in Table 16.

Table 16 The solubility of $[Ru(bpy)_2L](BF_4)_2$ (L = azpy, dmazpy, deazpy, azpym and deazpym)

Solvent	Solubility of complexes
Hexane	-
Toluene	-
Dichloromethane (CH_2Cl_2)	++
Chloroform ($CHCl_3$)	+
Ethyl acetate	-
Acetone	+++
Acetonitrile (CH_3CN)	+++
Dimethylformamide (DMF)	+++
Dimethylsulfoxide (DMSO)	+++
Ethanol (EtOH)	++
Methanol (MeOH)	+++
Water (H_2O)	+++

– nonsoluble + partially soluble ++ more soluble +++ well soluble

0.0012 g of all complexes were tested their solubilities in 10 mL of various solvents. The symbol of solubility, + represents the partially solubility of those complexes less than 0.0005 g, ++ represents the increase of solubility of complexes in the range 0.006-0.0010 g, +++ represents 0.0012 g of complexes completely soluble and – represents the non soluble 0.0012 g of complexes in 10 mL of solvents.

The solubility of complexes was used for recrystallization. The suitable solvents may be selected from solvent in which compounds have different solubilities.

3.6 Characterization of $[Ru(bpy)_2L](BF_4)_2$

The structures of $[Ru(bpy)_2L](BF_4)_2$ complexes (L = azpy, dmazpy, deazpy, azpym and deazpym) were characterized by using these following techniques.

3.6.1 Elemental analysis

3.6.2 Mass spectrometry

- Electrospray mass spectrometry (ES-MS)
- Fast atomic bombardment mass spectrometry (FAB-MS)

3.6.3 UV-Visible absorption spectroscopy (UV-Visible)

3.6.4 Infrared spectroscopy (IR)

3.6.5 Protons Nuclear Magnetic resonance spectroscopy

- ^1H NMR
- ^{13}C NMR
- ^1H-^1H Correlation spectroscopy (^1H-^1H COSY)
- Heteronuclear multiple quantum coherence correlation spectroscopy (HMQC)

3.6.6 Cyclic Voltammetry (CV)

3.6.1 Elemental analyses results of complexes

Elemental analysis is an useful technique to confirm the percent of C, H and N elements in complexes. The analytical data of $[Ru(bpy)_2L](BF_4)_2$ complexes (L = azpy, dmazpy, deazpy, azpym and deazpym) corresponded to the calculated values (Table 17)

Table 17 The analytical data of $[Ru(bpy)_2L](BF_4)_2$ (L = azpy, dmazpy, deazpy, azpym and deazpym)[a]

Compound	Formula	Elemental analysis (%)		
		C	H	N
$[Ru(bpy)_2azpy](BF_4)_2$	$RuC_{31}H_{25}N_7B_2F_8$	48.34 (48.86)	3.27 (3.53)	12.73 (12.36)
$[Ru(bpy)_2dmazpy](BF_4)_2$	$RuC_{33}H_{30}N_8B_2F_8$	48.73 (47.79)	3.72 (3.79)	13.78 (14.54)
$[Ru(bpy)_2deazpy](BF_4)_2$	$RuC_{35}H_{34}N_8B_2F_8$	49.96 (49.52)	4.07 (4.32)	13.32 (12.50)
$[Ru(bpy)_2azpym](BF_4)_2$	$RuC_{30}H_{24}N_8B_2F_8$	46.72 (46.68)	3.14 (3.23)	14.53 (14.96)
$[Ru(bpy)_2deazpym](BF_4)_2$	$RuC_{34}H_{33}N_9B_2F_8$	48.48 (46.31)	3.95 (4.10)	14.97 (14.92)

[a]Calculated values are in parentheses

3.6.2 Mass spectrometric results of complexes

Electrospray mass spectrometry (ES-MS) and fast atomic bombardment mass spectrometry (FAB-MS) are important techniques to confirm the structures and molecular mass of the complexes. Electrospray mass spectrum of $[Ru(bpy)_2deazpy](BF_4)_2$ and FAB mass spectra of the other complexes are listed in Table 18.

Table 18 Mass spectrometric data of $[Ru(bpy)_2L](BF_4)_2$ (L = azpy, dmazpy, deazpy, azpym and deazpym)

Compound	Expected molecular weight	m/z	Assignment	Rel. Abund. (%)
$[Ru(bpy)_2azpy](BF_4)_2$	770.3	684	$[M-BF_4]^+$	100
$[Ru(bpy)_2dmazpy](BF_4)_2$	813.3	727 640	$[M-BF_4]^+$ $[M-2BF_4]^+$	50 100
$[Ru(bpy)_2deazpy](BF_4)_2$	841.4	755.2 333.9	$[M-BF_4]^+$ $([M-2BF_4]^+)^{2+}$	35 100
$[Ru(bpy)_2azpym](BF_4)_2$	771.3	685 598	$[M-BF_4]^+$ $[M-2BF_4]^+$	40 100
$[Ru(bpy)_2deazpym](BF_4)_2$	842.4	669 641	$[M-BF_4]^+$ $[M-2BF_4,$ $-CH_2=CH_2]^+$	40 100

M = formula of a complex

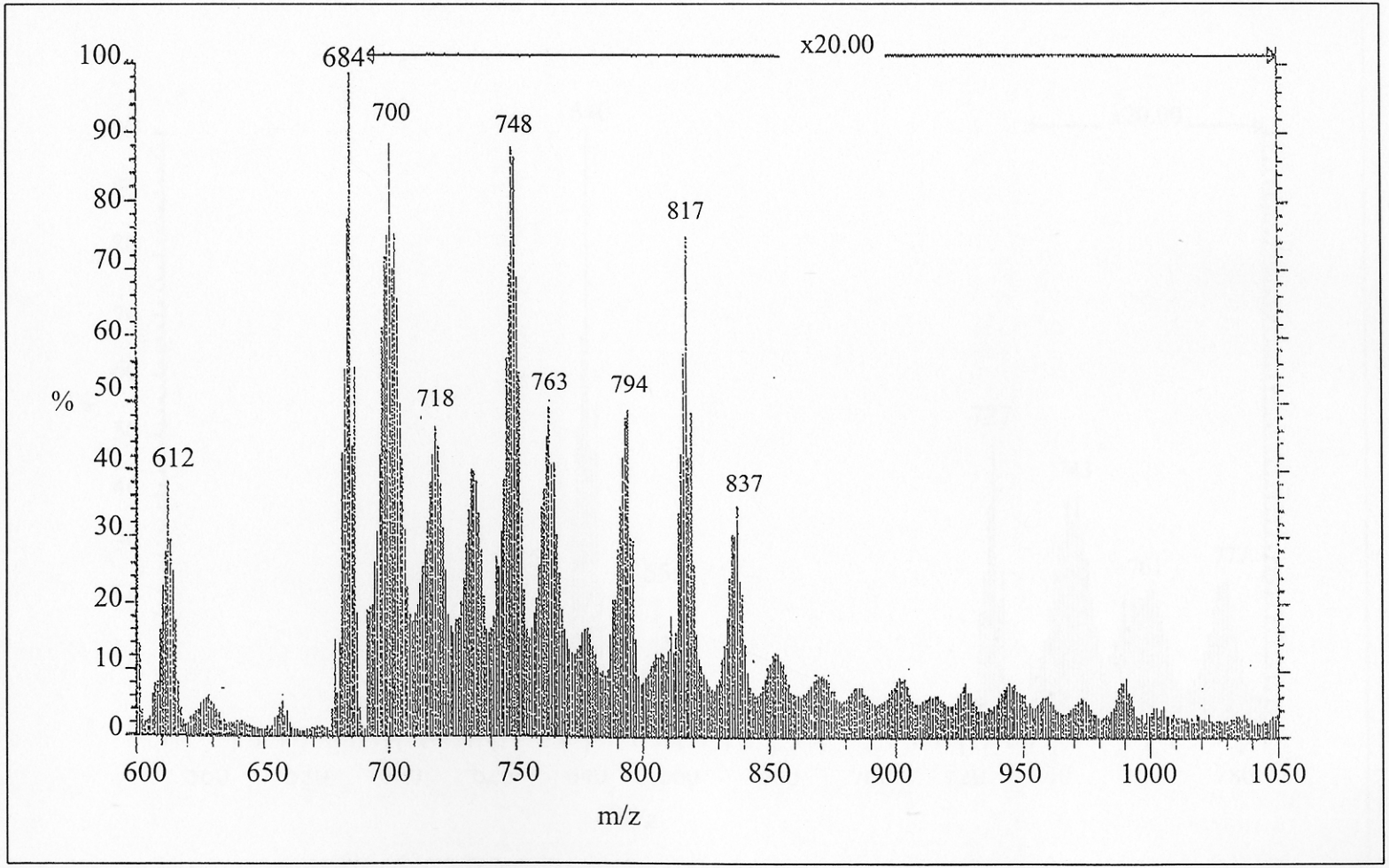

Figure 37 FAB mass spectrum of $[Ru(bpy)_2azpy](BF_4)_2$

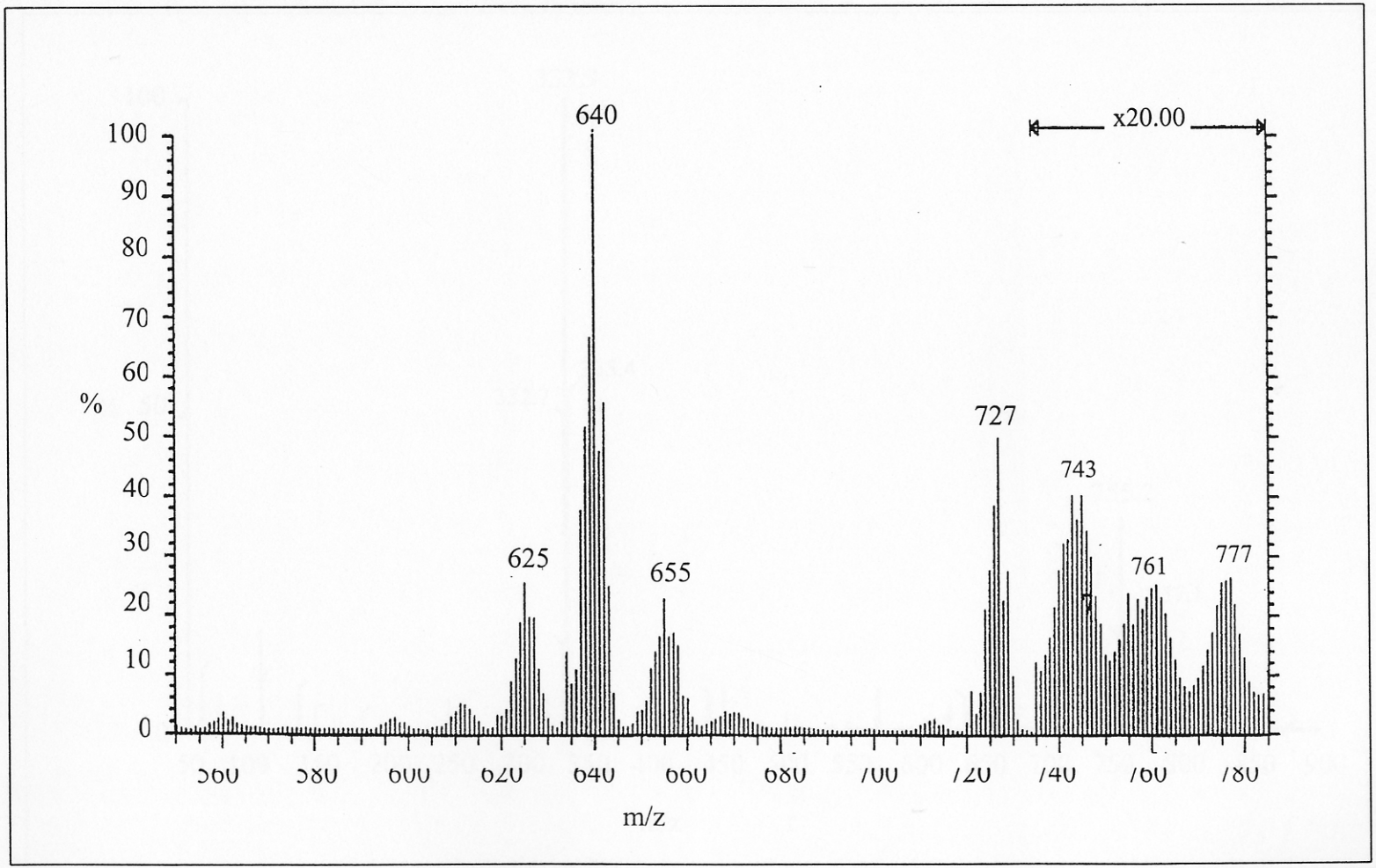

Figure 38 FAB mass spectrum of $[Ru(bpy)_2dmazpy](BF_4)_2$

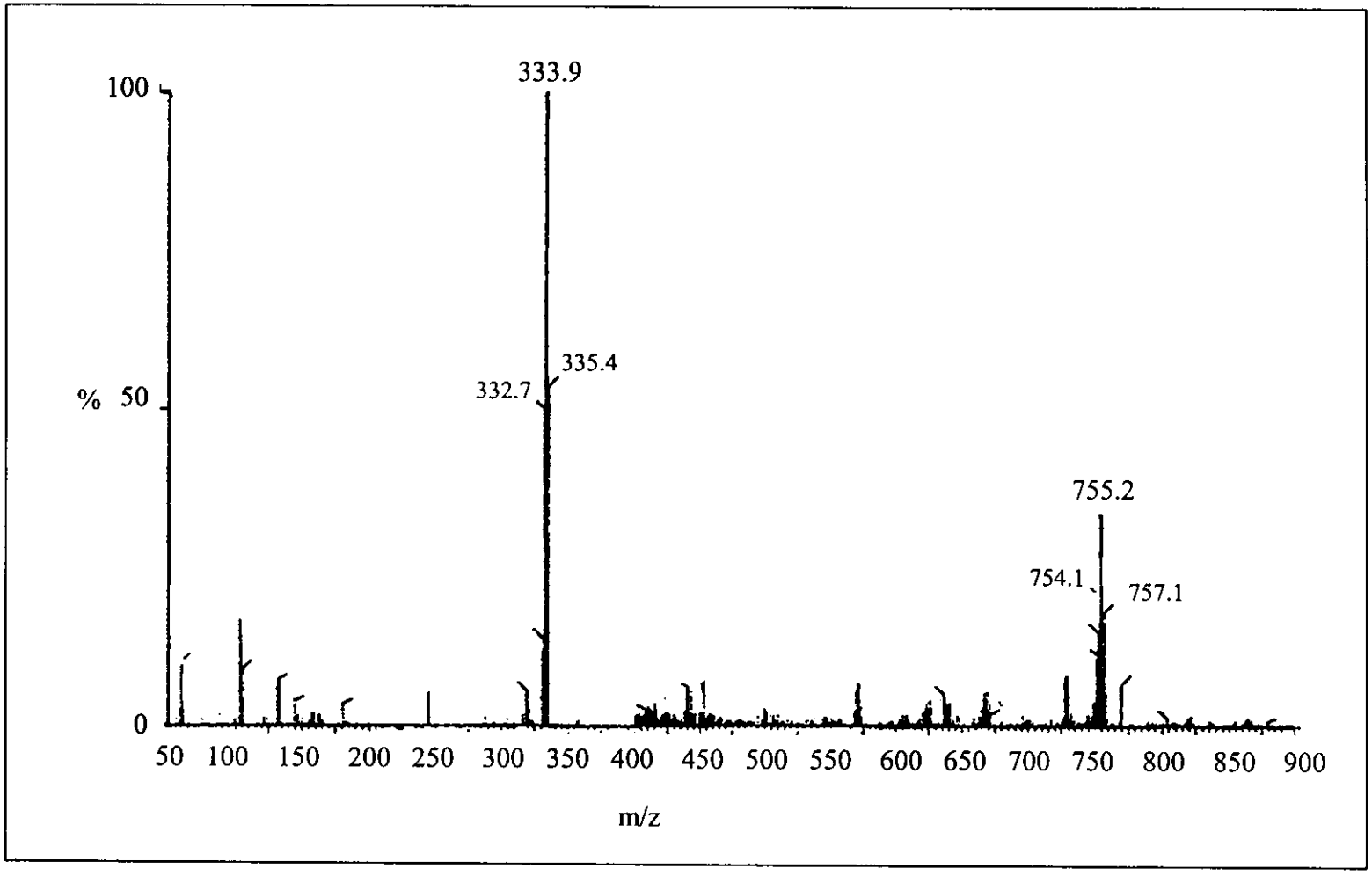

Figure 39 Electrospray mass spectrum of $[Ru(bpy)_2deazpy](BF_4)_2$

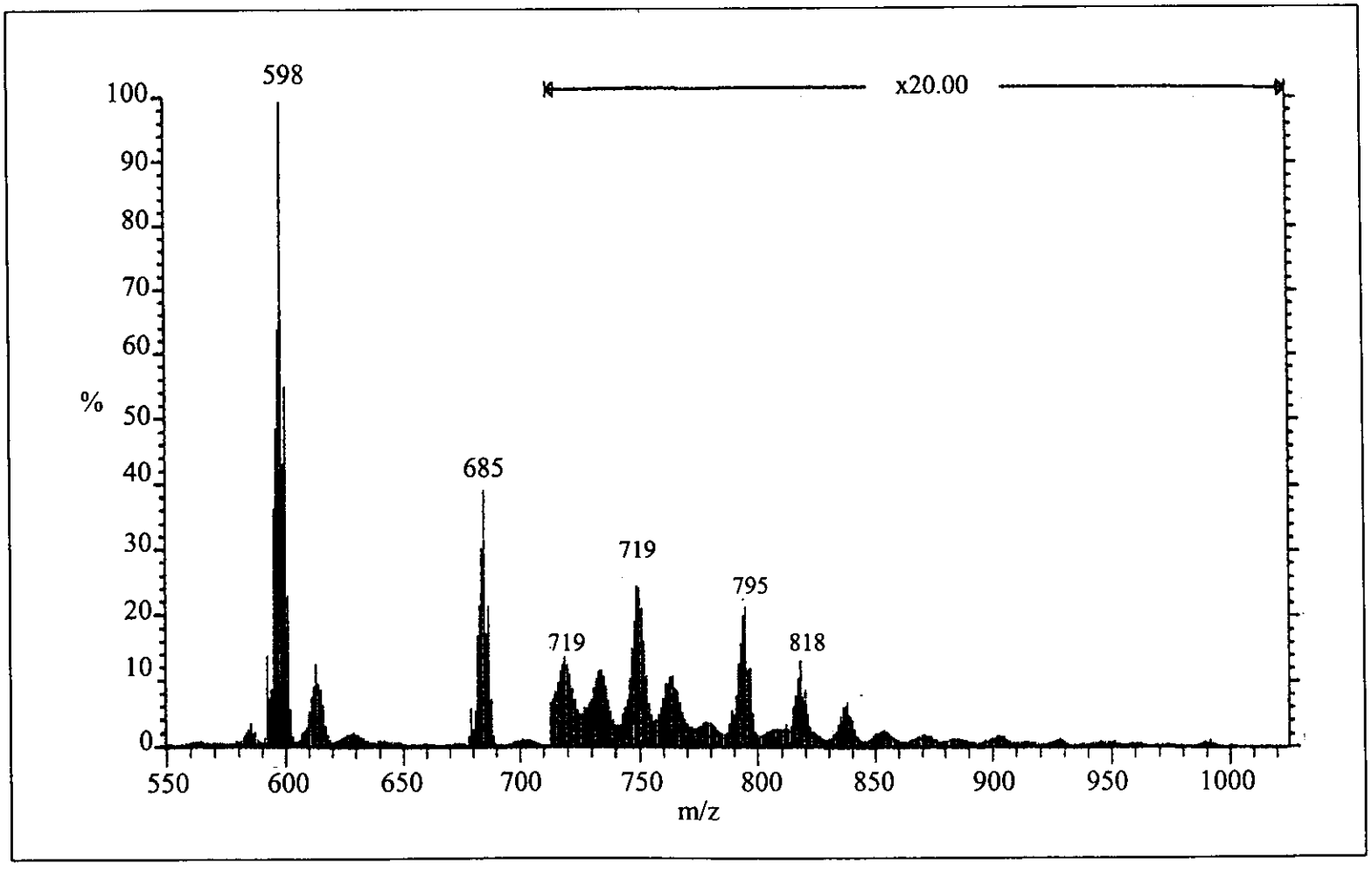

Figure 40 FAB mass spectrum of $[Ru(bpy)_2azpym](BF_4)_2$

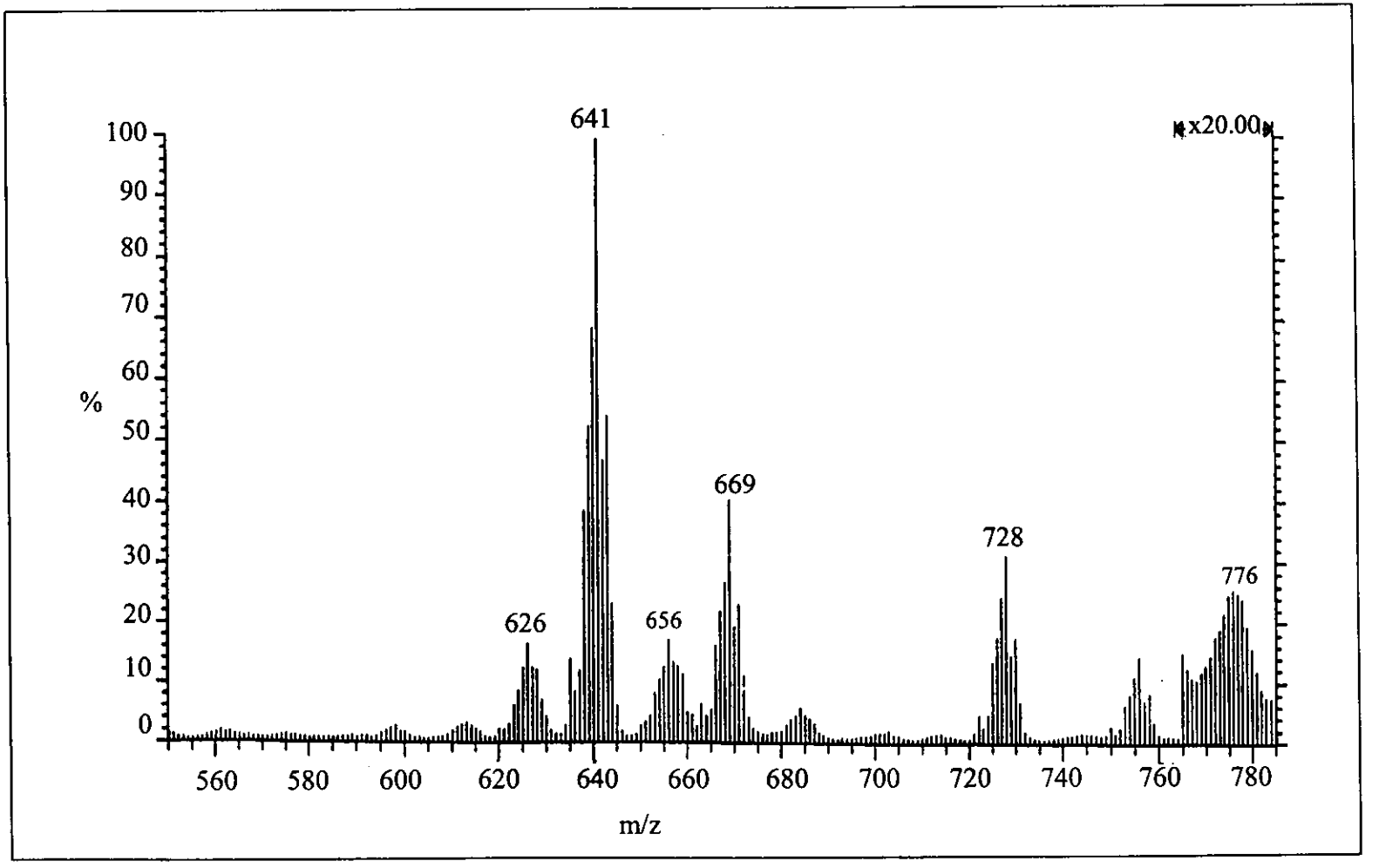

Figure 41 FAB mass spectrum of $[Ru(bpy)_2deazpym](BF_4)_2$

3.6.3 UV-Visible absorption spectroscopic results of complexes

The UV-Visible absorption spectra of the $[Ru(bpy)_2L](BF_4)_2$ complexes, where L = azpy, dmazpy, deazpy, azpym and deazpym in acetonitrile solution were measured at ambient temperature in the range 200-800 nm (Figure 42-46). The absorption data of azpy, dmazpy and deazpy complexes in various solvents are summarized in Table 19 and Table 20 for azpym and deazpym complexes.

Table 19 UV-Visible data of $[Ru(bpy)_2L](BF_4)_2$ (L = azpy, dmazpy and deazpy) in various solvents

Solvent	λ_{max}, nm (ε x 10^{-4}, $M^{-1}cm^{-1}$)		
	$[Ru(bpy)_2azpy]^{2+}$	$[Ru(bpy)_2dmazpy]^{2+}$	$[Ru(bpy)_2deazpy]^{2+}$
CH_2Cl_2	246 (2.5) 282 (4.9) 370 (1.4) 500 (1.0)	246 (2.3) 286 (5.6) 510 (2.0) 594 (3.1)	246 (2.5) 286 (6.3) 510 (2.2) 602 (3.9)
CH_3CN	246 (2.3) 280 (4.4) 362 (1.2) 498 (0.9)	246 (2.5) 284 (5.9) 504 (2.3) 580 (2.8)	246 (2.5) 284 (6.1) 506 (2.2) 588 (3.3)
Ethanol	246 (2.1) 280 (4.0) 368 (1.1) 496 (0.8)	246 (2.3) 284 (5.6) 506 (2.2) 584 (3.0)	246 (2.5) 284 (6.1) 508 (2.2) 594 (3.6)
Methanol	246 (2.1) 280 (4.0) 362 (1.1) 496 (0.8)	246 (2.5) 284 (5.3) 504 (2.0) 584 (2.6)	246 (2.5) 284 (5.8) 506 (2.1) 592 (3.3)
DMF	- 284 (4.7) 364 (1.3) 502 (0.9)	- 286 (6.3) 508 (2.4) 584 (2.9)	- 286 (6.1) 512 (2.3) 594 (3.2)
DMSO	- 284 (4.3) 364 (1.2) 502 (0.9)	- 288 (5.6) 510 (2.2) 590 (2.6)	- 288 (5.5) 512 (2.1) 598 (2.9)
H_2O	246 (2.4) 280 (4.1) 362 (1.2) 496 (0.9)	246 (2.4) 282 (5.1) 502 (1.8) 588 (1.9)	246 (2.1) 284 (4.5) 506 (1.6) 598 (2.0)

Table 20 UV-Visible data of $[Ru(bpy)_2L](BF_4)_2$ (L = azpym and deazpym) in various solvents

Solvent	λ_{max}, nm (ε^a x 10^{-4}, $M^{-1}cm^{-1}$)			
	$[Ru(bpy)_2azpym]^{2+}$		$[Ru(bpy)_2deazpym]^{2+}$	
CH_2Cl_2	254 (2.5)	278 (3.8)	246 (2.6)	286 (5.2)
	364 (1.5)	502 (0.8)	510 (1.8)	624 (3.8)
CH_3CN	254 (2.8)	276 (3.9)	246 (3.0)	284 (5.8)
	350 (1.5)	496 (0.8)	508 (2.0)	616 (3.9)
Ethanol	254 (2.3)	278 (3.4)	246 (2.6)	284 (5.1)
	354 (1.5)	496 (0.7)	508 (1.8)	620 (3.6)
Methanol	254 (2.7)	276 (3.8)	244 (3.0)	284 (5.5)
	354 (1.5)	498 (0.8)	508 (2.0)	622 (3.9)
DMF	-	280 (4.2)	-	288 (6.3)
	352 (1.6)	498 (0.8)	510 (2.2)	620 (4.0)
DMSO	-	280 (3.6)	-	288 (5.4)
	356 (1.4)	498 (0.8)	512 (1.9)	622 (3.5)
H_2O	254 (2.7)	274 (3.3)	244 (3.0)	284 (5.0)
	358(1.4)	496 (0.8)	512 (1.9)	636 (3.7)

[a] Molar extinction coefficient

In UV region, the absorption spectra of all complexes showed two intense bands which belong to the electronic transition of bpy ligands. In visible region, the absorption spectra of $[Ru(bpy)_2L](BF_4)_2$ complexes (L = azpy and azpym) exhibited only one intense band, whereas where L = dmazpy, deazpy and deazpym,

the complexes exhibit two intense bands which refer to metal-to-ligand charge transfer (MLCT).

In addition, the absorption bands of all complexes were not shifted when polarity of solvents is increased. The lowest energy absorption bands of MLCT transition shifted to lower energy for dmazpy, deazpy and deazpym complexes whereas, the absorption bands in azpym complex were similar to those in the azpy complex. The lowest energy of MLCT transition increased in the order : deazpym < deazpy < dmazpy < azpy ≈ azpym complexes.

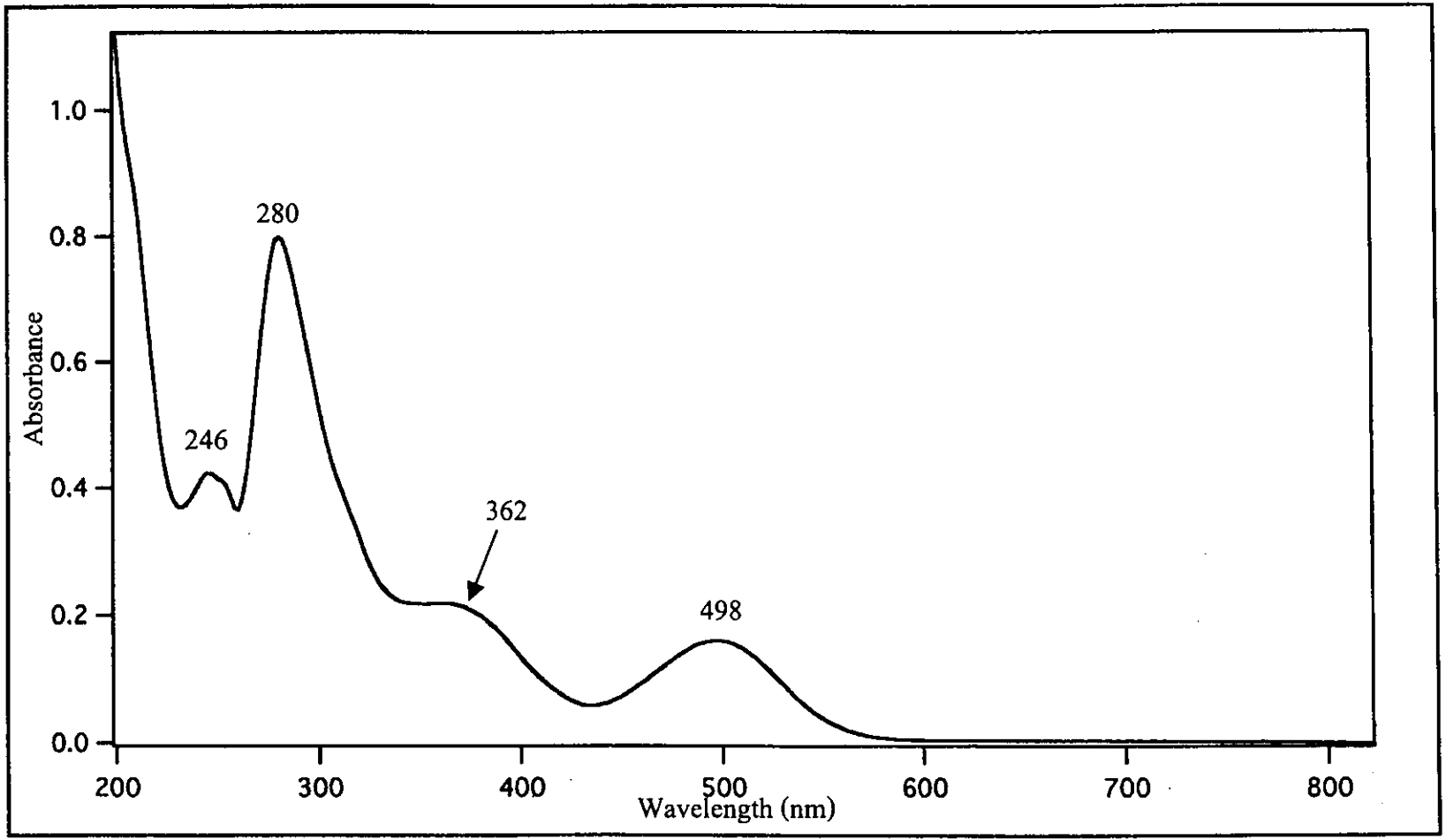

Figure 42 Absorption spectrum of $[Ru(bpy)_2azpy](BF_4)_2$ in CH_3CN solution

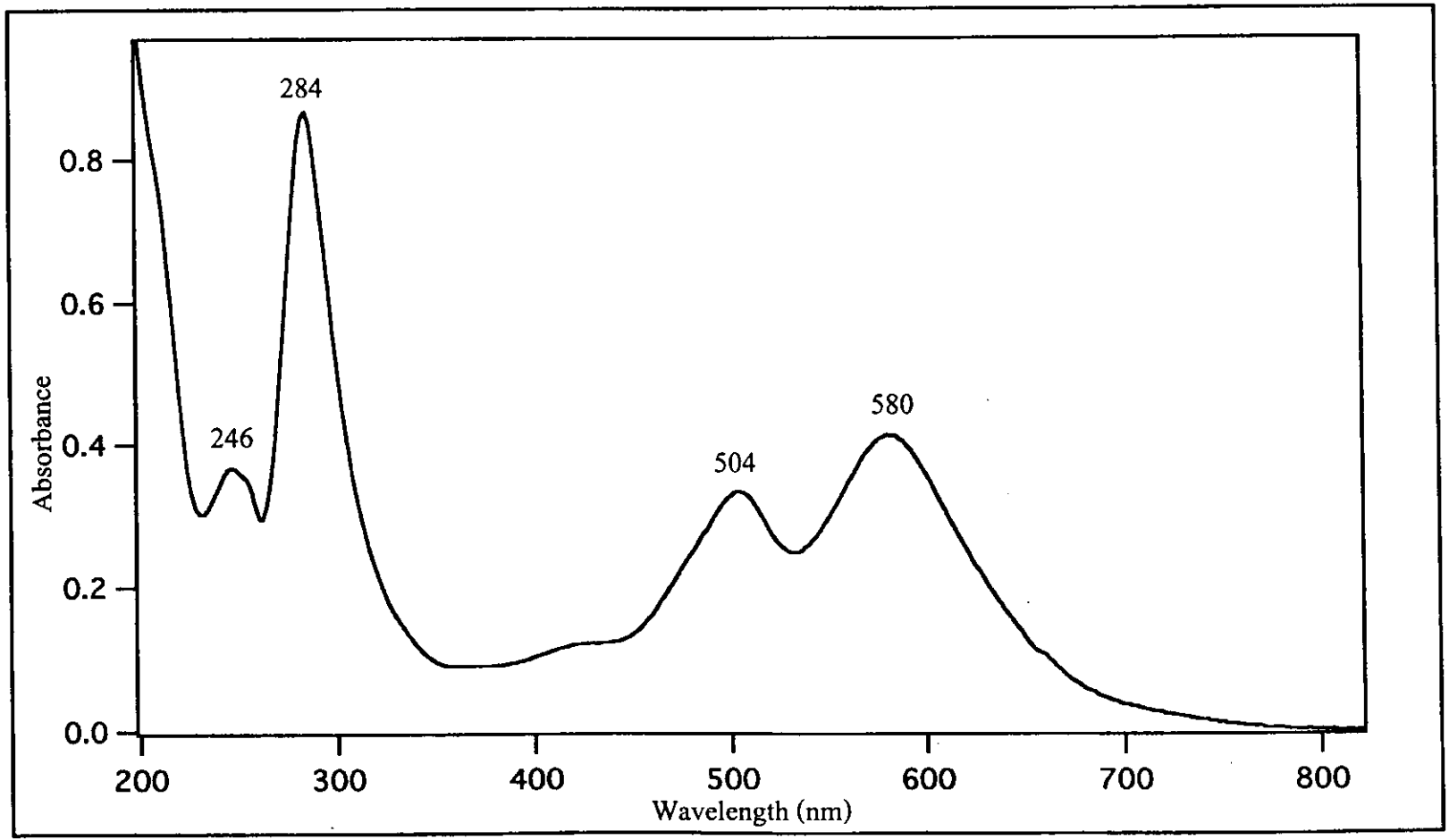

Figure 43 Absorption spectrum of $[Ru(bpy)_2dmazpy](BF_4)_2$ in CH_3CN solution

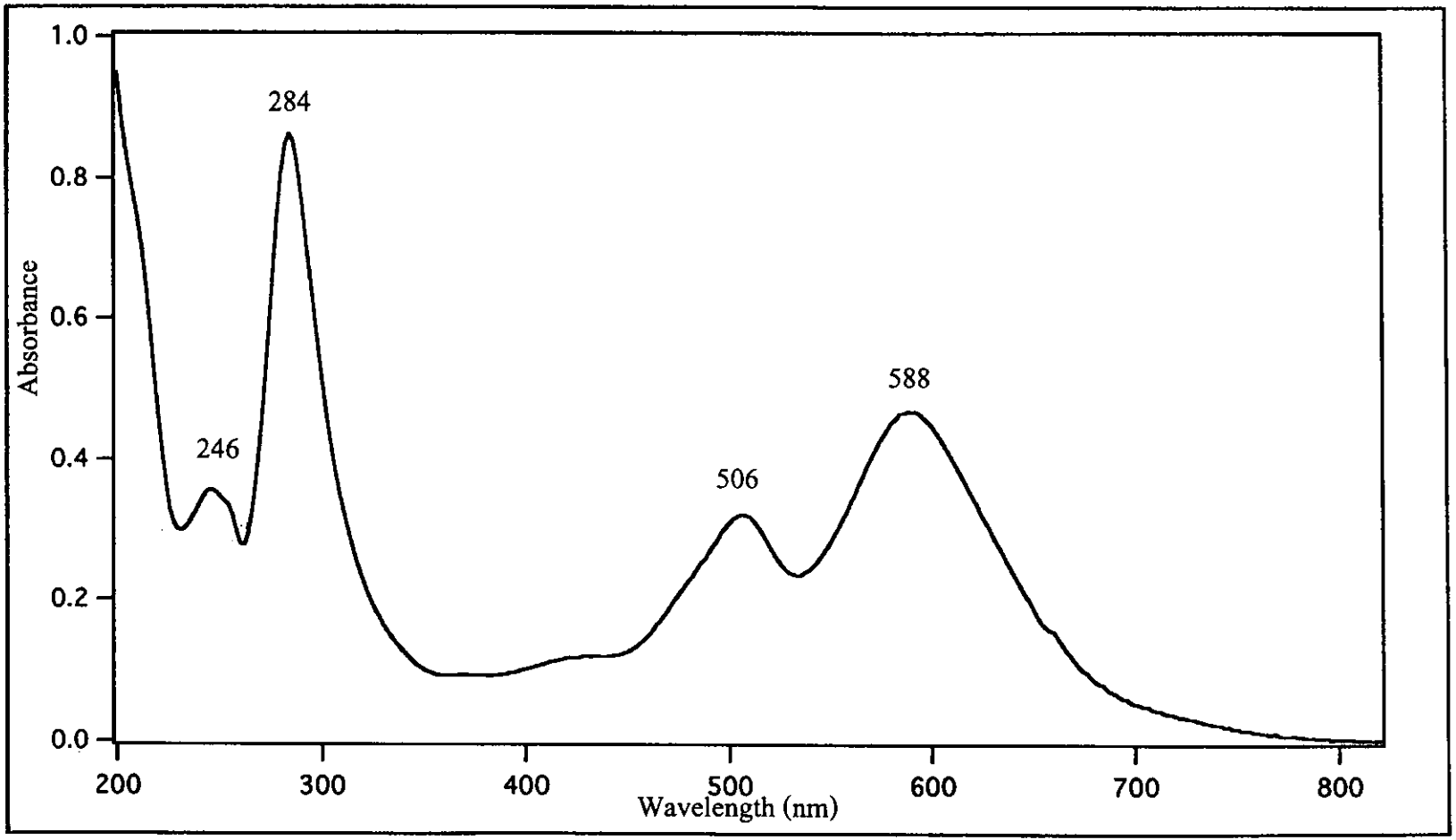

Figure 44 Absorption spectrum of $[Ru(bpy)_2deazpy](BF_4)_2$ in CH_3CN solution

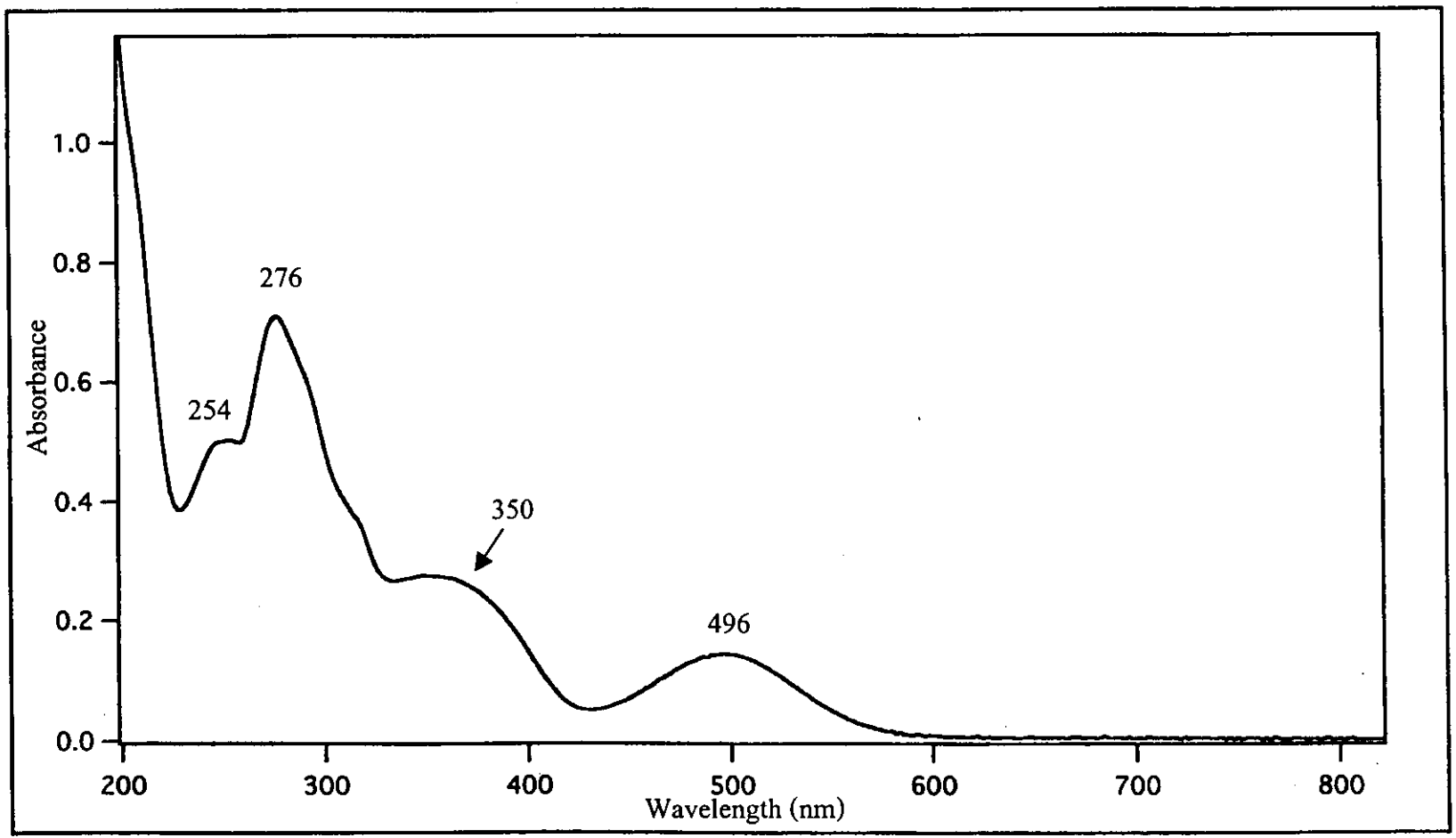

Figure 45 Absorption spectrum of $[Ru(bpy)_2azpym](BF_4)_2$ in CH_3CN solution

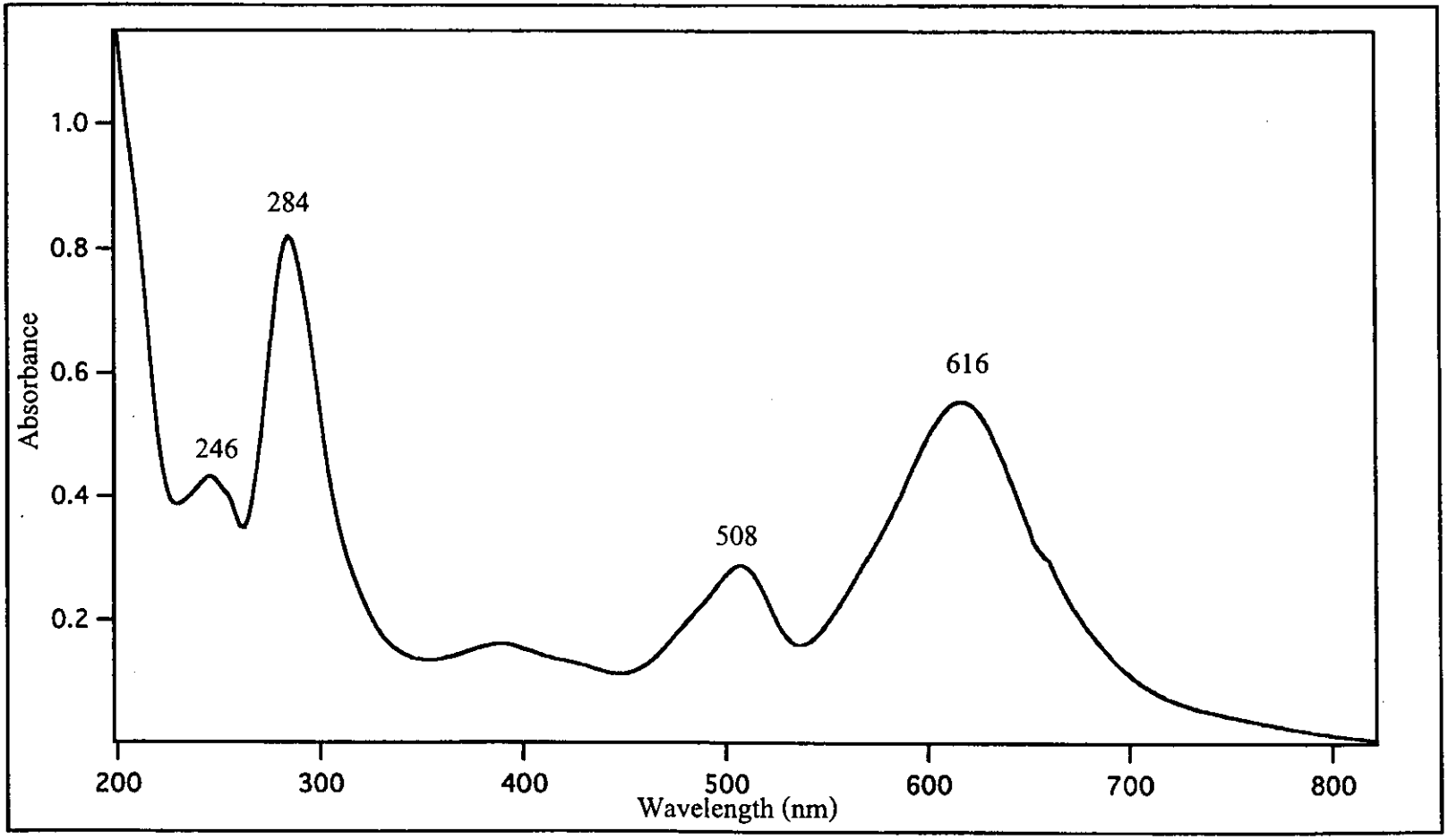

Figure 46 Absorption spectrum of $[Ru(bpy)_2deazpym](BF_4)_2$ in CH_3CN solution

3.6.4 Intrared spectroscopic results of complexes

Infrared spectroscopy is also an important technique to study the molecular structure of the complexes, vibrational spectra in the region 4,000-400 cm^{-1}, can be used to study the functional groups of ligands around a central metal atom.

Infrared data of the $[Ru(bpy)_2L](BF_4)_2$ complexes , where L = azpy, dmazpy, deazpy, azpym and deazpym in the range 1,600-400 cm^{-1} were significant. Some characteristic frequencies are shown in Table 21. The infrared spectra of the complexes are shown in Figure 47-51.

The IR spectra of $[Ru(bpy)_2L](BF_4)_2$ complexes (L = azpy, dmazpy, deazpy, azpym and deazpym) exhibited several characteristic strong bands. All of the complexes showed intense bands in the range 1,500-1,600 cm^{-1}, corresponding to C=N stretching. The N=N (azo) stretching modes in complexes occurred in the spectral region 1330-1260 cm^{-1}. The N=N stretching frequencies of complexes were varied. The N=N stretching modes of all complexes were shifted to lower frequencies by 100 cm^{-1} compared to those in free ligands. This was a good indication of N-coordination.

From Table 21 it can be seen that the N=N stretching vibration for the azpy complex gave a strong absorption at 1330 cm^{-1}. These bands shifted to lower energies as found in the dmazpy, deazpy, azpym and deazpym complexes, occurring at 1289, 1291, 1304 and 1263 cm^{-1}, respectively. This result indicated that the N=N bond of the azpy complex was stronger than those of dmazpy, deazpy, azpym and deazpym complexes. The decrease of N=N bond order in dmazpy, deazpy and deazpym complexes could be due to the substituents ($-NR_2$) which were electron donating groups and details were discussed later.

Table 21 Infrared data of $[Ru(bpy)_2L](BF_4)_2$ (L = azpy, dmazpy, deazpy, azpym and deazpym) in the KBr pellet

Vibrational modes	Wavenumber (cm^{-1})				
	$[Ru(bpy)_2L](BF_4)_2$ complexes				
	Azpy	Dmazpy	Deazpy	Azpym	Deazpym
N=N (azo) stretching	1330(s)	1289(s)	1291(s)	1304(s)	1263(s)
C=N stretching	1603(s)	1595(s)	1593(s)	1605(s)	1595(s)
C=C stretching	1603(s) 1447(s)	1595(s) 1526(m) 1446(s) 1380(s)	1593(s) 1446(m) 1413(m) 1358(m)	1605(s) 1447(s) 1401(s)	1595(s) 1467(m) 1447(m) 1384(s)
C-H bending of para disubstituted benzene	-	833(m)	833(m)	-	835(m)
C-H out of plane bending	765(s) 730(w) 696(m)	768(s) 743(m) 730(m)	770(s) 730(m)	769(s) 730(w) 698(m)	764(s) 745(m) 730(m)

s = strong, m = medium, w = weak

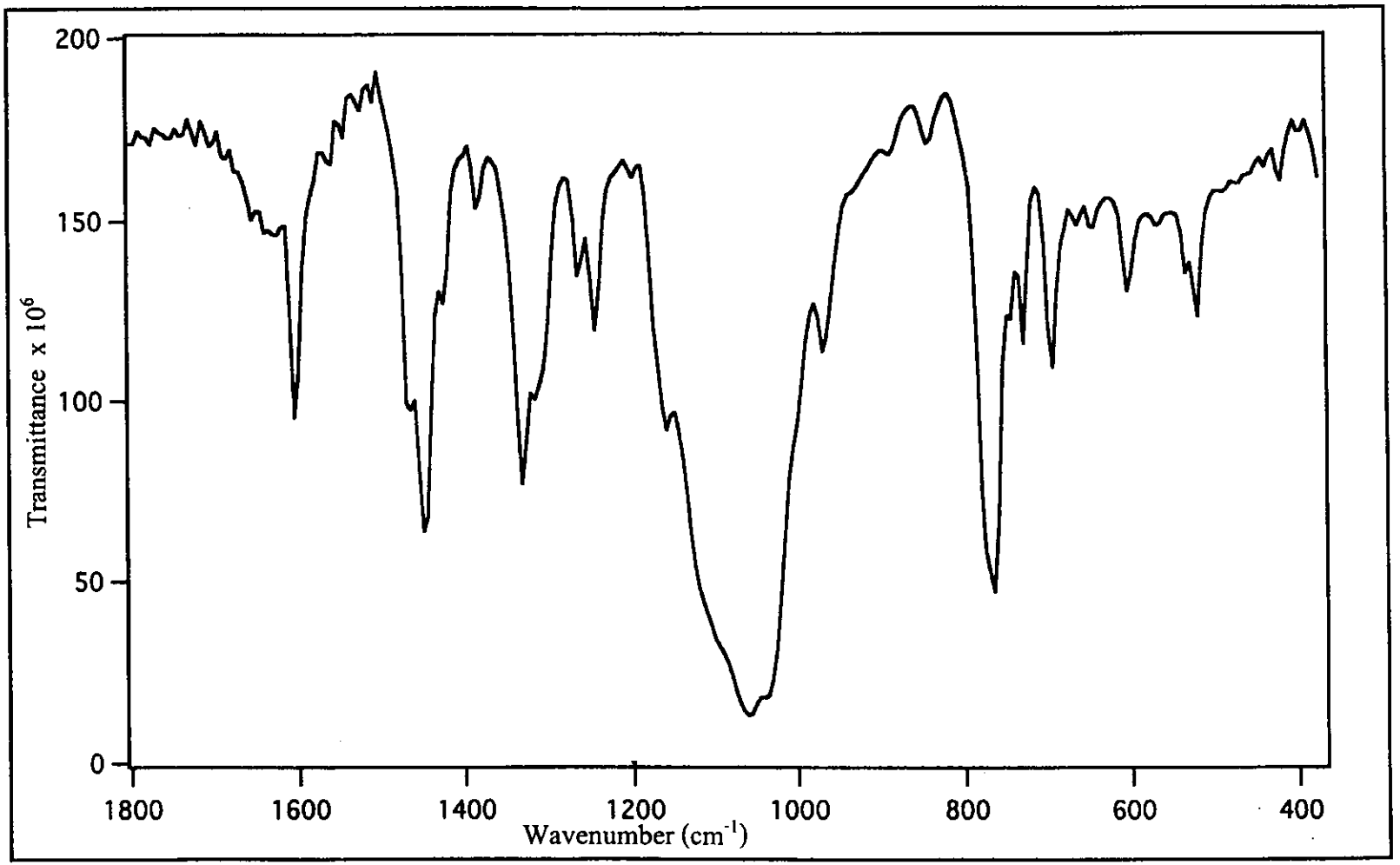

Figure 47 Infrared spectrum of $[Ru(bpy)_2azpy](BF_4)_2$ in the KBr pellet

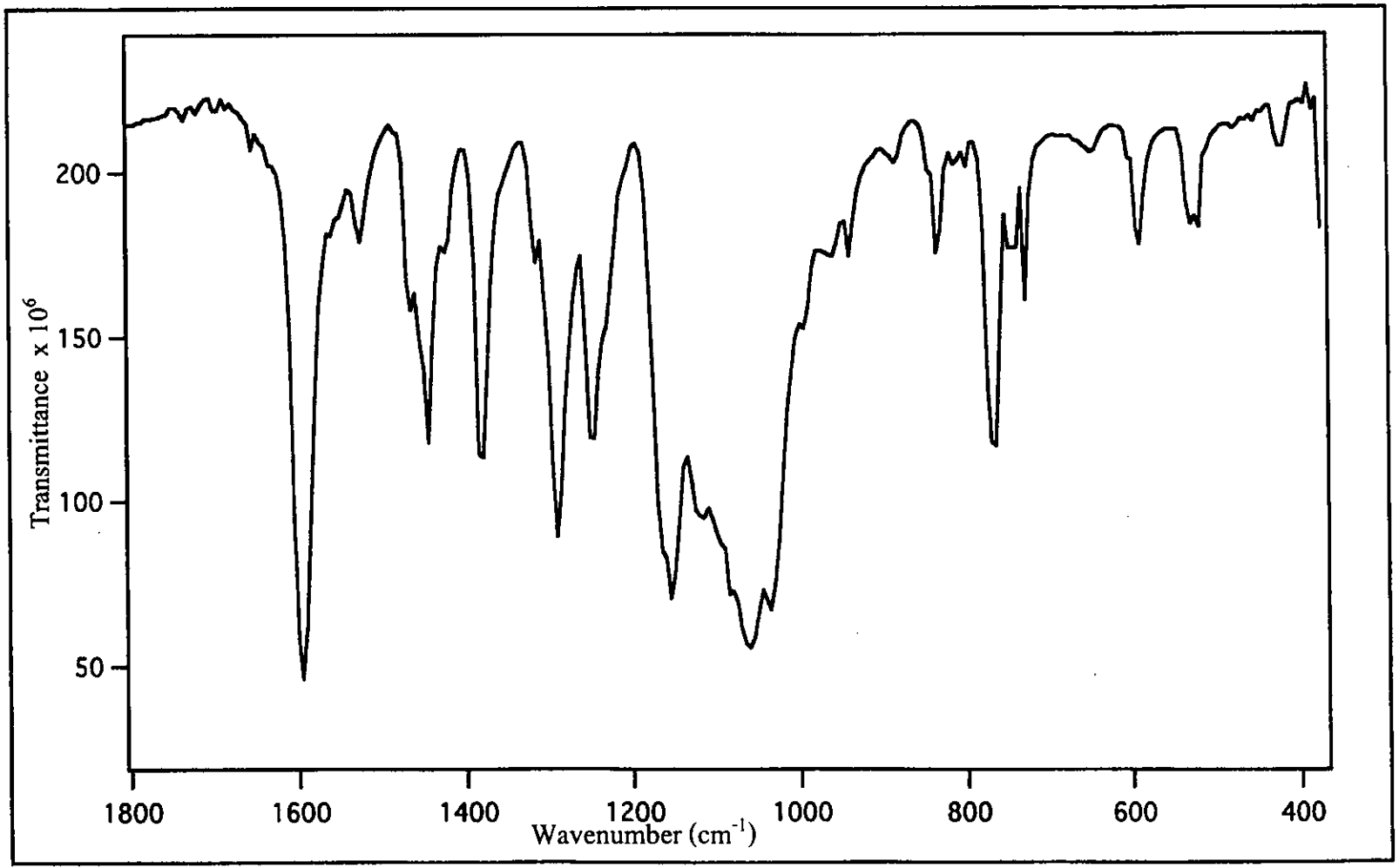

Figure 48 Infrared spectrum of $[Ru(bpy)_2dmazpy](BF_4)_2$ in the KBr pellet

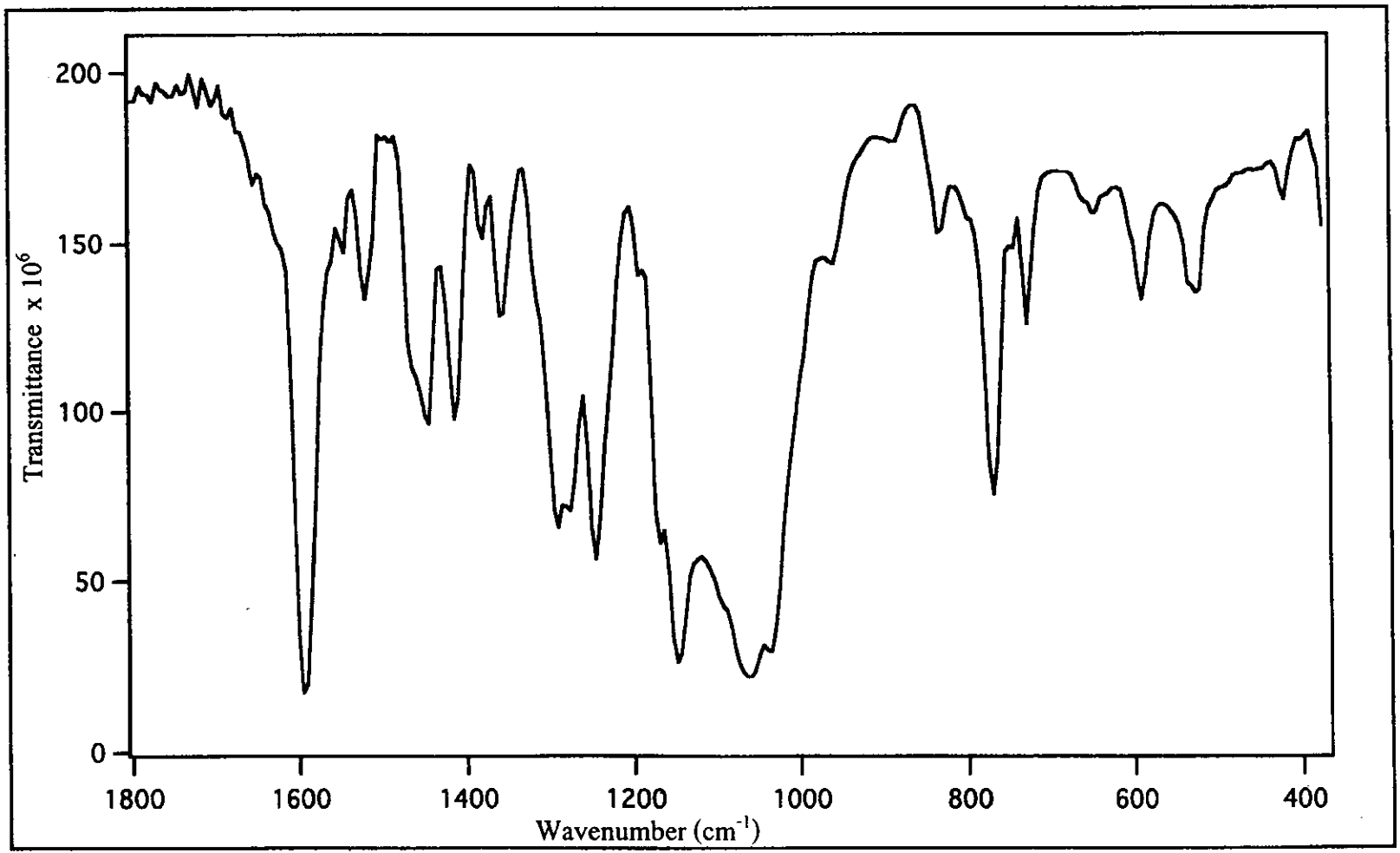

Figure 49 Infrared spectrum of $[Ru(bpy)_2deazpy](BF_4)_2$ in the KBr pellet

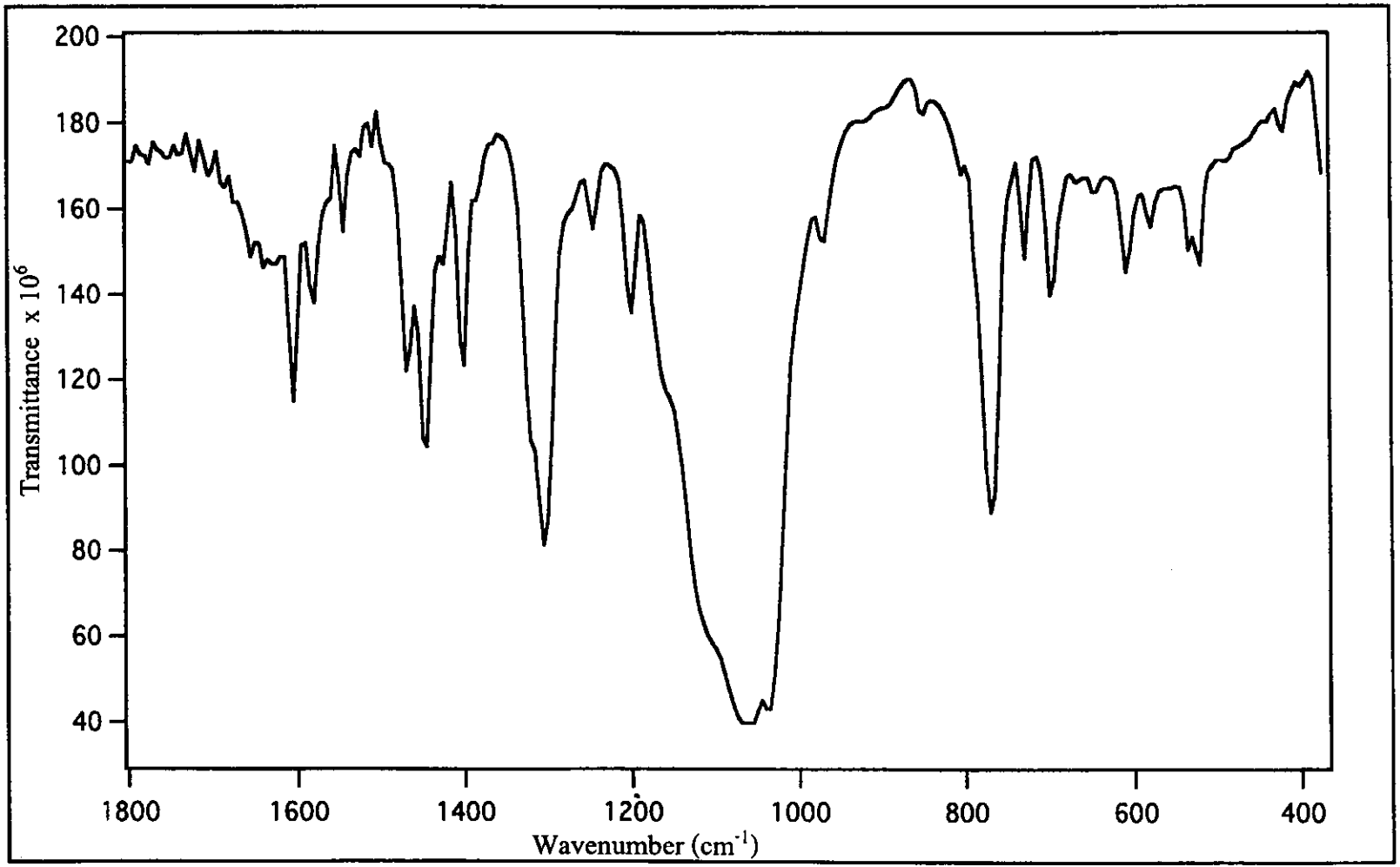

Figure 50 Infrared spectrum of $[Ru(bpy)_2azpym](BF_4)_2$ in the KBr pellet

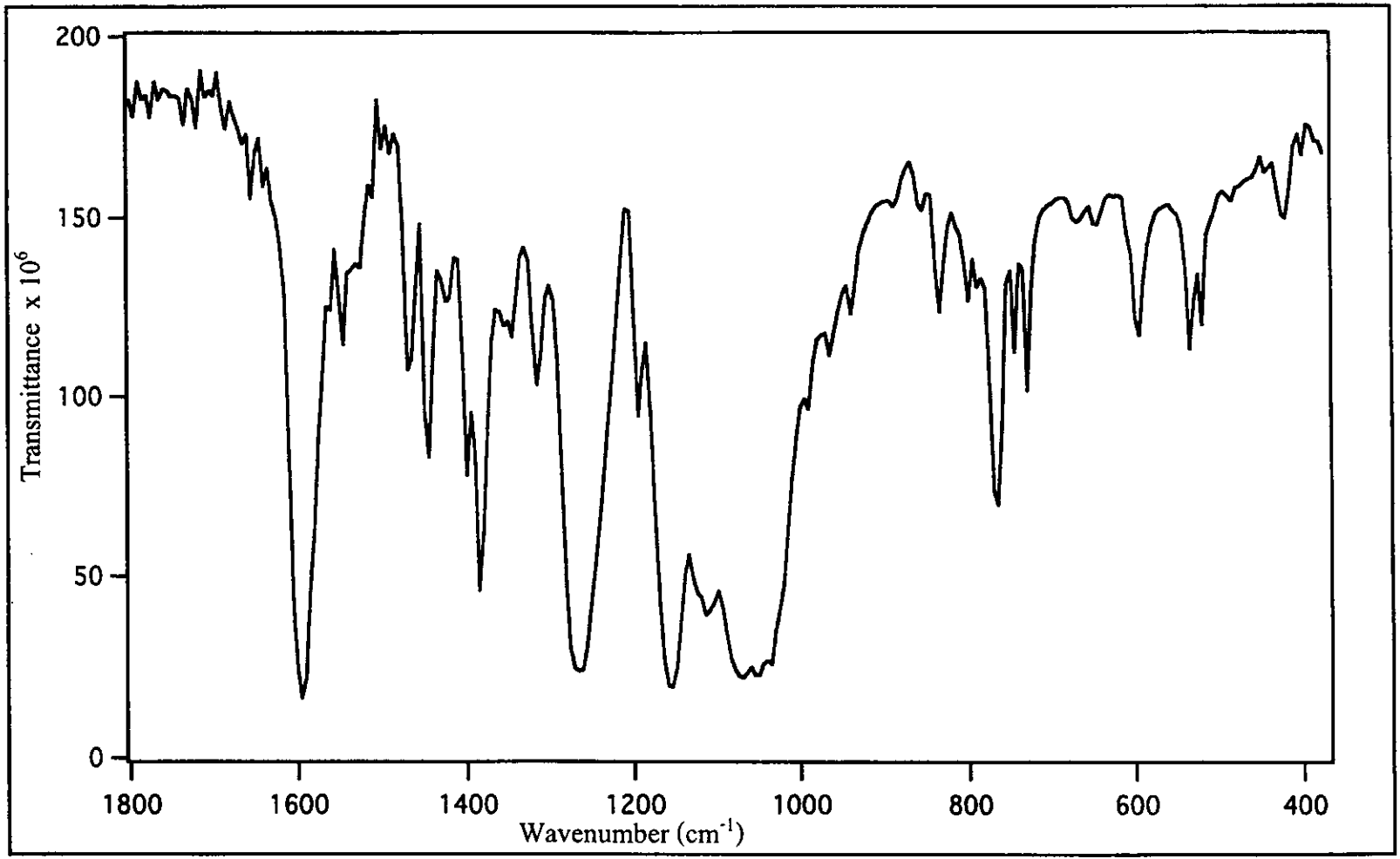

Figure 51 Infrared spectrum of $[Ru(bpy)_2deazpym](BF_4)_2$ in the KBr pellet

3.6.5 NMR spectroscopic results of complexes

NMR spectroscopy is an important technique to determine molecular structure because different protons in a molecular structure will show different chemical shifts. The structure of $[Ru(bpy)_2L](BF_4)_2$ complexes (L = azpy, dmazpy, deazpy, azpym and deazpym) were elucidated by using 1D and 2D NMR spectroscopic techniques.

^1H NMR spectrum gave the total number of protons in each complex and their chemical shifts were related to position in complexes which were based on ^1H-^1H COSY spectra. Furthermore, the ^{13}C NMR signals were determined from HMQC spectra. The chemical shifts (δ, ppm) and *J*-coupling (Hz) of complexes were reported in part per million (ppm) downfield from tetramethylsilane (TMS, $(CH_3)_4Si$) which was used as an internal standard. The NMR spectroscopic data of each complex are given in Table 22-26.

a) $[Ru(bpy)_2azpy](BF_4)_2$ complex

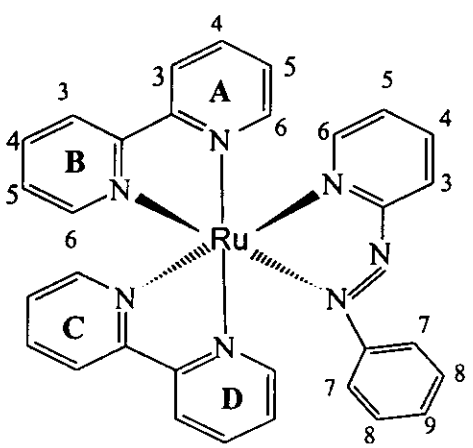

The ^{1}H NMR spectrum (Figure 52) of $[Ru(bpy)_2azpy](BF_4)_2$ complex in acetone-d_6 showed characteristic peaks of bipyridine rings of both bpy and azpy ligands and phenyl ring in azpy ligand which appeared 22 signals for 25 protons. This could be due to unsymmetric structure of complex. This mean the four pyridine rings in the bpy ligands were chemically and magnetically non-equivalent. The ^{1}H-^{1}H COSY spectrum (Figure 53) of this complex revealed that the seven signals at 8.99 (ddd), 8.42 (ddd), 8.25 (ddd), 7.83 (ddd), 7.40 (tt), 7.24 (ddd) and 7.17 (ddd) in azpy ligand could be assigned to H3, H4, H6, H5, H7, H8 and H9, respectively.

The ^{13}C NMR spectrum (Figure 54) and HMQC spectra (Figure 55) showed 28 resonances for 31 carbon atoms : twenty two methine carbons and six quaternary carbons (δ 168.22, 158.58, 157.99, 157.82, 156.76 and 156.61 ppm). The NMR data of this complex in acetone-d_6 solution are given in Table 22.

Table 22 The NMR data of $[Ru(bpy)_2azpy](BF_4)_2$ in acetone-d_6 solution

Position	^{1}H NMR			^{13}C NMR (C-Type)
	δ(ppm)	J (Hz)	Amount of H	δ, ppm
H3 (azpy)	8.99 (ddd)	8.0, 1.5, 1.0	1	129.82 (CH)
H3 (bpy)	8.97 (ddd)	8.0, 1.0, 1.0	1	126.99 (CH)
	8.95 (ddd)	8.0, 1.0, 1.0	1	126.69 (CH)
	8.64 (ddd)	8.0, 1.0, 1.0	1	126.13 (CH)
	8.50 (ddd)	8.0, 1.0, 1.0	1	125.87 (CH)
H4 (azpy)	8.42 (ddd)	8.0, 8.0, 1.5	1	142.00 (CH)
H4 (bpy)	8.35 (ddd)	8.0, 8.0, 1.5	2	141.98, 141.78 (CH)
	8.32 (ddd)	8.0, 8.0, 1.5	1	141.54 (CH)
H6 (bpy)	8.32 (ddd)	5.5, 1.5, 1.0	1	154.91 (CH)
H6 (azpy)	8.25 (ddd)	6.0, 1.5, 1.0	1	151.82 (CH)
H4 (bpy)	8.10 (ddd)	8.0, 8.0, 1.5	1	140.87 (CH)
H6 (bpy)	7.99 (ddd)	6.0, 1.5, 1.0	1	153.49 (CH)
	7.96 (ddd)	5.5, 1.5, 1.0	1	152.60 (CH)
H5 (azpy)	7.83 (ddd)	7.5, 1.5, 6.0	1	130.40 (CH)
H5 (bpy)	7.73 (ddd)	7.5, 1.5, 6.0	1	130.44 (CH)
	7.70 (ddd)	8.0, 1.5, 6.0	1	130.44 (CH)
	7.68 (ddd)	7.5, 1.5, 6.0	1	130.12 (CH)
H6 (bpy)	7.66 (ddd)	5.5, 1.5, 1.0	1	154.16 (CH)
H5 (bpy)	7.54 (ddd)	7.5, 1.5, 6.0	1	130.03 (CH)
H7 (azpy)	7.40 (tt)	7.5, 1.5	1	132.63 (CH)
H8 (azpy)	7.24 (dd)	8.5, 7.5	2	130.73 (CH)
H9 (azpy)	7.17 (dd)	8.5, 1.5	2	123.67 (CH)
Quaternary carbons (C)				168.22, 158.58, 157.99, 157.82, 156.76, 156.61

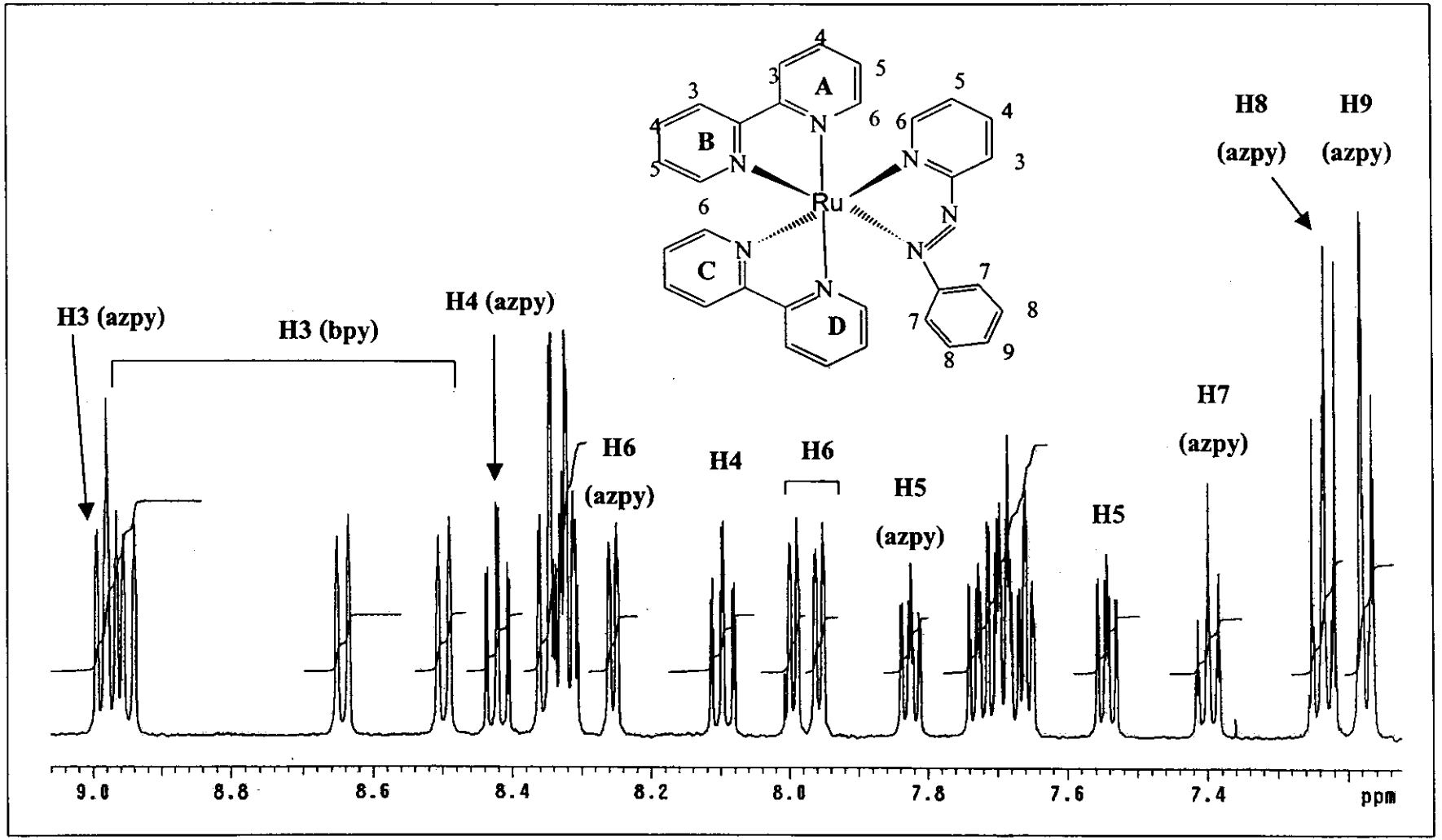

Figure 52 ^{1}H NMR spectrum of $[Ru(bpy)_2azpy](BF_4)_2$ in acetone-d_6 solution

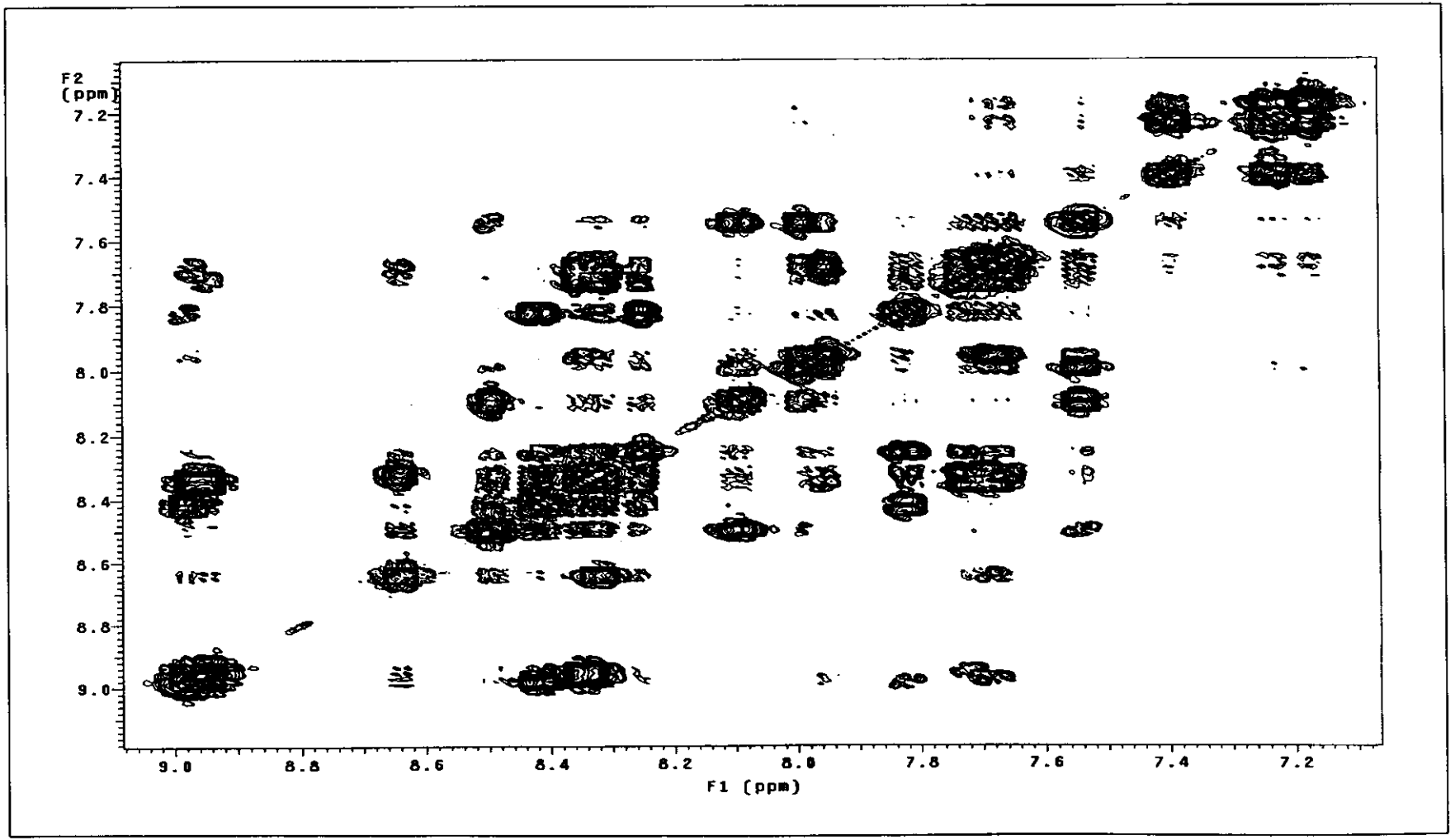

Figure 53 ^{1}H-^{1}H COSY spectrum of $[Ru(bpy)_2azpy](BF_4)_2$ in acetone-d_6 solution

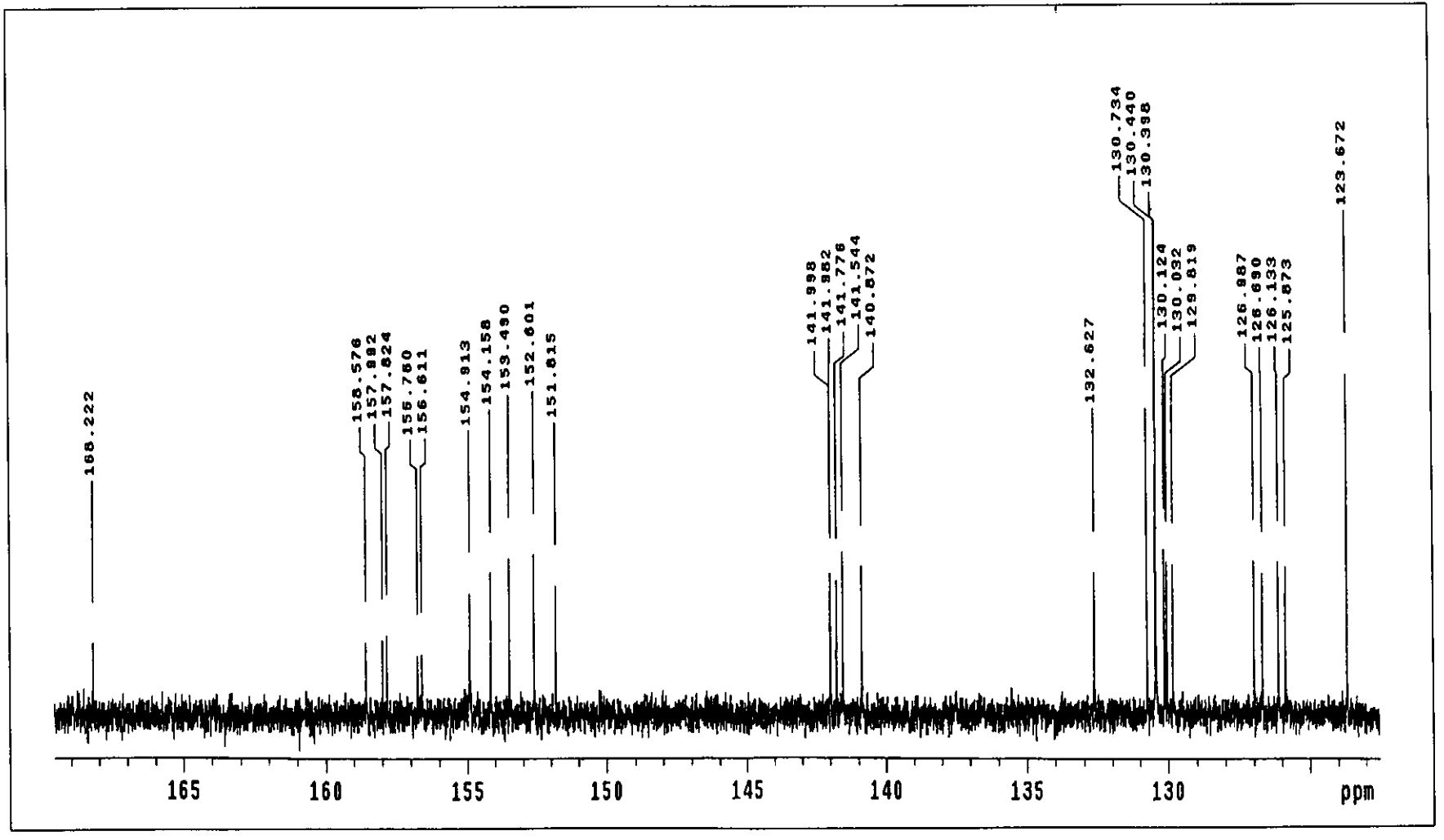

Figure 54 ^{13}C NMR spectrum of $[Ru(bpy)_2azpy](BF_4)_2$ in acetone-d_6 solution

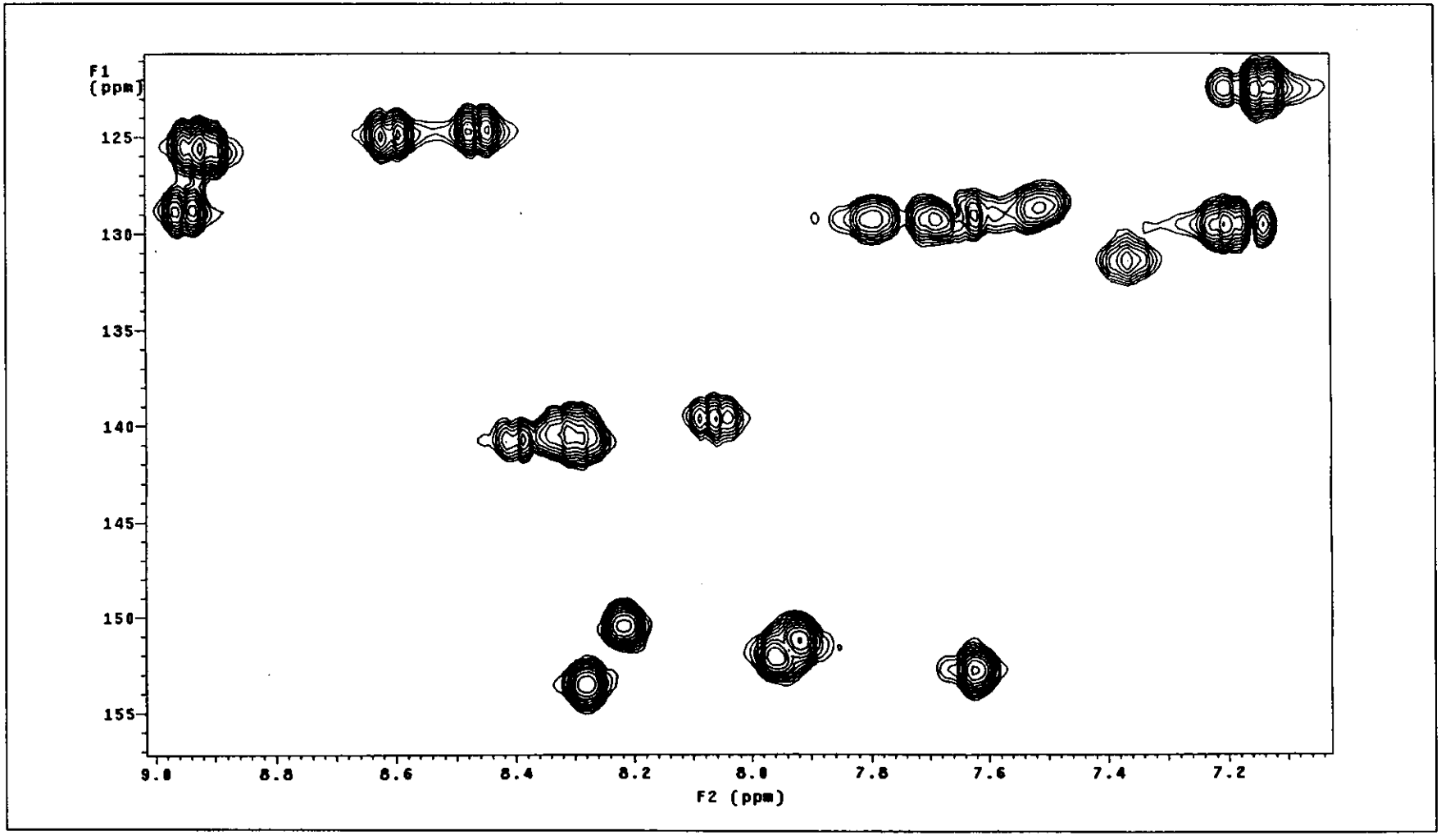

Figure 55 HMQC spectrum of $[Ru(bpy)_2azpy](BF_4)_2$ in acetone-d_6 solution

b) $[Ru(bpy)_2dmazpy](BF_4)_2$ complex

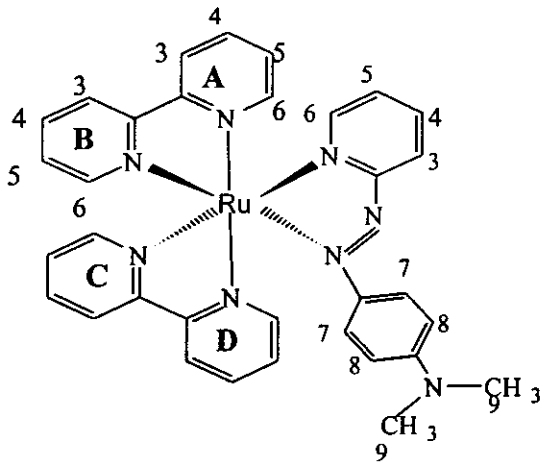

The ^1H NMR spectrum of $[Ru(bpy)_2dmazpy](BF_4)_2$ complex (Figure 56) in acetone-d_6 showed characteristic peaks of bipyridine rings of both bpy and dmazpy ligands and phenyl ring in dmazpy ligand which appeared 23 signals for 30 protons. There were 23 signals observed in this complex which was not a symmetric molecule. This means the four pyridine rings in the bpy ligands are chemically and magnetically non-equivalent. The ^1H-^1H COSY spectrum (Figure 57) of this complex revealed that seven signals at 8.68 (ddd), 8.27 (ddd), 8.01 (ddd), 7.56 (ddd), 7.42 (d), 6.52 (d) and 3.07 (s) in dmazpy ligand could be assigned to H3, H4, H6, H5, H7, H8 and H9, respectively.

The ^{13}C NMR spectrum (Figure 58) and HMQC spectra (Figure 59) showed 29 resonances for 33 carbon atoms : twenty one methine carbons, a methyl (δ 40.24 ppm) and seven quaternary carbons (δ168.09, 158.56, 158.40, 158.27, 157.40, 155.71 and 148.42 ppm). The NMR data of this complex in acetone-d_6 solution are given in Table 23.

Table 23 The NMR data of $[Ru(bpy)_2dmazpy](BF_4)_2$ in acetone-d_6 solution

Position	^{1}H NMR			^{13}C NMR (C-Type)
	δ(ppm)	J (Hz)	Amount of H	δ(ppm)
H3 (bpy)	8.95 (ddd)	8.0, 1.0, 1.0	1	126.83 (CH)
	8.94 (ddd)	8.0, 1.0, 1.0	1	126.60 (CH)
	8.74 (ddd)	8.0, 1.0, 1.0	1	126.20 (CH)
	8.70 (ddd)	8.0, 1.0, 1.0	1	126.14 (CH)
H3 (dmazpy)	8.68 (ddd)	8.0, 1.5, 1.0	1	127.61 (CH)
H4 (bpy)	8.32 (ddd)	8.0, 8.0, 1.5	1	141.28 (CH)
	8.31 (ddd)	8.0, 8.0, 1.5	1	141.09 (CH)
	8.28 (ddd)	8.0, 8.0, 1.5	1	141.09 (CH)
H6 (bpy)	8.28 (ddd)	6.0, 1.5, 1.0	1	154.72 (CH)
H4 (dmazpy)	8.27 (ddd)	8.0, 8.0, 1.5	1	141.02 (CH)
H4 (bpy)	8.21 (ddd)	8.0, 8.0, 1.5	1	140.66 (CH)
H6 (bpy)	8.10 (ddd)	6.0, 1.5, 1.0	1	153.20 (CH)
H6 (dmazpy)	8.01 (ddd)	5.5, 1.5, 1.0	1	151.28 (CH)
H6 (bpy)	7.94 (ddd)	6.0, 2.0, 1.0	1	152.80 (CH)
H5 (bpy)	7.70 (ddd)	7.5, 1.5, 5.5	1	130.09 (CH)
	7.65 (ddd)	7.5, 1.5, 5.5	1	130.05 (CH)
	7.64 (ddd)	7.5, 1.5, 5.5	1	129.93 (CH)
	7.60 (ddd)	7.5, 1.5, 5.5	1	129.74 (CH)
H5 (dmazpy)	7.56 (ddd)	8.0, 1.5, 6.0	1	127.57 (CH)
H6 (bpy)	7.55 (ddd)	6.0, 1.5, 1.0	1	153.58 (CH)
H7 (dmazpy)	7.42 (d)	9.5	2	127.51 (CH)
H8 (dmazpy)	6.52 d)	9.5	2	112.80 (CH)
H9 (dmazpy)	3.07 s	-	6	40.24 (CH_3)

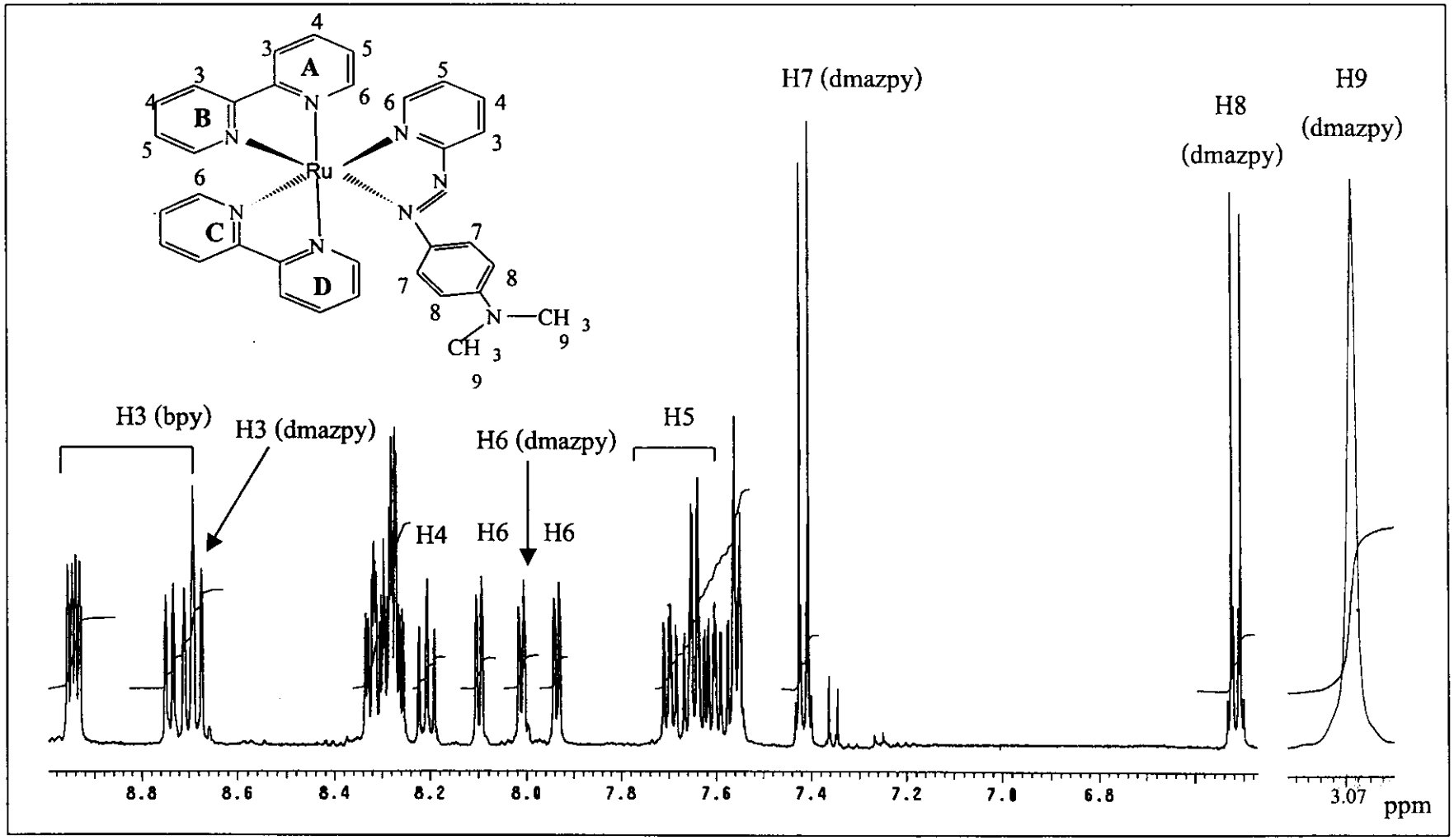

Figure 56 ^{1}H NMR spectrum of $[Ru(bpy)_2dmazpy](BF_4)_2$ in acetone-d_6 solution

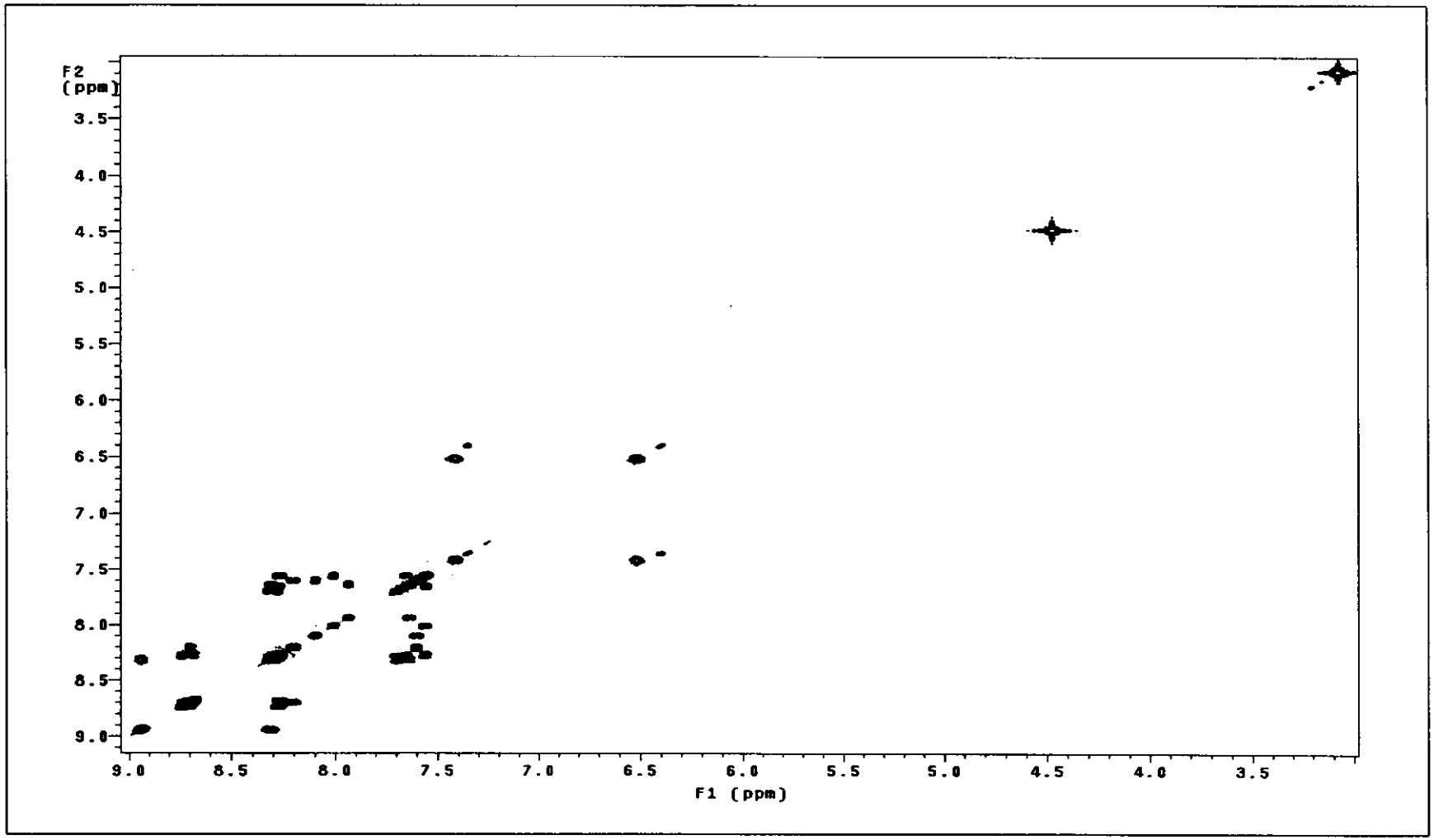

Figure 57 ^{1}H-^{1}H COSY spectrum of $[Ru(bpy)_2dmazpy](BF_4)_2$ in acetone-d_6 solution

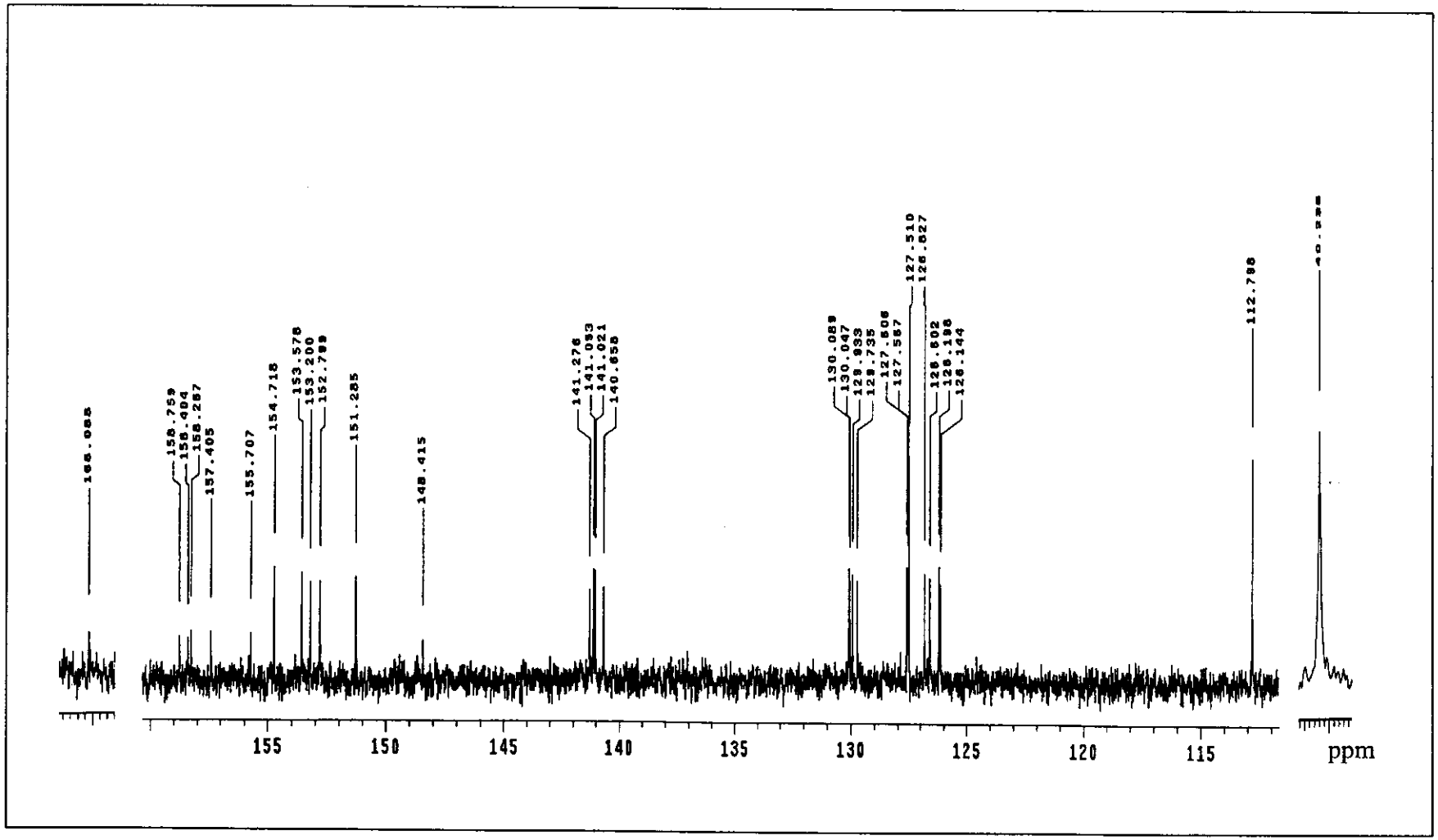

Figure 58 ^{13}C NMR spectrum of $[Ru(bpy)_2dmazpy](BF_4)_2$ in acetone-d_6 solution

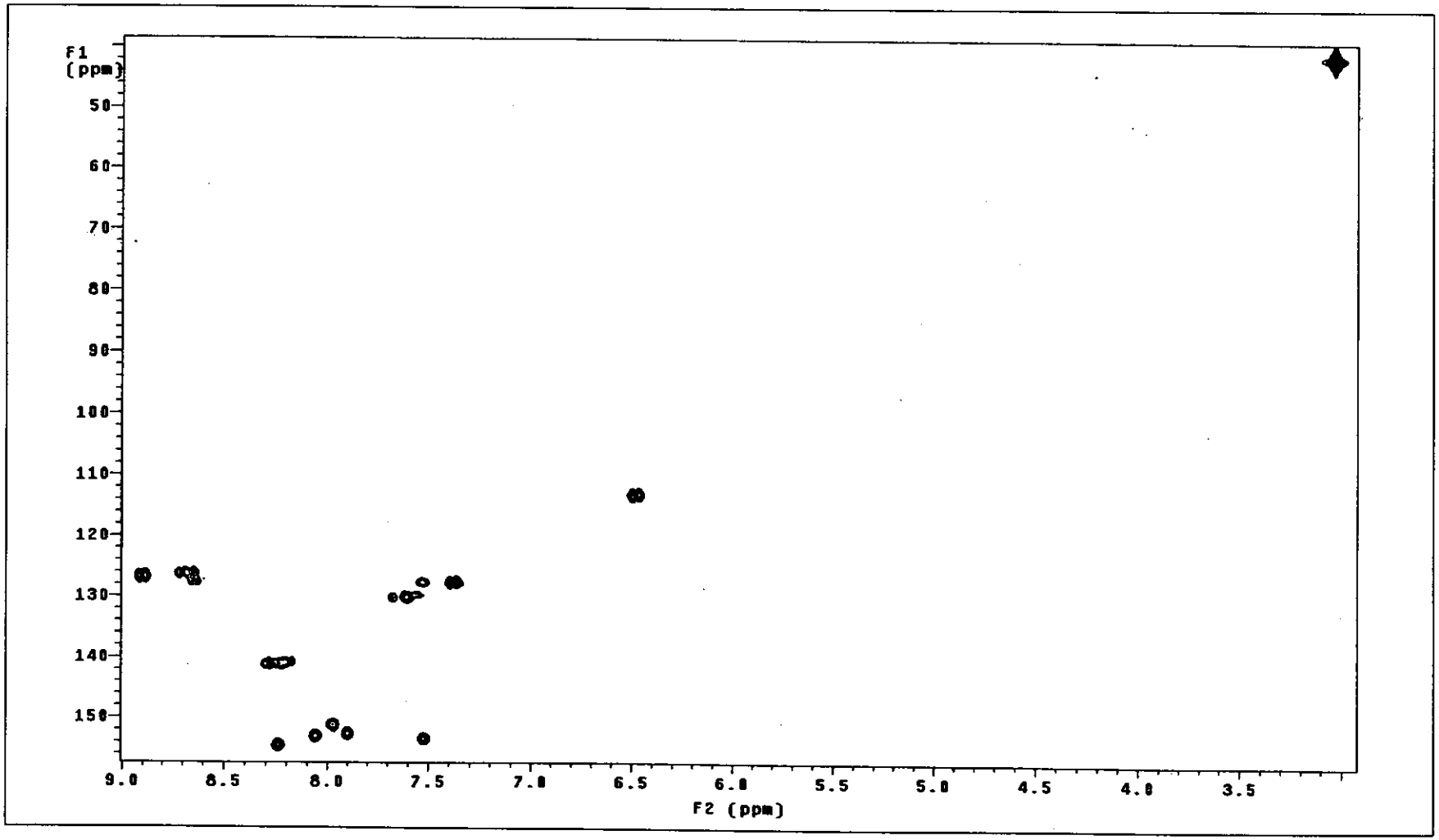

Figure 59 HMQC spectrum of $[Ru(bpy)_2dmazpy](BF_4)_2$ in acetone-d_6 solution

c) $[Ru(bpy)_2deazpy](BF_4)_2$ complex

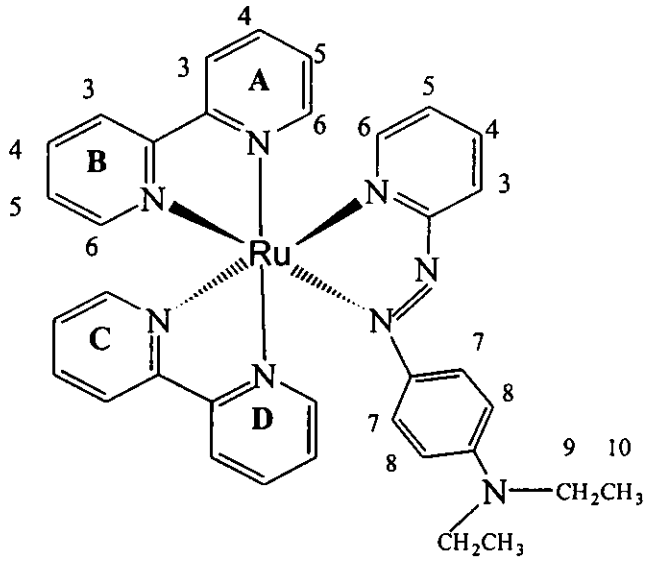

The ^{1}H NMR spectrum of $[Ru(bpy)_2deazpy](BF_4)_2$ complex (Figure 60) in acetone-d_6 showed characteristic peaks of bipyridine rings of both bpy and deazpy ligands and phenyl ring in deazpy ligand which appeared 25 signals for 34 protons. Since the complex ion was unsymmetric. Then four pyridine rings in the bpy ligands were chemically and magnetically non-equivalent. The ^{1}H-^{1}H COSY spectrum (Figure 61) of this complex revealed that the eight signals at 8.64 (ddd), 8.25 (ddd), 7.98 (ddd), 7.53 (ddd), 7.42 (d), 6.53 (d), 3.47 (q) and 1.14 (t) in deazpy ligand could be assigned to H3, H4, H6, H5, H7, H8, H9 and H10, respectively.

The ^{13}C NMR spectrum (Figure 62) and HMQC spectra (Figure 63) showed 31 resonances for 35 carbon atoms : twenty two methine carbons, a methene carbons (δ 45.68 ppm), a methyl carbons (δ 12.61 ppm) and seven quaternary carbons (δ 168.12, 158.47, 158.10, 158.00, 157.13, 153.44 and 147.91 ppm). The NMR data of this complex in acetone-d_6 solution are given in Table 24.

Table 24 The NMR data of $[Ru(bpy)_2deazpy](BF_4)_2$ in acetone-d_6 solution

Position	^{1}H NMR			^{13}C NMR (C-Type)
	δ(ppm)	J (Hz)	Amount of H	δ(ppm)
H3 (bpy)	8.92 (ddd)	8.0, 1.0, 1.0	1	126.46 (CH)
	8.91 (ddd)	8.0, 1.0, 1.0	1	126.24 (CH)
	8.73 (ddd)	8.0, 1.0, 1.0	1	125.83 (CH)
	8.70 (ddd)	8.0, 1.0, 1.0	1	125.80 (CH)
H3 (deazpy)	8.64 (ddd)	8.0, 1.5, 1.0	1	127.01 (CH)
H4 (bpy)	8.31 (ddd)	7.5, 8.0, 1.5	1	140.91 (CH)
	8.30 (ddd)	7.5, 8.0, 1.5	1	140.74 (CH)
H6 (bpy)	8.28 (ddd)	6.0, 2.0, 1.0	1	154.37 (CH)
H4 (bpy)	8.27 (ddd)	8.0, 8.0, 1.5	1	140.70 (CH)
H4 (deazpy)	8.25 (ddd)	8.0, 8.0, 1.5	1	140.65 (CH)
H4 (bpy)	8.21 (ddd)	8.0, 8.0, 1.5	1	140.28 (CH)
H6 (bpy)	8.10 (ddd)	6.0, 2.0, 1.0	1	152.89 (CH)
H6 (deazpy)	7.98 (ddd)	6.0, 1.5, 1.0	1	150.89 (CH)
H6 (bpy)	7.93 (ddd)	6.0, 2.0, 1.0	1	152.48 (CH)
H5 (bpy)	7.70 (ddd)	7.5, 1.5, 5.5	1	129.75 (CH)
	7.65 (ddd)	7.5, 1.5, 5.5	1	129.72 (CH)
	7.63 (ddd)	7.5, 1.5, 5.5	1	129.60 (CH)
	7.60 (ddd)	7.5, 1.5, 5.5	1	129.43 (CH)
H6 (bpy)	7.56 (ddd)	5.5, 2.0, 1.0	1	153.25 (CH)
H5 (deazpy)	7.53 (ddd)	8.0, 1.5, 6.0	1	126.96 (CH)
H7 (deazpy)	7.42 9d)	9.5	2	127.69 (CH)
H8 (deazpy)	6.53 (d)	9.5	2	112.38 (CH)
H9 (deazpy)	3.48(q) 3.47(q)	7.0, 7.0	4	45.68 (CH_2)
H10 (deazpy)	1.14 (t)	7.0	6	12.61 (CH_3)

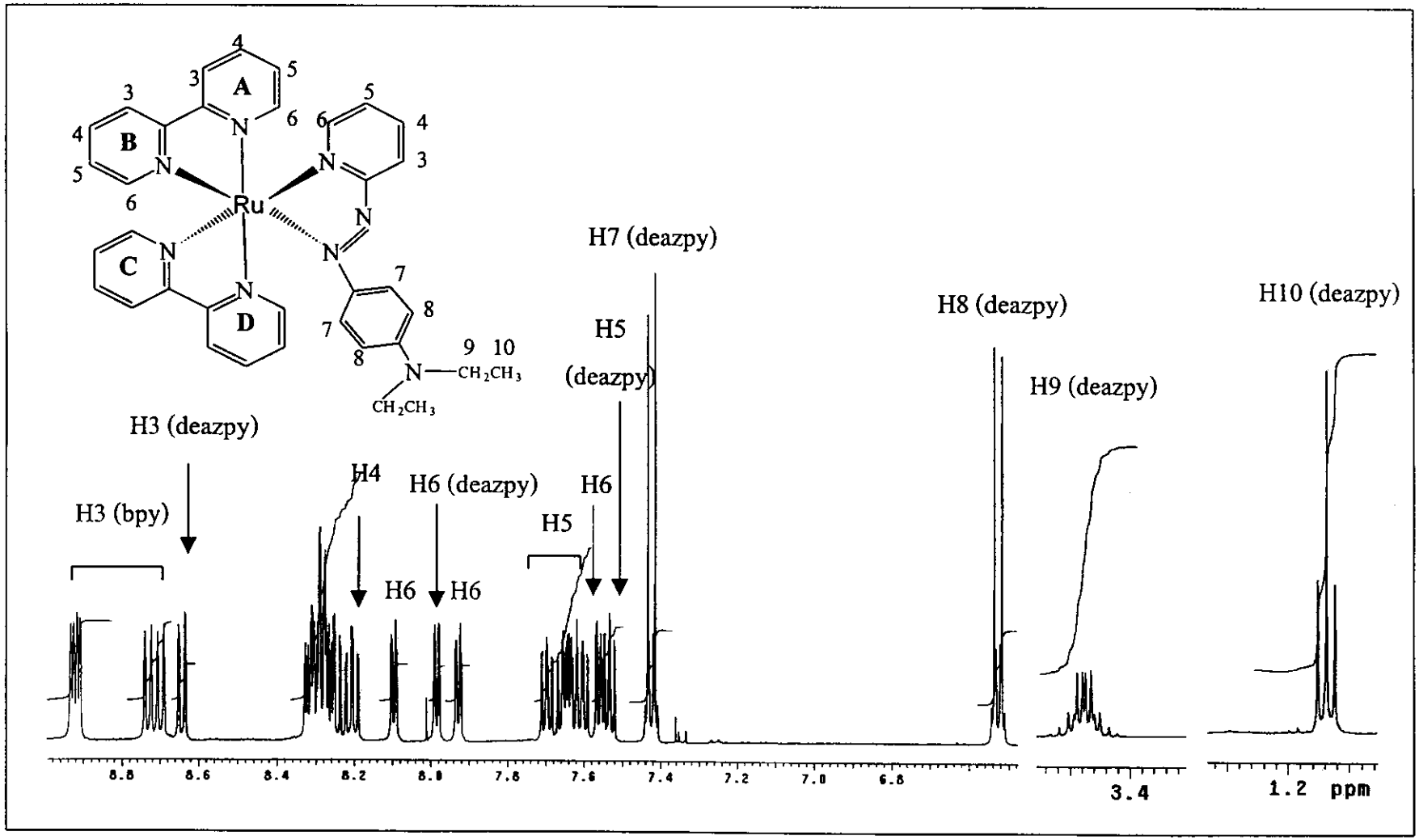

Figure 60 ^{1}H NMR spectrum of $[Ru(bpy)_2deazpy](BF_4)_2$ in acetone-d_6 solution

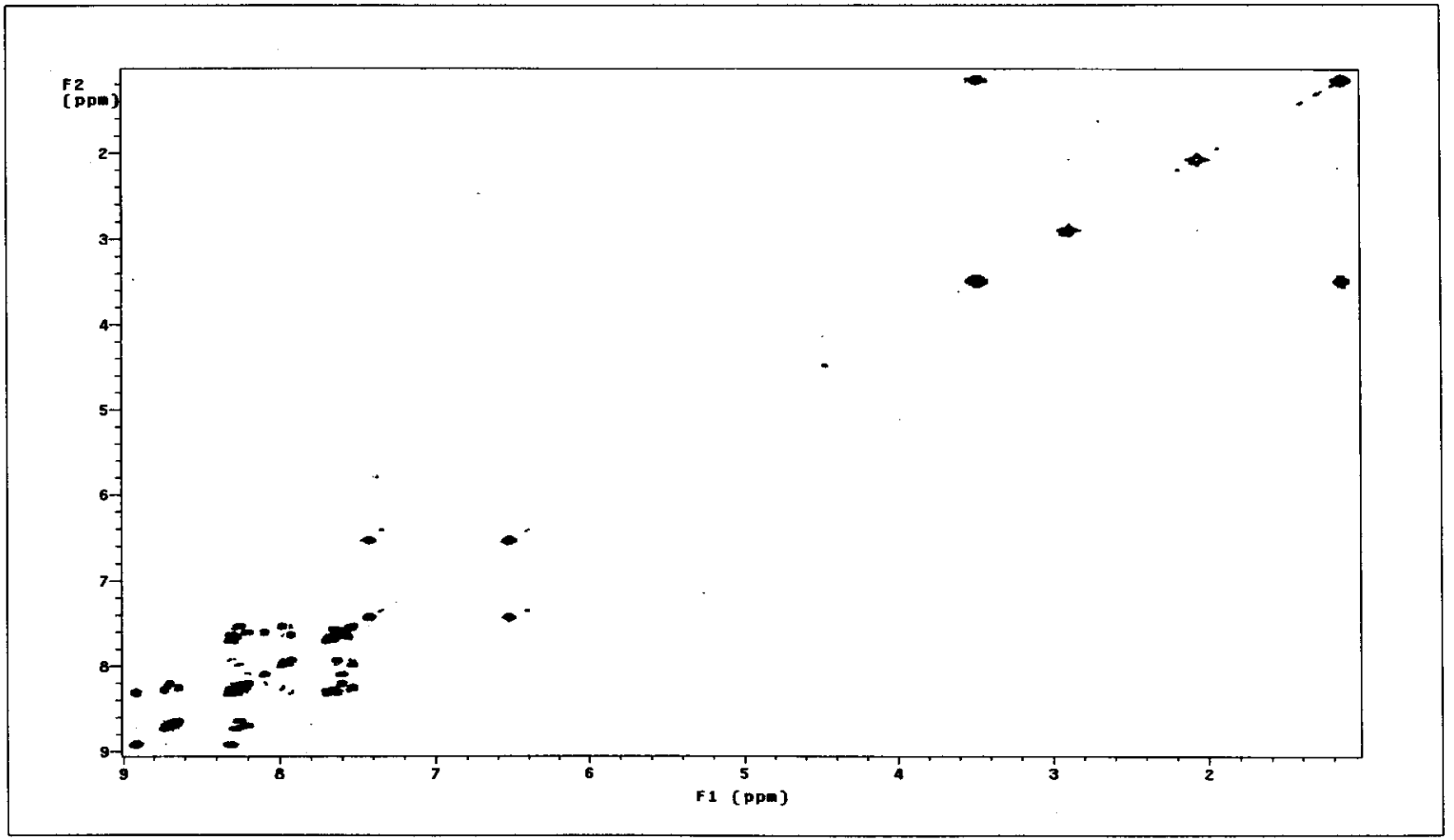

Figure 61 ^{1}H-^{1}H COSY spectrum of $[Ru(bpy)_2deazpy](BF_4)_2$ in acetone-d_6 solution

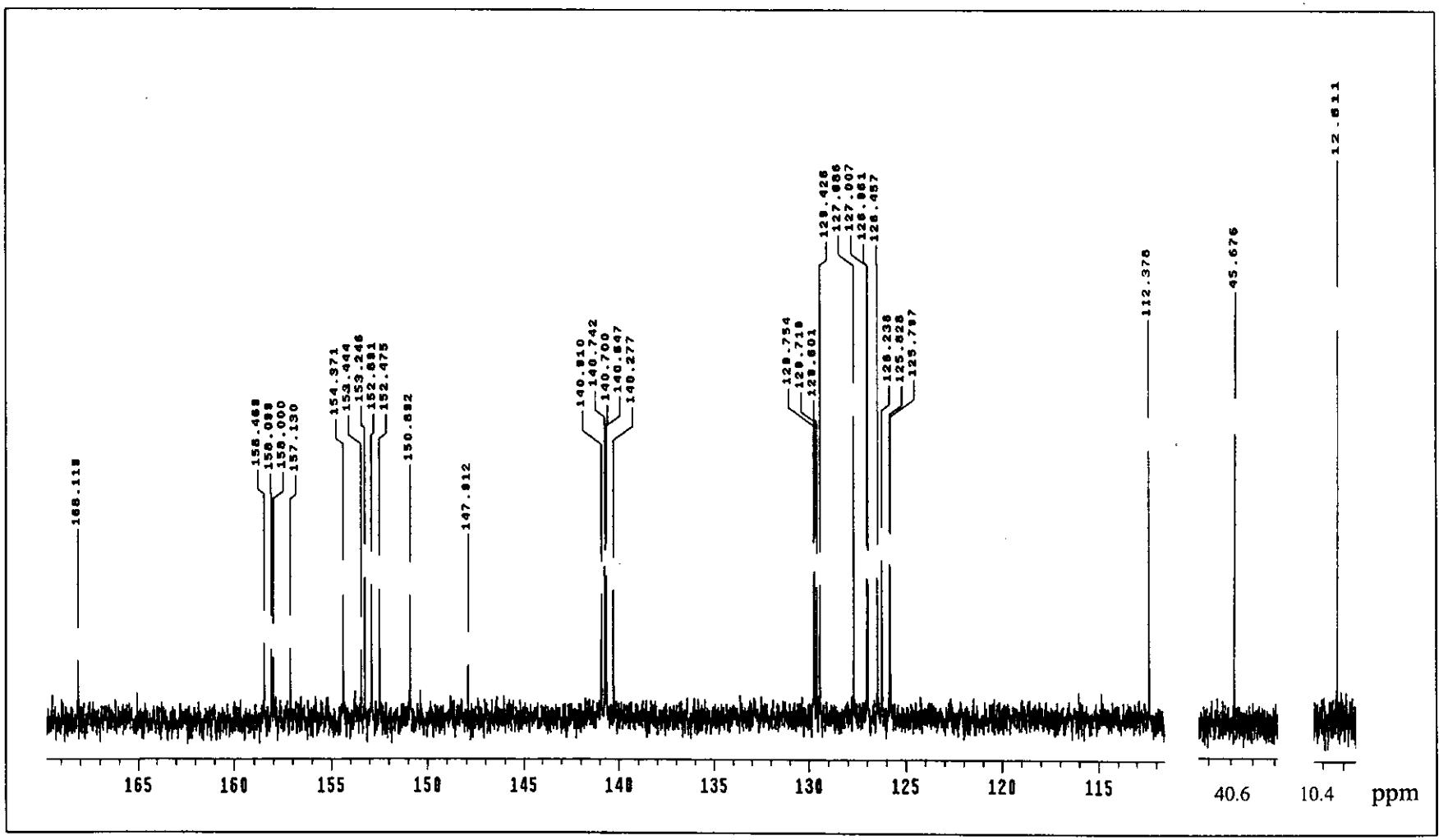

Figure 62 ^{13}C NMR spectrum of $[Ru(bpy)_2deazpy](BF_4)_2$ in acetone-d_6 solution

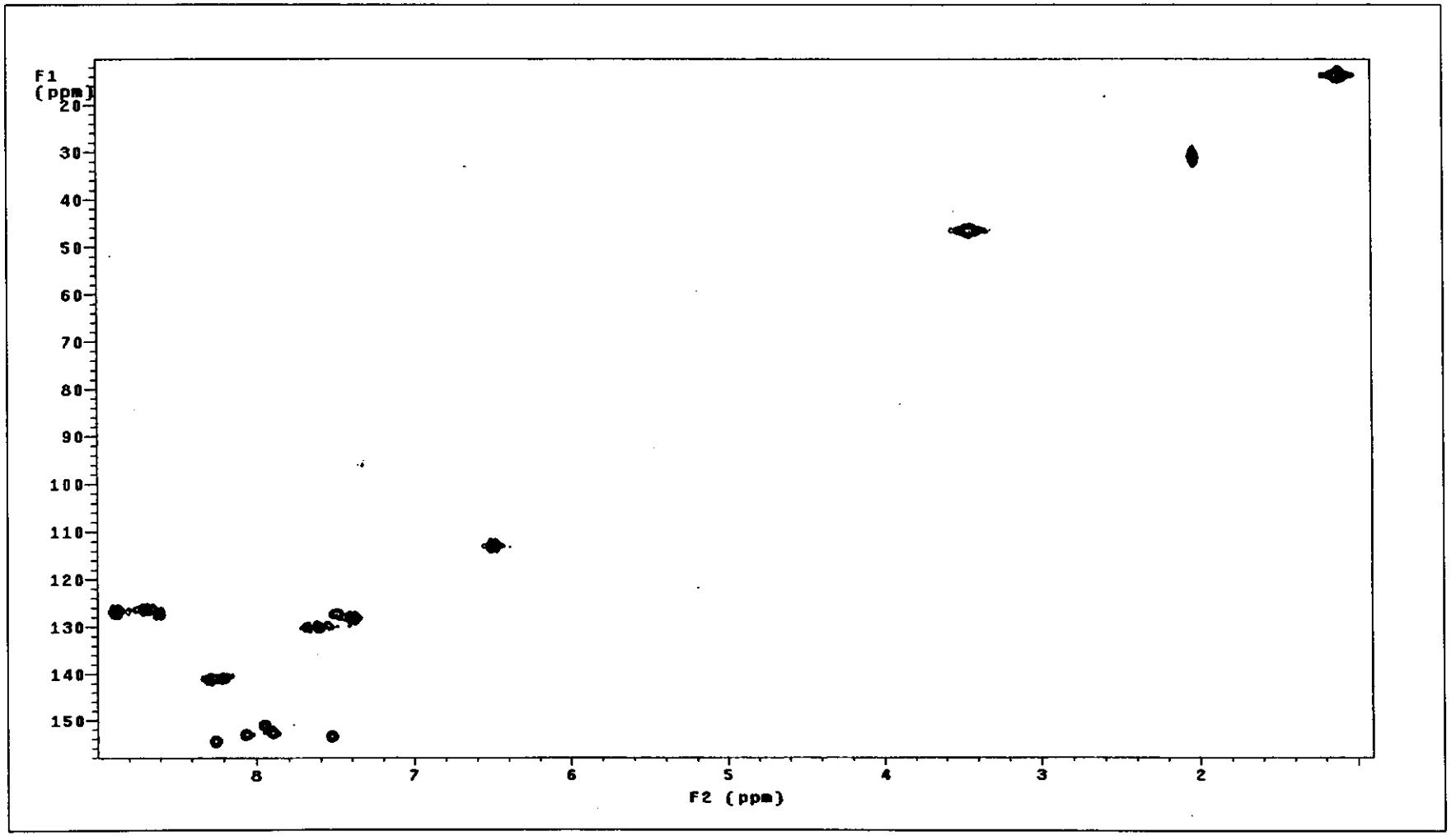

Figure 63 HMQC spectrum of $[Ru(bpy)_2deazpy](BF_4)_2$ in acetone-d_6 solution

d) $[Ru(bpy)_2azpym](BF_4)_2$ complex

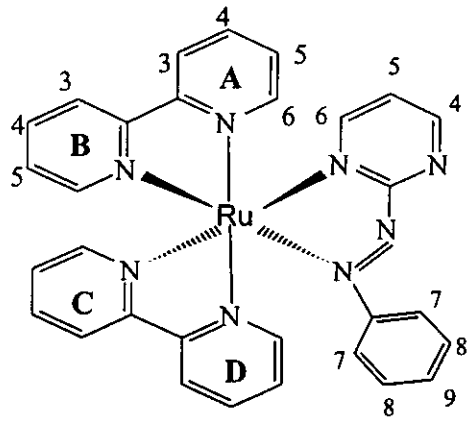

The ^{1}H NMR spectrum of $[Ru(bpy)_2azpym](BF_4)_2$ complex (Figure 64) in acetone-d_6 showed characteristic peaks of bipyridine rings of bpy ligand and broad peaks of azpym ligand which appeared 18 signals for 24 protons. Since the complex ion was unsymmetric, then four pyridine rings in the bpy ligands were chemically and magnetically non-equivalent. The ^{1}H-^{1}H COSY spectrum (Figure 65) of this complex revealed that the two signals at 9.33 (broad) and 7.26 (broad) in azpym ligand could be assigned to H4, H5 and H6 in pyrimidine ring and H7, H8 and H9 in phenyl ring, respectively.

The ^{13}C NMR spectrum (Figure 66) and HMQC spectra (Figure 67) showed 20 resonances for 20 carbon atoms of bpy ligand: sixteen methine carbons and four quaternary carbons (δ 160.56, 157.99, 157.42 and 157.31 ppm). For azpym ligand did not show signals in ^{13}C NMR and HMQC spectra. The NMR data of this complex in acetone-d_6 solution are given in Table 25.

Table 25 The NMR data of $[Ru(bpy)_2azpym](BF_4)_2$ in acetone-d_6 solution

Position	^{1}H NMR			^{13}C NMR (C-Type)
	δ(ppm)	J (Hz)	Amount of H	δ, ppm
H4, H5, H6 (azpym)	9.33 (broad)	-	3	-
H3 (bpy)	8.98 (d)	8.0	1	126.45 (CH)
	8.96 (d)	8.0	1	126.78 (CH)
	8.66 (d)	8.0	1	125.85 (CH)
	8.52 (d)	8.0	1	125.61 (CH)
H4 (bpy)	8.38 (ddd)	8.0, 8.0, 1.5	1	142.06 (CH)
	8.36 (ddd)	8.0, 8.0, 1.5	1	141.75 (CH)
	8.35 (ddd)	8.0, 8.0, 1.5	1	141.59 (CH)
H6 (bpy)	8.34 (d)	5.5	1	154.68 (CH)
H4 (bpy)	8.12 (ddd)	8.0, 8.0, 1.5	1	140.86 (CH)
H6 (bpy)	7.95 (d)	5.5	1	154.34 (CH)
	7.93 (d)	5.5	1	154.34 (CH)
	7.82 (d)	5.5	1	153.09 (CH)
H5 (bpy)	7.77 (ddd)	7.5, 1.5, 5.5	1	100.33 (CH)
	7.73 (ddd)	7.5, 1.5, 5.5	1	130.23 (CH)
	7.69 (ddd)	7.5, 1.5, 5.5	1	129.89 (CH)
	7.56 (ddd)	7.5, 1.5, 5.5	1	129.58 (CH)
H7 , H8 , H9 (azpym)	7.26 (broad)	-	5	-
Quaternary carbons (C)				160.56, 157.99 157.42, 157.31

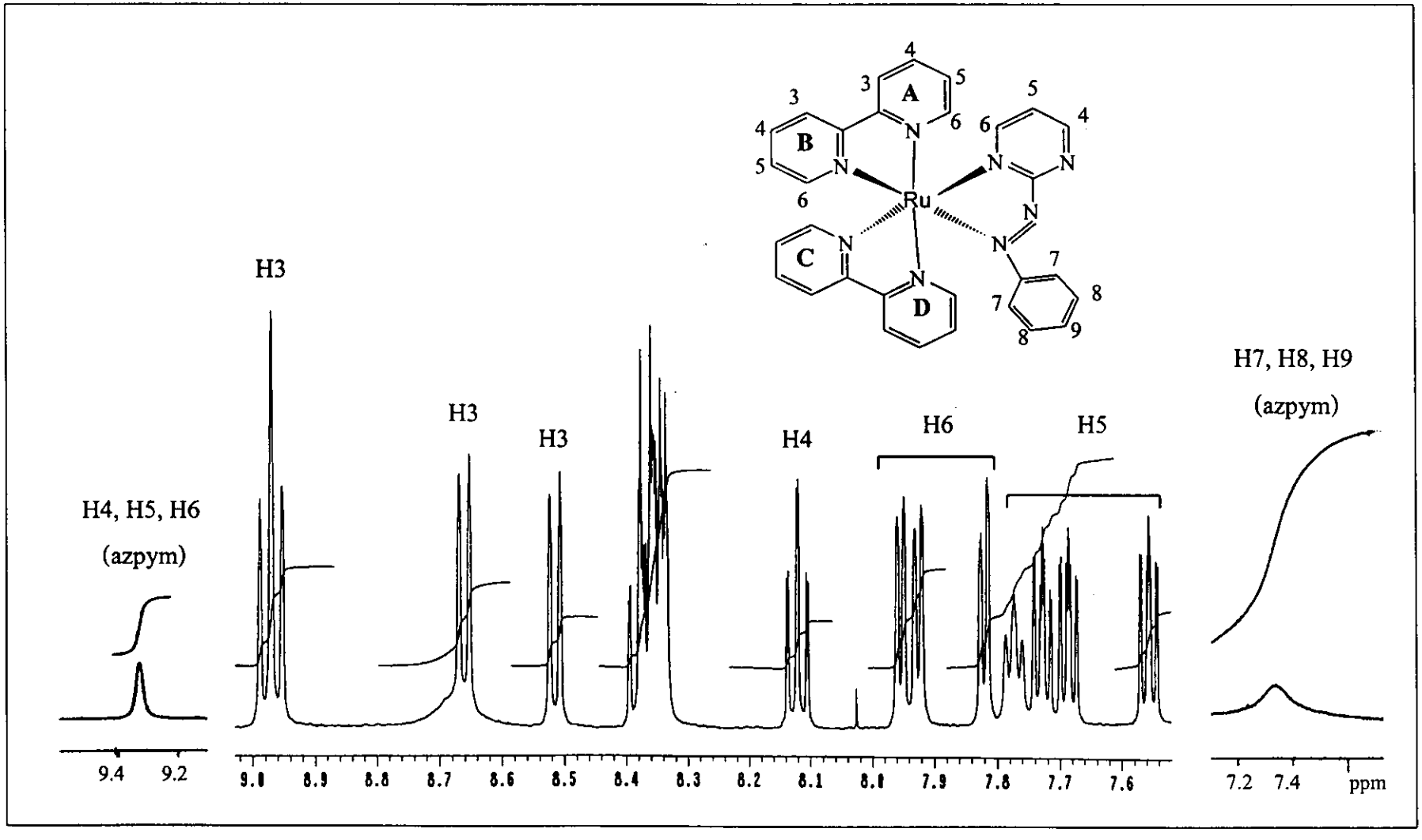

Figure 64 ^{1}H NMR spectrum of $[Ru(bpy)_2azpym](BF_4)_2$ in acetone-d_6 solution

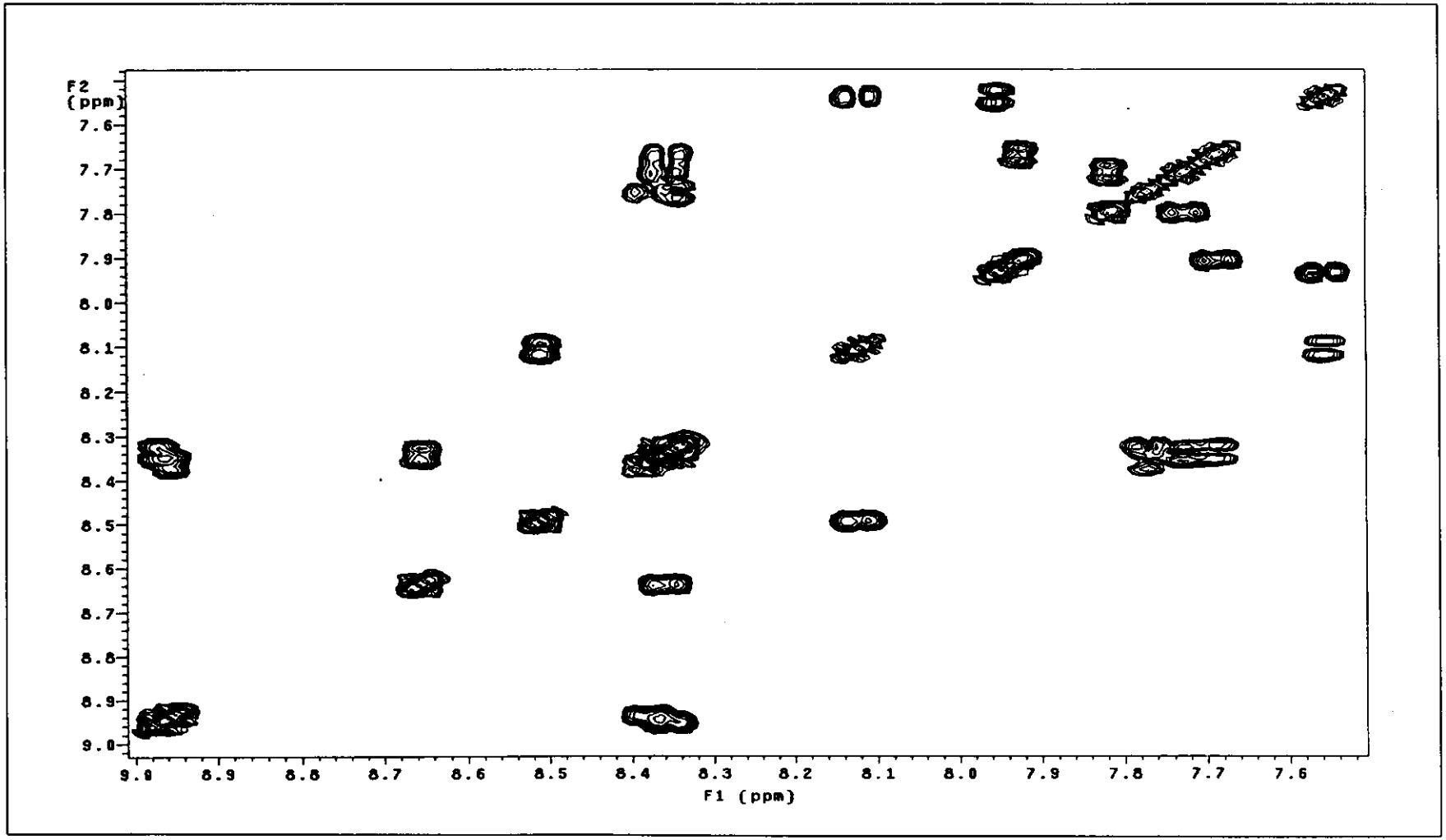

Figure 65 ^{1}H-^{1}H COSY spectrum of $[Ru(bpy)_2azpym](BF_4)_2$ in acetone-d_6 solution

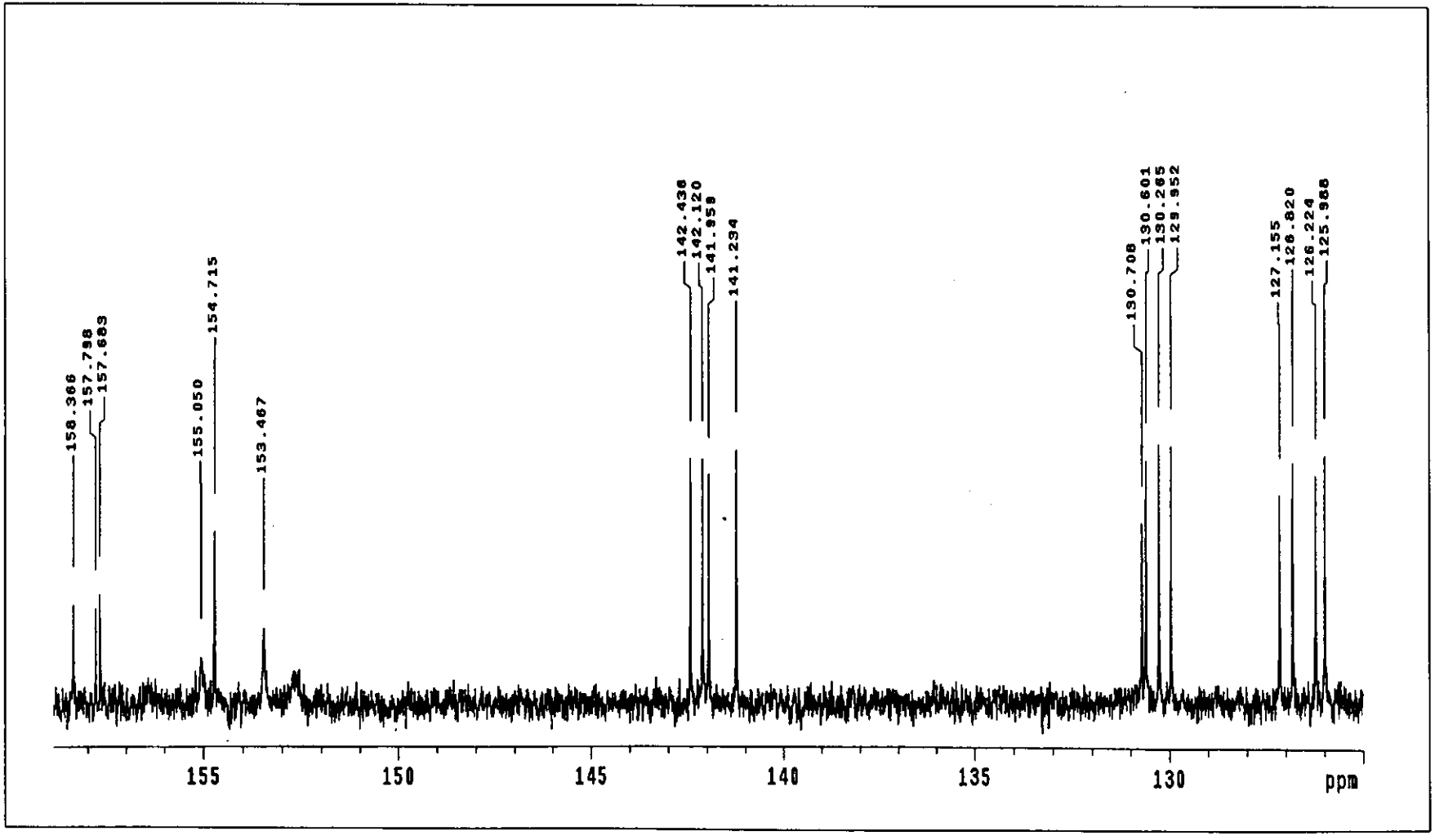

Figure 66 ^{13}C NMR spectrum of $[Ru(bpy)_2azpym](BF_4)_2$ in acetone-d_6 solution

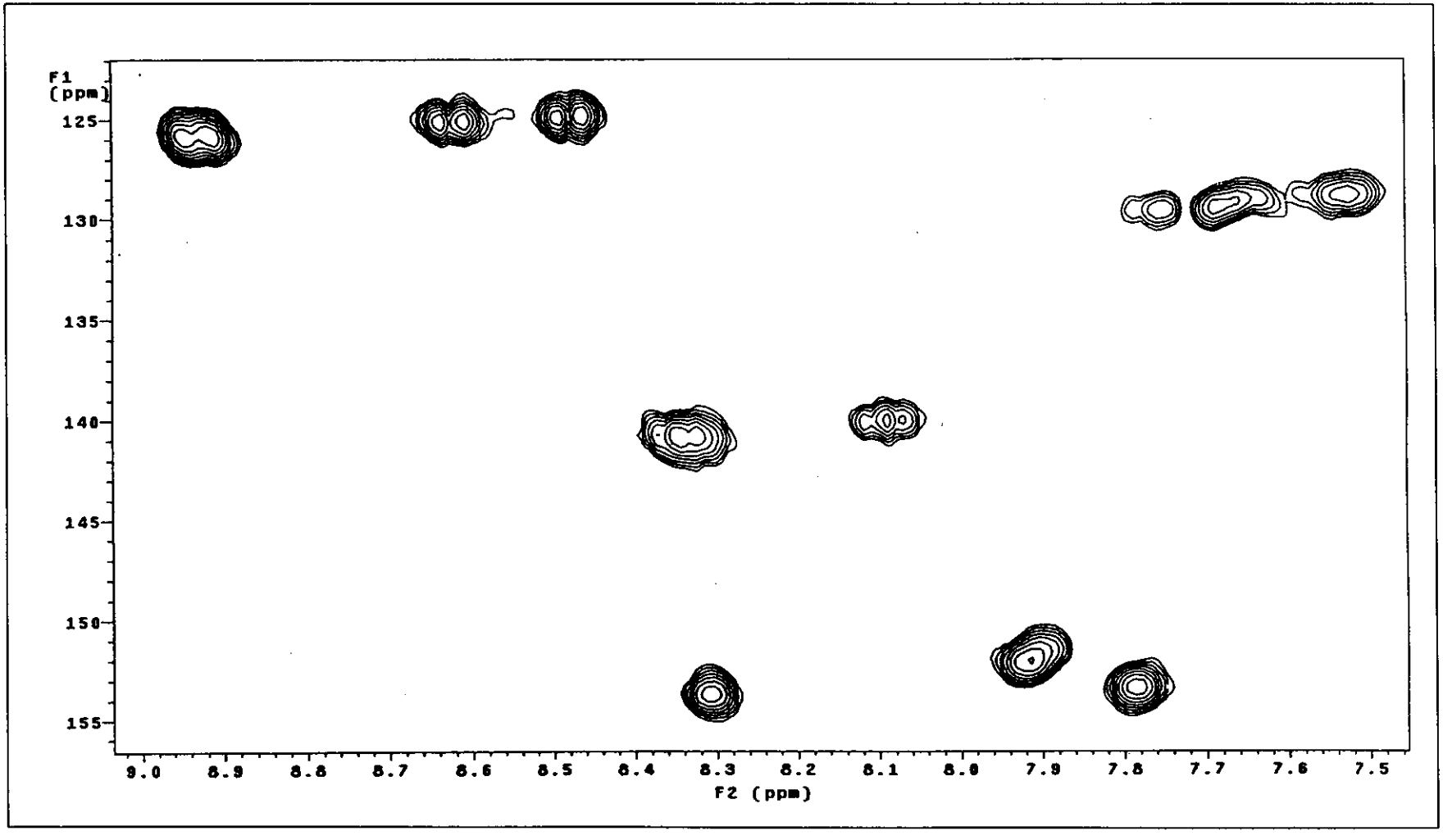

Figure 67 HMQC spectrum of $[Ru(bpy)_2azpym](BF_4)_2$ in acetone-d_6 solution

e) $[Ru(bpy)_2deazpym](BF_4)_2$ complex

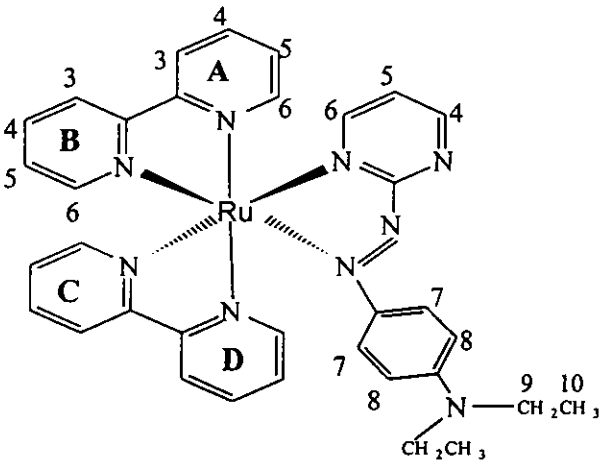

The ^{1}H NMR spectrum of $[Ru(bpy)_2deazpym](BF_4)_2$ complex (Figure 68) in acetone-d_6 showed characteristic peaks of bipyridine rings of both bpy and deazpym ligands and phenyl ring in deazpym ligand which appeared 24 signals for 33 protons. Since the complex ion was unsymmetric. Then four pyridine rings in the bpy ligands were chemically and magnetically non-equivalent. The ^{1}H-^{1}H COSY spectrum (Figure 69) of this complex revealed that the seven signals at 9.13 (dd), 8.34 (dd), 7.57 (d), 7.46 (dd), 6.61 (d), 3.55 (q) and 1.16 (t) in deazpym ligand could be assigned to H4, H6, H7, H5, H8, H9 and H10, respectively.

The ^{13}C NMR spectrum (Figure 70) and HMQC spectra (Figure 71) showed 32 resonances for 34 carbon atoms : twenty one methine carbons, two methene carbons (δ 46.31, 40.84 ppm), two methyl carbons (δ 19.27, 12.94 ppm) and seven quaternary carbons (δ 174.66, 158.65, 158.32, 158.67, 157.33, 155.18 and 149.88 ppm). The NMR data of this complex in acetone-d_6 solution are given in Table 26.

Table 26 The NMR data of $[Ru(bpy)_2dezpym](BF_4)_2$ in acetone-d_6 solution

Position	^{1}H NMR			^{13}C NMR (C-Type)
	δ(ppm)	J (Hz)	Amount of H	δ(ppm)
H4 (deazpym)	9.13 (dd)	5.0, 2.0	1	161.75 (CH)
H3 (bpy)	8.92 (ddd)	8.0, 1.0, 1.0	1	126.90 (CH)
	8.91 (ddd)	8.0, 1.0, 1.0	1	125.67 (CH)
	8.77 (ddd)	8.0, 1.0, 1.0	1	126.30 (CH)
	8.75 (ddd)	8.0, 1.5, 1.0	1	126.24 (CH)
H4 (bpy)	8.35 (ddd)	8.0, 8.0, 1.5	1	141.45 (CH)
H6 (deazpym)	8.34 (dd)	5.5, 2.0	1	160.41 (CH)
H6 (bpy)	8.33 (ddd)	5.0, 1.5, 1.0	1	154.77 (CH)
H4 (bpy)	8.32 (ddd)	8.0, 8.0, 1.5	1	141.32 (CH)
	8.30 (ddd)	8.0, 8.0, 1.5	1	141.26 (CH)
	8.23 (ddd)	8.0, 8.0, 1.5	1	140.92 (CH)
H6 (bpy)	8.08 (ddd)	5.5, 1.5, 1.0	1	153.14 (CH)
	7.90 (ddd)	5.5, 1.5, 1.0	1	152.88 (CH)
	7.75 (ddd)	5.5, 1.5, 1.0	1	153.86 (CH)
H5 (bpy)	7.73 (ddd)	7.5, 1.5, 5.5	1	130.28 (CH)
	7.68 (ddd)	7.5, 1.5, 5.5	1	130.15 (CH)
	7.63 (ddd)	7.5, 1.5, 5.5	1	129.99 (CH)
	7.62 (ddd)	7.5, 1.5, 5.5	1	129.89 (CH)
H7 (deazpym)	7.57 (d)	9.5	2	129.162 (CH)
H5 (deazpym)	7.46 (dd)	5.0, 2.0	1	120.79 (CH)
H8 (deazpym)	6.61 (d)	9.5	2	113.47 (CH)
H9 (deazpym)	3.55 (q) 3.54 (q)	7.0, 7.0	4	46.31 (CH_2) 40.84 (CH_2)
H10 (deazpym)	1.16 (t)	7.0	6	19.27, 12.94 (CH_3)

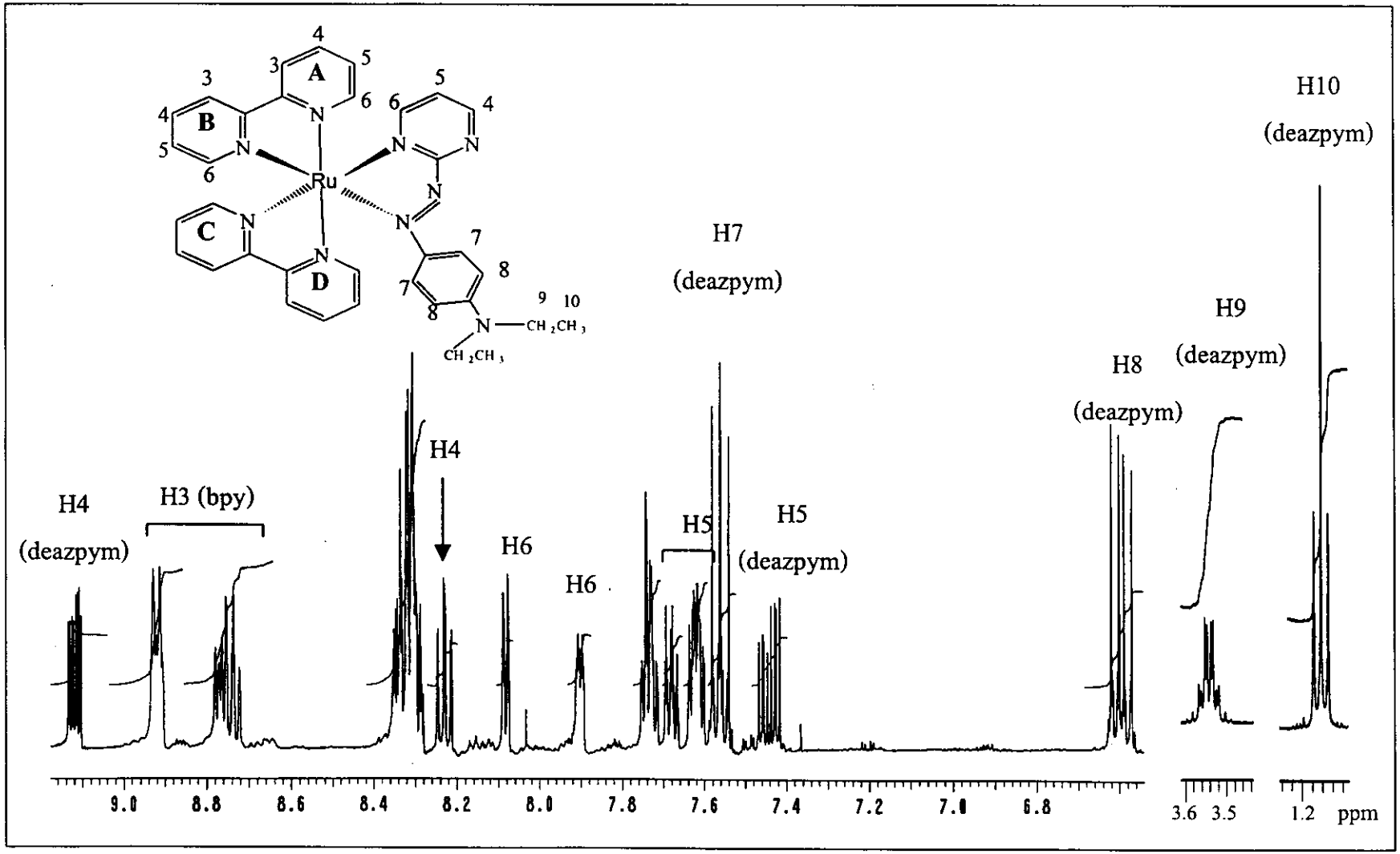

Figure 68 ^{1}H NMR spectrum of $[Ru(bpy)_2deazpym](BF_4)_2$ in acetone-d_6 solution

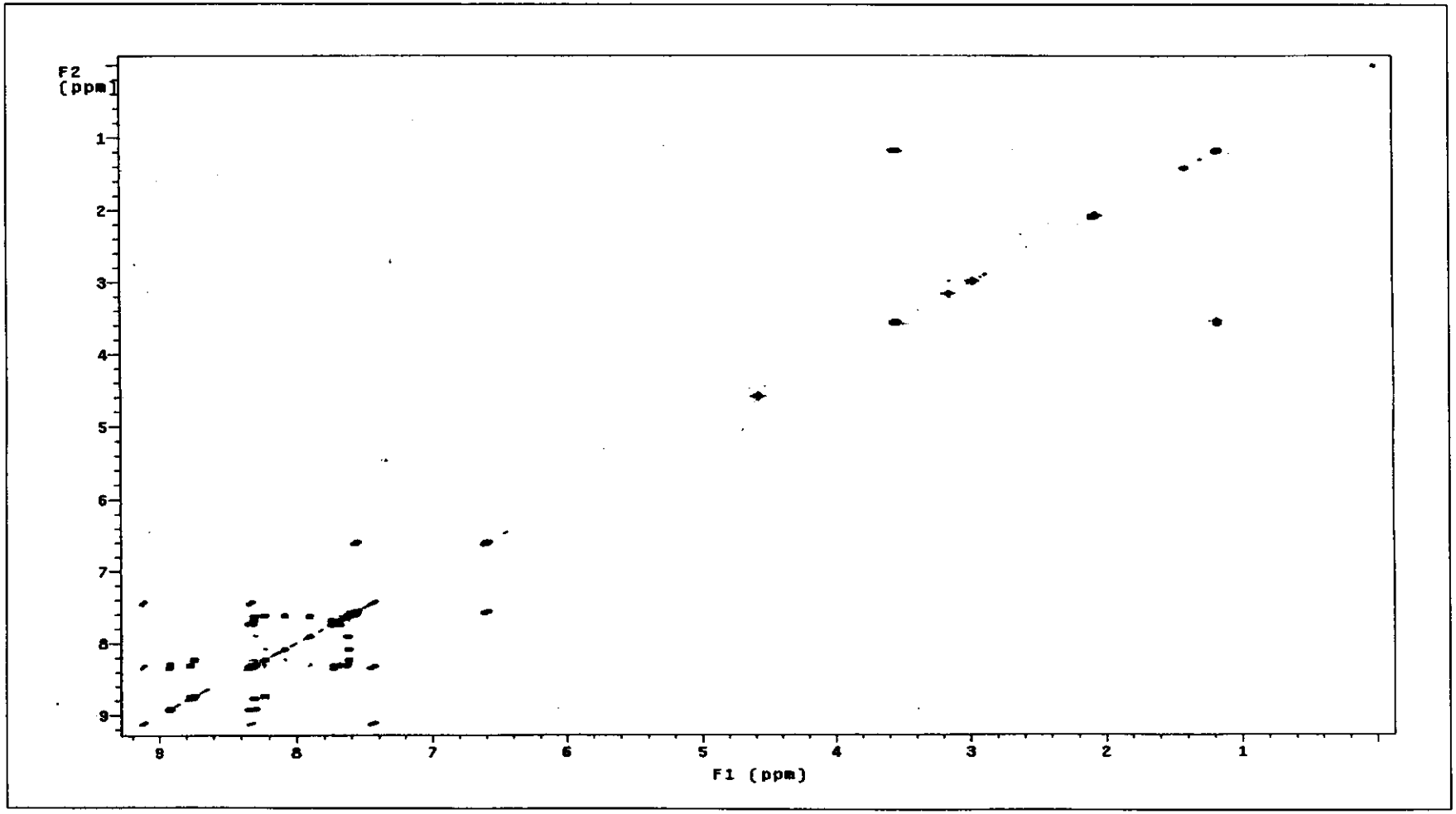

Figure 69 ^{1}H-^{1}H COSY spectrum of $[Ru(bpy)_2deazpym](BF_4)_2$ in acetone-d_6 solution

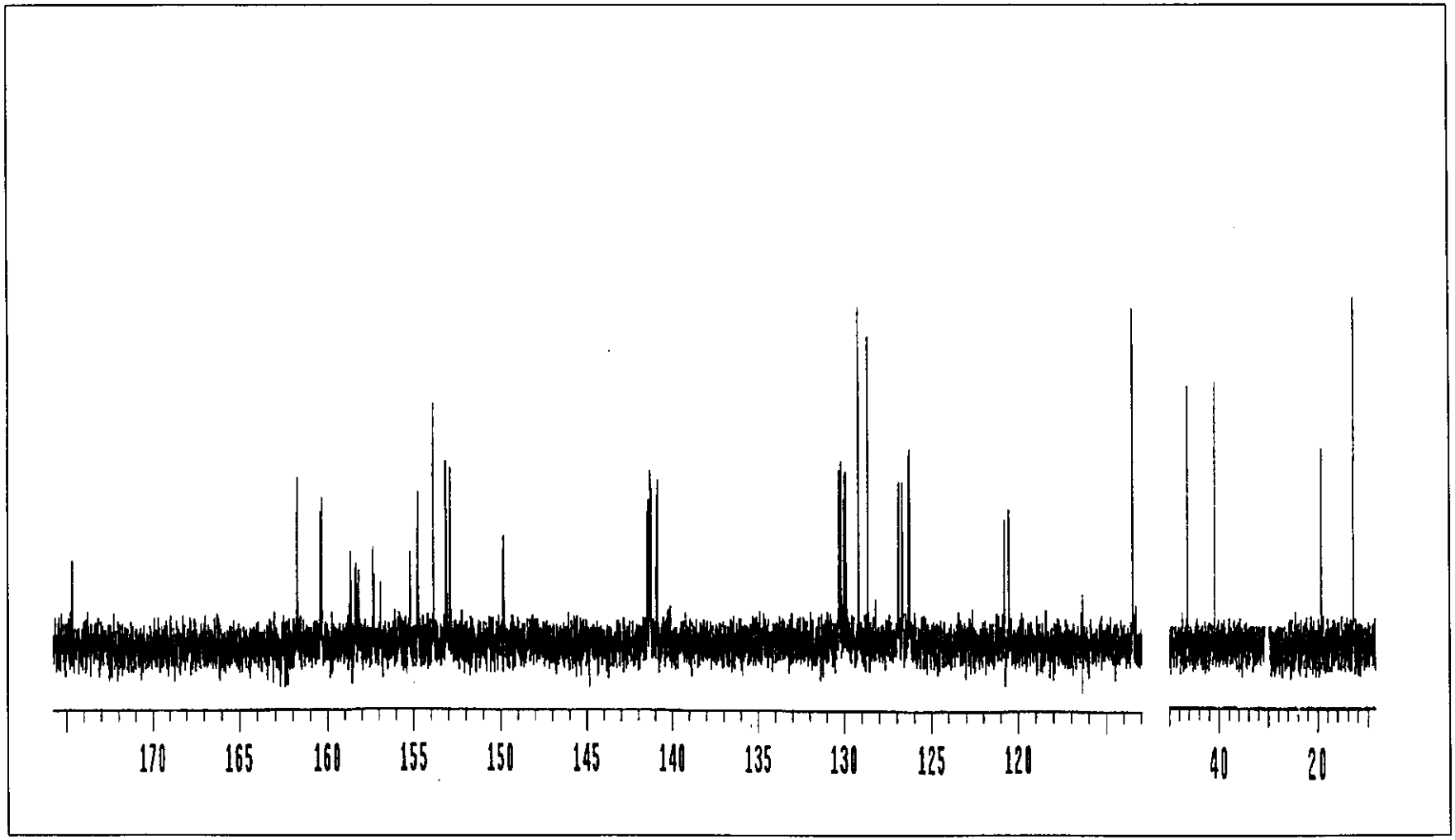

Figure 70 ^{13}C NMR spectrum of $[Ru(bpy)_2deazpym](BF_4)_2$ in acetone-d_6 solution

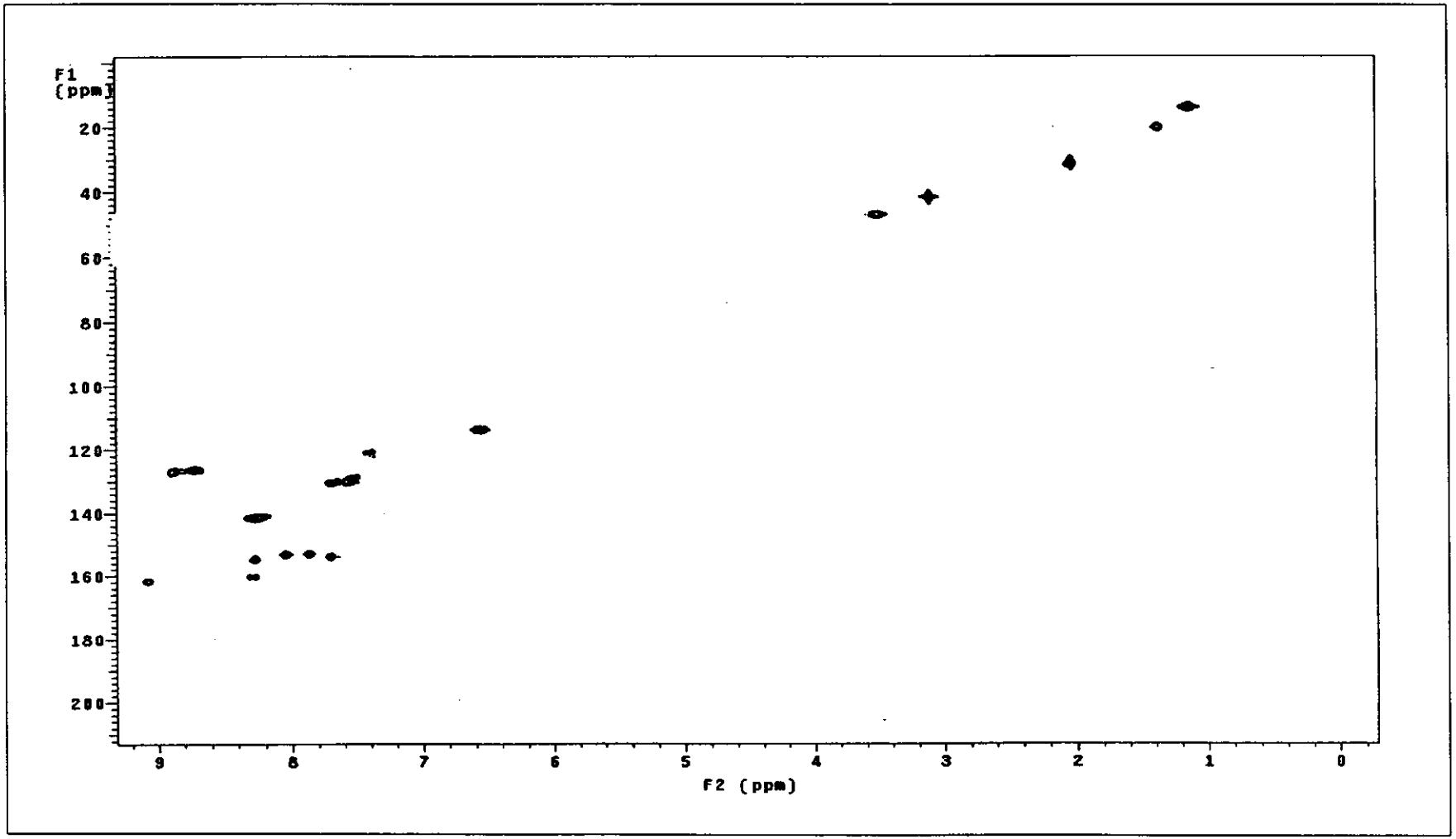

Figure 71 HMQC spectrum of $[Ru(bpy)_2deazpym](BF_4)_2$ in acetone-d_6 solution

3.6.6 Cyclic Voltammetric results of complexes

Cyclic voltammetry is a method of studying the oxidation-reduction processes in detail. Cyclic voltammograms of $[Ru(bpy)_2L]^{2+}$ (L= bpy, azpy, dmazpy, deazpy, azpym and deazpym ligands in acetonitrile solution are shown in Figure 72-77, respectively. The summary of the cyclic voltammetric data is given in Table 27.

Table 27 Cyclic voltammetric data of $[Ru(bpy)_2L]^{2+}$ (L= bpy, azpy, dmazpy, deazpy, azpym and deazpym ligands in 0.1 M TBAH acetonitrile at scan rate 100 mV/s (ferrocene as an internal standard, ΔE_p = 75 mV)

Complex	$E_{1/2}$, V (ΔE_p, mV)					
	Oxidation		Reduction			
	Ru (II/II)	Ligand with substituents	I	II	III	IV
$[Ru(bpy)_3]^{2+}$	+0.91 (85)	-	-1.74 (85)	-1.93 (85)	-2.17 (85)	-
$[Ru(bpy)_2azpy]^{2+}$	+1.21 (100)	-	-0.87 (80)	-1.61 (70)	-2.07 (85)	-2.40 (95)
$[Ru(bpy)_2dmazpy]^{2+}$	-	+0.71 (70)	-1.02 (75)	-1.75 (85)	-2.07 (85)	-2.27 (85)
$[Ru(bpy)_2deazpy]^{2+}$	-	+0.74 (75)	-1.04 (80)	-1.76 (75)	-2.07 (85)	-2.23 (85)
$[Ru(bpy)_2azpym]^{2+}$	-	-	-0.67 (80)	-1.48 (90)	-2.04 (85)	-2.38 (85)
$[Ru(bpy)_2deazpym]^{2+}$	-	+0.77 (90)	-0.86 (75)	-1.64 (65)	-2.04 (80)	-2.25 (85)

Cyclic Voltammogram of the $[Ru(bpy)_2L]^{2+}$ complexes, where L = azpy, dmazpy, deazpy, azpym and deazpym, gave similar patterns but the peak potentials were shifted. These complexes displayed signals in oxidation and reduction potentials.

Oxidation potential

The cyclic voltammogram of $[Ru(bpy)_3]^{2+}$ and $[Ru(bpy)_2azpy]^{2+}$ complexes showed the redox couple of Ru(II/III) at $E_{1/2}$ = +0.91 (ΔE_p = 85 mV) and +1.21 V (ΔE_p = 100 mV), respectively (Figure 84, Appendix A). Whereas, the oxidation potentials of $[Ru(bpy)_2L]^{2+}$ complexes (L = dmazpy, deazpy, azpym and deazpym) were not observed within the solvent window in the range 0.0 to 1.4 V. For the substituted complexes showed only quasi-reversible couple at less positive (Figure 85, Appendix A). The $[Ru(bpy)_2dmazpy]^{2+}$ complex showed quasi-reversible couple at $E_{1/2}$ = +0.71 V (ΔE_p = 70 mV). For $[Ru(bpy)_2deazpy]^{2+}$ and $[Ru(bpy)_2deazpym]^{2+}$ complexes gave similar results to those in dmazpy complex at $E_{1/2}$ = +0.74 V (ΔE_p = 75 mV) and $E_{1/2}$ = +0.77 V (ΔE_p = 90 mV), respectively.

Reduction potential

The complexes were studied in the range –2.5 to 0.0 V. Cyclic voltammogram of $[Ru(bpy)_2L]^{2+}$ complexes (L = azpy, dmazpy, deazpy, azpym and deazpym) occurred four couples. Each couple in this region was reversible couple which could individually transfer one electron. The couple I-II belonged to the third ligands. Whereas, the III and IV couples belonged to the bpy ligands which occurred in the range –2.0 to –2.4 V of all complexes and will be discussed in detail later.

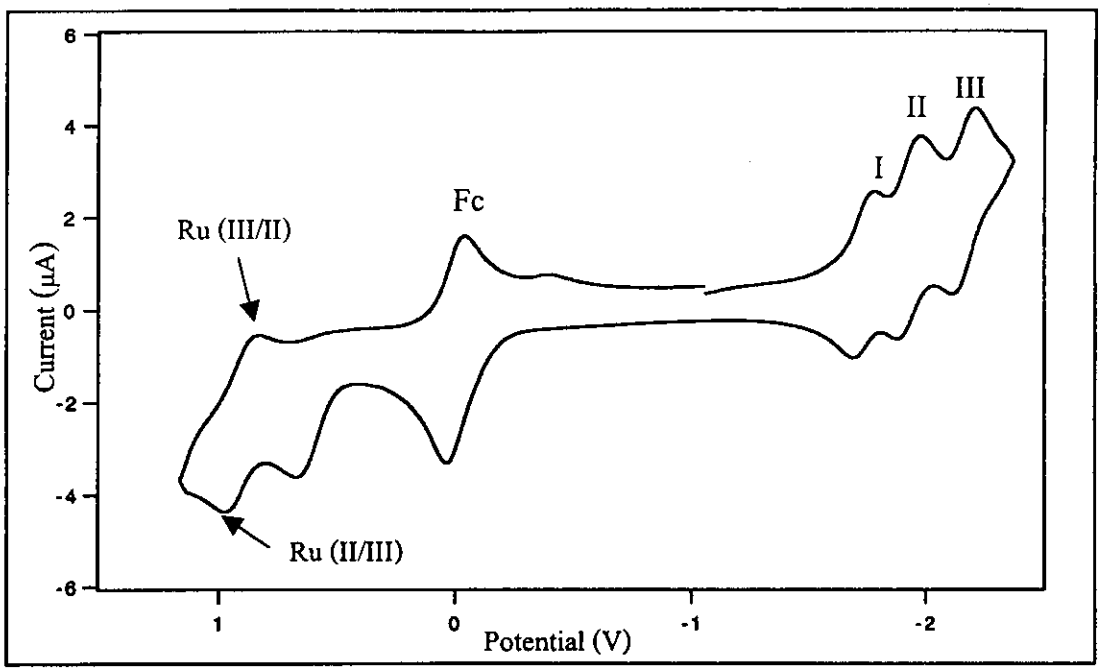

Figure 72 Cyclic voltammogram of $[Ru(bpy)_3]^{2+}$ in CH_3CN at scan rate 100 mV/s

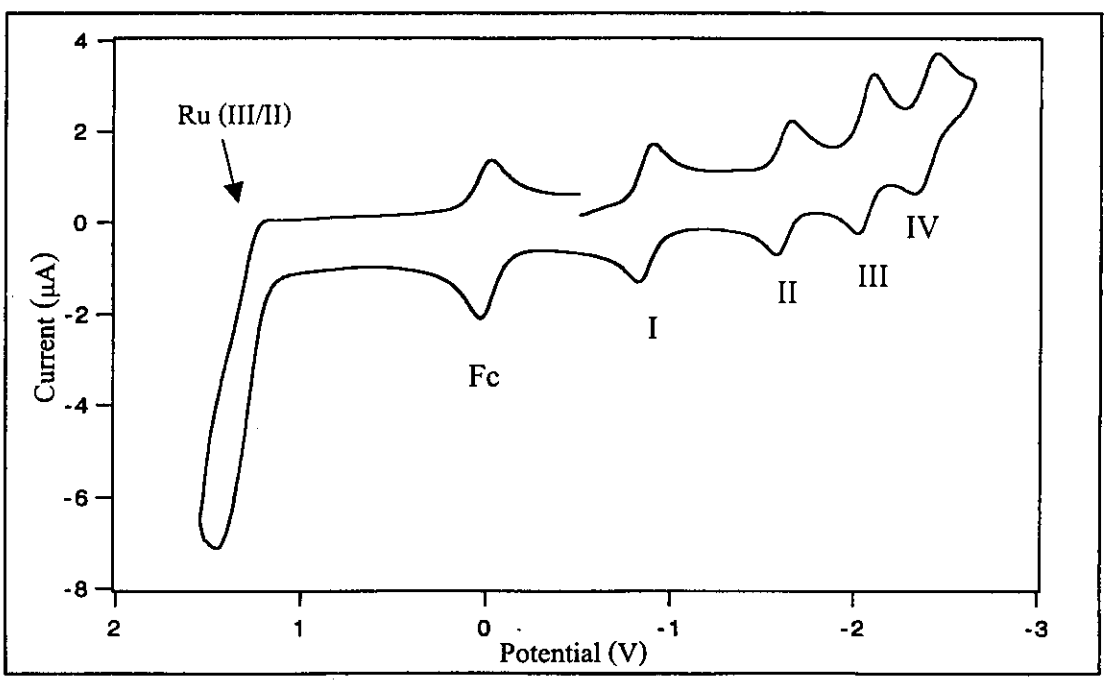

Figure 73 Cyclic voltammogram of $[Ru(bpy)_3azpy]^{2+}$ in CH_3CN at scan rate 100 mV/s

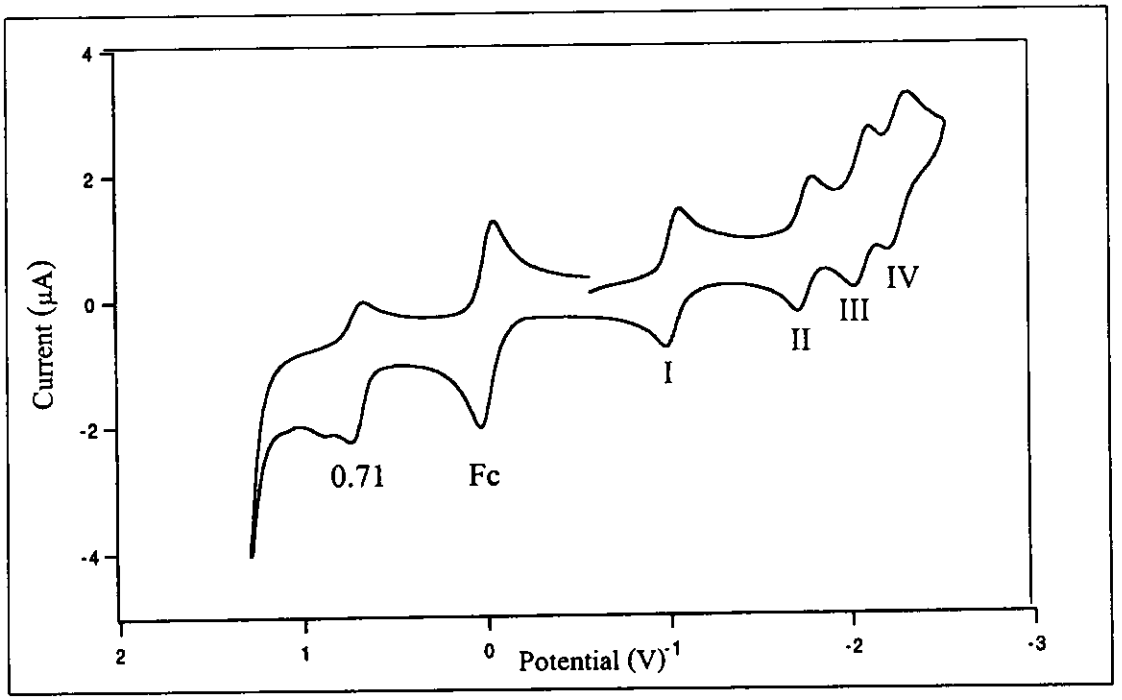

Figure 74 Cyclic voltammogram of $[Ru(bpy)_2dmazpy]^{2+}$ in CH_3CN at scan rate 100 mV/s

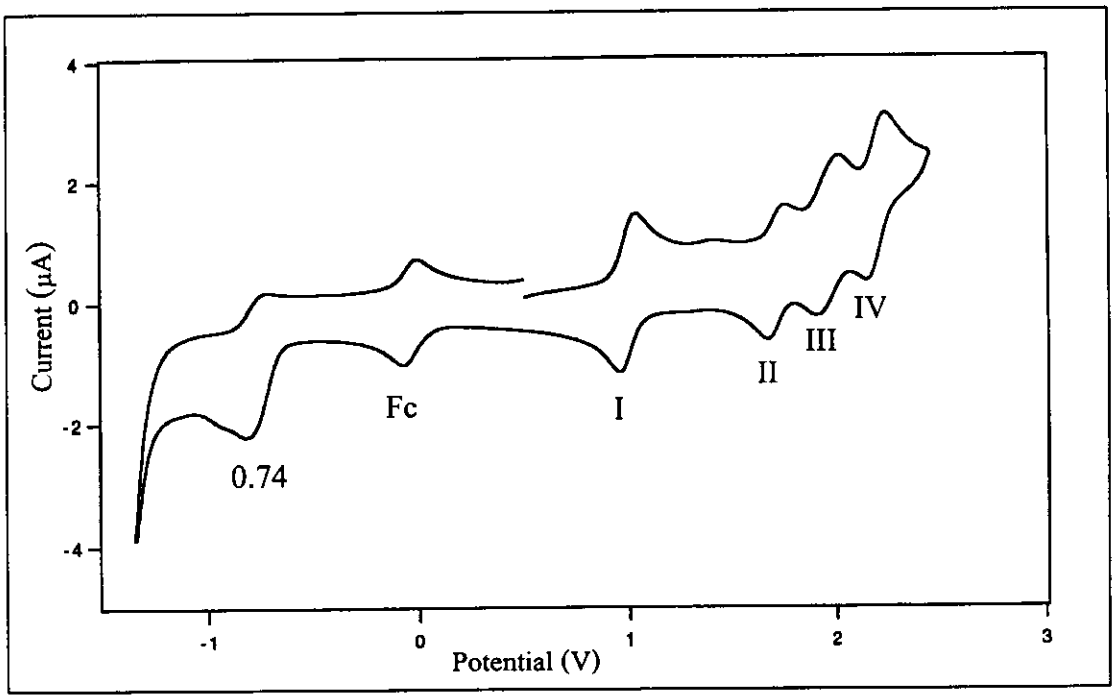

Figure 75 Cyclic voltammogram of $[Ru(bpy)_2deazpy]^{2+}$ in CH_3CN at scan rate 100 mV/s

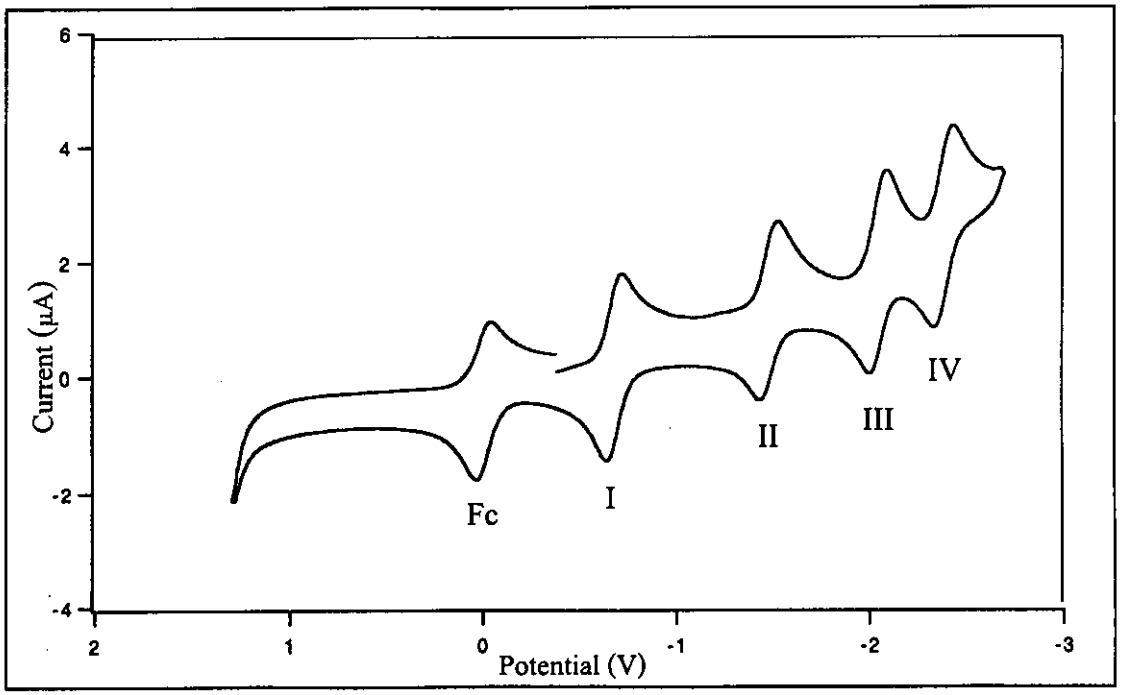

Figure 76 Cyclic voltammogram of $[Ru(bpy)_3azpym]^{2+}$ in CH_3CN at scan rate 100 mV/s

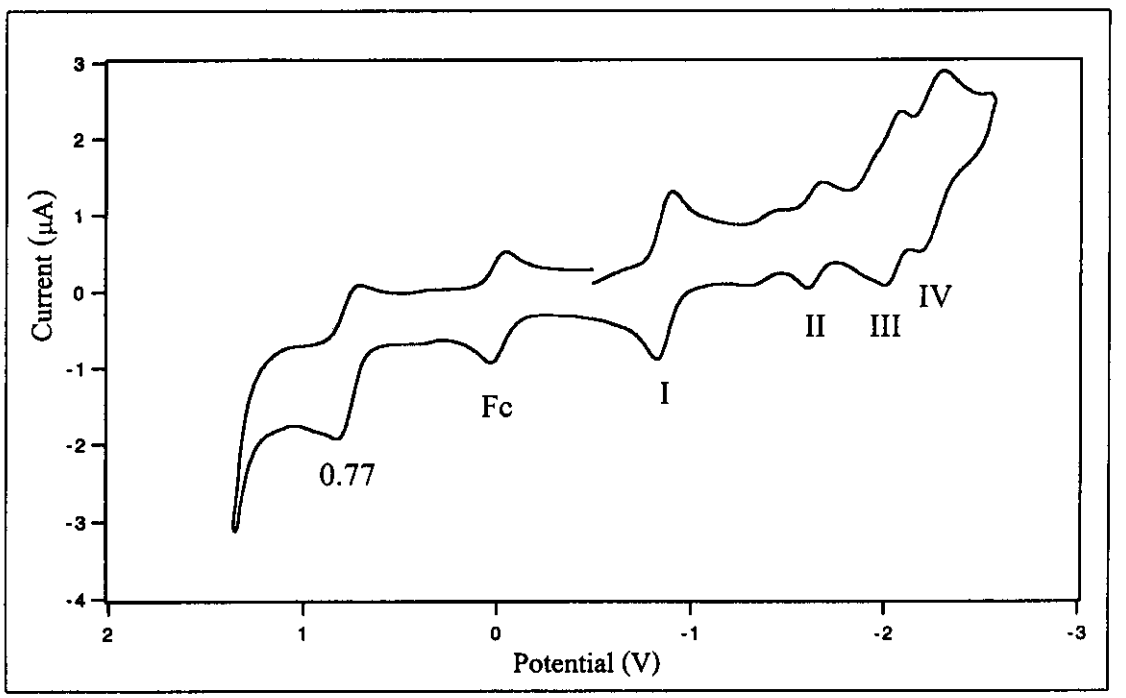

Figure 77 Cyclic voltammogram of $[Ru(bpy)_2deazpym]^{2+}$ in CH_3CN at scan rate 100 mV/s